

# UC Riverside

## UC Riverside Electronic Theses and Dissertations

### Title

Perception Learning, Prediction and Motion Planning for Energy Efficient Driving of Connected and Automated Vehicles

### Permalink

<https://escholarship.org/uc/item/4vh9b4j6>

### Author

Ye, Fei

### Publication Date

2019

Peer reviewed|Thesis/dissertation

UNIVERSITY OF CALIFORNIA  
RIVERSIDE

Perception Learning, Prediction and Motion Planning for Energy Efficient Driving of  
Connected and Automated Vehicles

A Dissertation submitted in partial satisfaction  
of the requirements for the degree of

Doctor of Philosophy

in

Electrical Engineering

by

Fei Ye

September 2019

Dissertation Committee:

Dr. Matthew J. Barth, Chairperson  
Dr. Hamed Mohsenian-Rad  
Dr. Peng Hao

Copyright by  
Fei Ye  
2019

The Dissertation of Fei Ye is approved:

---

---

---

Committee Chairperson

University of California, Riverside

## Acknowledgments

First and foremost, I would like to sincerely thank my advisor Prof. Matthew J. Barth, whose valuable guidance and continuous support during my pursuit of Ph.D. degree have made all these work possible. I'm grateful and fortunate to be advised by Prof. Barth who has guided me through the gate of research opportunities and exciting challenges in the realm of intelligent vehicles and intelligent transportation systems. His insightful knowledge and great personality have always been a powerful source of inspiration and encouragement I could ever ask for. Working with him is a rewarding experience for me both technically and non-technically. I would not have come to this far without his lasting support and wisdom advice.

I would like to thank my other committee members for serving on my proposal and dissertation, Dr. Hamed Mohsenian-Rad, Dr. Guoyuan Wu and Dr. Peng Hao whose valuable advice and feedback have greatly improved the research in this dissertation. In addition, I would like to give my special thank to Dr. Guoyuan Wu, and Dr. Peng Hao who leading most of the research projects I have participated in at CE-CERT. I'm honored to work with them and benefit greatly from their profound knowledge and insight on connected and automated vehicles research. I learned a lot from so many inspiration discussions and "white-board" moments we had together. They are incredible helpful and most importantly, showed me what a great researcher should be like. I am grateful also to Dr. Kanok Boriboonsomsin and Mike Todd for their managements and valuable guidance in our collaborative projects and whose effectiveness and communication skills I will always strive for.

It is very fortunate for me to work and learn with so many exceptional fellows and collaborators, especially Dr. Shaocheng Wang, Dr. Peng Wang, Dr. Hongsheng Yu and Danial Esaid. I want to thank my lab colleagues, Dr. Ji Luo, Dr. Xuwei Qi, Dr. George Scora, Chao Wang, Ziran

Wang, Nigel Williams, Danyang Tian, Zhouqiao Zhao, Zhensong Wei, Xishun Liao, Alexander Vu and many others. I also want to special thank Alta Vasquez and Carolyn Ray who help me in many aspects during my study in CE-CERT.

During my time at UC Riverside, I have met many great people and have a wonderful memory because of them. I would like to thank my best friends Zhu Yan, Meng Zhao, Xing Zheng, Luting Yang, Han Zhou, Zhenjun Cui, Hongsheng Yu, Xiaonian Shan, Weixia Li and many others for accompanying me, supporting me and enriching my life throughout this enjoyable journey.

I would like to acknowledge and thank all the fund supported for my Ph.D. study: The Department of Electrical Engineering of UC Riverside, CE-CERT at UC Riverside, the U.S. Department of Energy, The National Center for Sustainable Transportation (NCST), Honda R&D, Women In Engineer(WIE), and Dr. Nora Hackett, for fully or partially supporting my studies built in this dissertation.

I would also like to express my gratitude to my host and managers at Mitsubishi Electric Research Laboratory, Dr. Jianlin Guo, Dr. Stefano Di Cairano, Dr. Phil Orlik, Dr. Keyong Jin Kim and Dr. Heejin Ahn, who enriched my summer in 2018.

Finally, I would like to dedicate this dissertation to my parents, Song Ye and Wei Xue for their unconditional love, understanding and support throughout my life. I'm extremely fortunate to have my parents as the most powerful and warmest bay who are always respectful and supporting me to live my life and purse my dreams.

*To my dad Song Ye and my mom Wei Xue for their love and support*

## ABSTRACT OF THE DISSERTATION

Perception Learning, Prediction and Motion Planning for Energy Efficient Driving of Connected and Automated Vehicles

by

Fei Ye

Doctor of Philosophy, Graduate Program in Electrical Engineering  
University of California, Riverside, September 2019  
Dr. Matthew J. Barth, Chairperson

The uninterrupted growth in transportation activities has been exerting significant pressure on our socio-economics and environment in recent years. However, emerging technologies such as connected and automated vehicles (CAVs), transportation electrification, and edge computing have been stimulating increasingly dedicated efforts by engineers, researchers and policymakers to tackle these transportation-related problems, including those that are focused on energy and the environment. With the advancement towards vehicle connectivity and automation, vehicles can reduce the energy consumption, emissions and improve urban mobility and safety through environmentally-friendly eco-driving strategies, vehicle electrification, and driving coordination.

In this dissertation, we developed predictive models and trajectory planning algorithms using machine learning and optimization techniques to address four key challenge: 1) Driving in real-world scenarios with constrains and interaction from downstream vehicle's trajectory and traffic; 2) Extracting essential traffic information from sparse vehicle trajectory data in a connected vehicle environment; 3) Evaluating and quantifying the behavior of a complex Vehicle-Powertrain Eco-Operation System; and 4) Optimal scheduling and coordinating automated vehicles in terms

of mobility benefits and energy savings considering the tradeoff between solution optimality and computational efficiency for online performance.

This research first starts with developing an electric vehicle energy consumption model based on real world data and integrating it into eco-driving algorithms considering the regenerative braking effect. By introducing a hybrid modeling approach which provides variables with actual physical meaning instead of the exhaustive method used in conventional data-driven approaches, we feature knowledge-driven variable selection and data-driven statistical synthesis together to further improve the estimation accuracy.

Many of the existing eco-driving algorithms, including the eco-approach and departure (EAD) algorithm, are not flexible enough to effectively handle customized powertrain characteristics, interaction with other traffic, road grade, and traveling with the presence of the downstream vehicles. Therefore, when considering the real-world deployment of the EAD application, it is beneficial to further explore the dynamic states from downstream vehicles and incorporate these into the trajectory planning process. A machine learning technique has been applied to the snippet of downstream vehicle trajectory (which may be obtained from onboard sensors, such as radar) to predict trajectories using real-world data. By integrating the prediction on future states of the preceding vehicle into the trajectory planner, the resulting enhanced EAD algorithm provides an eco-friendly speed trajectory in the presence of preceding traffic and queues at intersections with additional 2 – 34 % energy savings and emission reduction compared to the EAD algorithms without prediction.

This dissertation also describes a technique to integrate vehicle dynamics and powertrain operations, using a comprehensive simulation study that was designed and tested for both electric buses and plug-in hybrid electric buses driving across total 11 signalized intersections in a test corri-

dor. The overall simulation framework incorporates a two-layer vehicle optimal trajectory planning module that seamlessly integrates a graph-based trajectory planning algorithm and a deep learning-based trajectory planning algorithm while interacting with the environment calibrated using real-world data. It was found that deep learning-based EAD algorithms can achieve a good balance between solution optimality and computational efficiency. Besides, a dynamic queue prediction in the connected vehicle environment has been developed to better plan the bus trajectory for greater energy consumption. Over 20.0% energy savings can be achieved across various traffic conditions when co-optimizing vehicle dynamics and powertrain operations. In addition, an extra around 5% energy efficiency improvement for a test PHEV bus was shown when introducing 20% connected vehicles in the network.

With a partially connected vehicle network, we not only improve the longitudinal control of the vehicle to obtain better energy efficiency but also extract essential traffic condition information such as lane-level traffic information that can be used for better lane selection. We developed a Lane-Hazard Prediction (LHP) application that can detect lane-level hazards effectively and efficiently. A machine learning approach was developed with feature extraction from the spatial-temporal domain to achieve sustainable high accurate lane-level prediction of a downstream hazard within tenths of seconds after it occurred by crowdsourcing sparse connected vehicle trajectories. The LHP application then guides the application-equipped vehicles with suggestions for proper lateral maneuvers far ahead of the hazard to avoid traffic jams. Results demonstrate that LHP-equipped vehicles may gain significant mobility and safety benefits without compromising the mobility and safety performance of the overall traffic under various traffic conditions and penetration rate of connectivity in the vehicle network.

Finally, a Bi-level Optimal Edge Computing (BOEC) methodology was developed under the fully connectivity vehicle network to maximize both the vehicle mobility benefit and energy saving by optimizing the vehicle coordination and motion planning. For the on-ramp scenario, the first-level edge computing is conducted in the roadside unit (RSU) that collects connected vehicle data, dynamically assigning each vehicle into an associated cluster group based on its state and potential merging conflict and periodically solved for the clustered vehicles with their optimal scheduling sequence and arrival time at the merge bottleneck point. Once the clustered vehicles have their assigned arrival time at the merge point, the second-level edge computing determines the optimal vehicle trajectory to guarantee vehicles meet the assigned arrival time with the minimum energy cost. It is shown that the computational cost of vehicle trajectory planning approaches can satisfy the objective of real-time performance with 63.4%-66.8% energy savings.

# Contents

<b>List of Figures</b>	<b>xiv</b>
<b>List of Tables</b>	<b>xvi</b>
<b>1 Introduction</b>	<b>1</b>
1.1 Background and Problem Statement . . . . .	1
1.2 Related Work . . . . .	8
1.3 Contributions . . . . .	13
1.4 Organization . . . . .	14
<b>2 Data-Driven Modeling Combined with Physical Concept Modeling of Electric Vehicle Energy Consumption</b>	<b>16</b>
2.1 Background . . . . .	17
2.2 Electric Vehicle Drivetrain Configuration . . . . .	19
2.3 Real-World Data Acquisition and Processing . . . . .	20
2.3.1 Data Acquisition . . . . .	21
2.3.2 Data Processing . . . . .	21
2.4 Hybrid Modeling Approach . . . . .	23
2.4.1 Power Flows at the Battery Terminal . . . . .	23
2.4.2 Regenerative Braking Factor . . . . .	24
2.4.3 Hybrid Approach for EV Energy Consumption Rate Estimation . . . . .	25
2.5 Experimental Setup and Results . . . . .	27
2.5.1 Variable Selection and Model Calibration . . . . .	27
2.5.2 Metrics for Model Accuracy Evaluation . . . . .	30
2.5.3 Comparative Results and Discussion . . . . .	30
2.6 Summary and Discussion . . . . .	31
<b>3 Prediction-based Eco-Approach and Departure at Signalized Intersections</b>	<b>33</b>
3.1 Introduction . . . . .	34
3.2 Background . . . . .	35
3.2.1 Existing Eco-Approach and Departure Applications . . . . .	35
3.2.2 State-of-the-art Approaches for Vehicle Movement Prediction . . . . .	37

3.3	Short-Term Vehicle Speed Trajectory Prediction . . . . .	39
3.3.1	Learning-based Vehicle Speed Forecasting Models . . . . .	39
3.3.2	Data Descriptions . . . . .	41
3.3.3	RBF Model Architecture and Calibration . . . . .	42
3.3.4	Evaluating the Performance of Vehicle Speed Forecasting Models . . . . .	44
3.3.5	Summary . . . . .	46
3.4	Enhanced Trajectory Planning Algorithm (EVTPA) with the Consideration of Preceding Traffic . . . . .	48
3.4.1	System Architecture . . . . .	48
3.4.2	Formulation of the Enhanced Trajectory Planning Algorithm (EVTPA) Model . . . . .	49
3.4.3	Validation of the Trajectory Planning Algorithm with Traffic . . . . .	55
3.5	Summary and Discussion . . . . .	60
<b>4</b>	<b>An Advanced Simulation Study of an Integrated Vehicle-Powertrain Eco-Operation System for Electric Buses</b>	<b>61</b>
4.1	Introduction . . . . .	62
4.2	System Framework . . . . .	64
4.3	Simulation Study . . . . .	67
4.3.1	Simulation Tools . . . . .	67
4.3.2	Simulation Network Model . . . . .	68
4.3.3	Simulation Scenarios . . . . .	69
4.4	Powertrain Model for EVs . . . . .	70
4.5	Dynamic Queue Prediction . . . . .	72
4.5.1	Queue Location and Time Forecasting . . . . .	72
4.5.2	Methodology Overview . . . . .	76
4.5.3	Numerical Experiments . . . . .	82
4.6	Simulation Evaluation and Analysis . . . . .	85
4.6.1	Calibration Results . . . . .	85
4.6.2	Energy Consumption Evaluation . . . . .	87
4.6.3	Mobility Analysis . . . . .	87
4.6.4	Improvements . . . . .	88
4.7	Summary and Discussion . . . . .	89
<b>5</b>	<b>Anomaly Detection in Traffic with Partial Connectivity</b>	<b>90</b>
5.1	Introduction . . . . .	91
5.2	Framework . . . . .	93
5.3	Lane Hazard Prediction Model . . . . .	94
5.4	Lateral Driver Response Model . . . . .	97
5.5	Prediction Evaluation and Simulation Setup . . . . .	97
5.5.1	Lane Hazard Prediction Evaluation . . . . .	97
5.5.2	Simulation Tools . . . . .	98
5.5.3	Simulation Network Model . . . . .	99
5.5.4	Simulation Scenarios . . . . .	100
5.6	Results and Discussion . . . . .	101
5.6.1	Prediction Performance . . . . .	101

5.6.2	Mobility Performance . . . . .	103
5.6.3	Safety Performance . . . . .	104
5.7	Summary and Conclusions . . . . .	106
<b>6</b>	<b>Bi-Level Optimal Edge Computing Model in Connected Vehicle Environment</b>	<b>107</b>
6.1	Background . . . . .	108
6.2	System Framework . . . . .	109
6.3	Optimal Vehicle Merge Scheduling by Edge Computing . . . . .	111
6.4	Optimal Vehicle Trajectory Planning . . . . .	114
6.4.1	Heuristic Vehicle Trajectory Planning . . . . .	115
6.4.2	QP-Based Optimal Trajectory Planning . . . . .	118
6.4.3	Graph-Based Optimal Trajectory Planning . . . . .	120
6.5	Experiment Setup and Test Scenario . . . . .	122
6.5.1	Simulation Setup . . . . .	122
6.5.2	Energy Consumption Model and Evaluation Metrics . . . . .	123
6.6	Experimental Results and Performance Comparison . . . . .	124
6.6.1	Simulation Validation of the Proposed MILP-based Optimal Scheduling . . . . .	125
6.6.2	Simulation Validation of the Proposed Vehicle Trajectory Planner . . . . .	126
6.7	Summary and Discussion . . . . .	127
<b>7</b>	<b>Conclusions and Future Work</b>	<b>128</b>
7.1	Conclusions . . . . .	128
7.2	Selected Paper and Patent Coverage . . . . .	131
7.3	Future Work . . . . .	133

# List of Figures

1.1	Total Green House Gas (GHG) emission in California by sector 2016 [1]	2
1.2	Total U.S. Energy consumption by transportation sector 2018 (Source: [2])	2
1.3	Energy consumption by sector, 1949-2018 (Source:[2])	3
1.4	Overview of Connectivity, Automation, and Intelligence, the intersection of three is a potentially better solution	5
1.5	Connected and Automated System Structure	7
2.1	Schematic of EV’s drivetrain [42].	19
2.2	(a) CONSULT III plus kit to collect test vehicle’s energy consumption and other vehicle activities data; and (b) GPS data logger.	20
2.3	One of the field test loops consisting of SR-91 and Magnolia Ave., Riverside, California.	22
2.4	Structure of the fuzzy logic model of regenerative braking factor [45].	25
3.1	Human-machine interface for the EAD system without the predictive model at different traffic conditions: (a) no preceding vehicle, the interface displays the advisory speed, the SPaT information, and the distance to the approaching intersection; (b) with preceding vehicle, only displays the SPaT information and the distance to the approaching intersection, control is handed over to humans.	36
3.2	RBF-based vehicle speed predictor structure.	40
3.3	Vehicle speed forecasting results with 3 second prediction horizon using RBF-NN.	44
3.4	Results of the predicted vehicle speed at different driving scenarios (black line: ground truth; red line: the predicted average speed within a 3-second horizon using RBF-NN; cyan starred line: prediction results from MLP-NN; and dark blue line: prediction results from GP).	47
3.5	Prediction-based EAD system architecture.	48
3.6	Prediction-based EAD system architecture.	51
3.7	The proposed methodology for determining if the preceding vehicle will join the queue at the approaching intersection.	52
3.8	A comparison of different driving strategies.	56
3.9	Impact of the proposed prediciton-based EAD system on vehicle speed distribution.	58

4.1	System framework . . . . .	64
4.2	Simulated network on University Ave with signal control and bus stops. . . . .	68
4.3	Time-distance discretized into cell regions, where each blue line represents a single vehicle trajectory traveling through signalized corridors, and the horizontal red and green line segments indicate the signal phase over time. . . . .	73
4.4	Queue shockwave and vehicle critical points. . . . .	74
4.5	Schematic of proposed forecasting method. . . . .	76
4.6	Detailed view of the forecasted and the observed vehicle states in the queue (red circle: ground truth of the vehicle states joining the queue; green circle: dissipation states of vehicles in the queue; blue star: prediction results of vehicles joining and departing the queue) . . . . .	83
4.7	Queue end forecasting error of a vehicle approaching the intersection . . . . .	84
4.8	Average acceleration and deceleration before and after calibration. . . . .	85
4.9	Comparative results of the VPEO bus and the baseline bus at various traffic conditions including no traffic ( $v/c$ : 0.17), light traffic ( $v/c$ : 0.35), moderate traffic ( $v/c$ : 0.7), and heavy traffic ( $v/c$ : 1.0): (a) the average energy consumption, and (b) the average speed. . . . .	88
5.1	Framework of lane hazard prediction application . . . . .	92
5.2	Illustration of scaling and partitioning on an example network . . . . .	94
5.3	Road network of I-270N in real world and VISSIM. . . . .	99
5.4	ROC curve of LHP under different penetration rates. . . . .	101
5.5	Reaction time of LHP under different penetration rates. . . . .	102
5.6	Sensitivity analysis of penetration rate on mobility benefits: (a) user benefits and (b) system benefits. . . . .	103
5.7	Sensitivity analysis of penetration rate on safety benefits: (a) user benefits and (b) system benefits. . . . .	105
6.1	Flow diagram and framework of bi-level optimal edge computing for on-ramp merging	110
6.2	Heuristic vehicle speed trajectory planning . . . . .	115
6.3	Flow diagram of heuristic vehicle trajectory planner . . . . .	117
6.4	Graph-based optimal trajectory planner illustration . . . . .	120
6.5	Simulation software components and interface block diagram . . . . .	122
6.6	An example of the assigned merge time difference using the MILP-based model and the FIFO-based model . . . . .	124

# List of Tables

2.1	Related work on EV's energy consumption. . . . .	18
2.2	Parameter calibration results of Type I energy consumption rate with the entire dataset. . . . .	28
2.3	Parameter calibration results of Type I energy consumption rate with the split datasets. . . . .	28
2.4	Parameter calibration results of Type II energy consumption rate with the entire dataset. . . . .	29
2.5	Comparison results of forecast accuracy between models. . . . .	31
3.1	Comparative results of vehicle speed forecasting models based on different methods . . . . .	45
3.2	Fuel consumption and pollutant emission comparison evaluation conducted using motor vehicle emission simulator (MOVES Model) . . . . .	59
4.1	Performance of the proposed queue location and time forecasting model . . . . .	82
4.2	Route 14 EB stops along the University Avenue. . . . .	86
4.3	Comparative Results on Energy Savings for VPEO-bus . . . . .	89
5.1	Parameters calibration results of the LHP model . . . . .	96
6.1	Performance comparison between the optimal MILP-Based scheduling model and the FIFO-based approach . . . . .	125
6.2	Fuel consumption and pollutant emission comparison evaluation conducted using motor vehicle emission simulator (MOVES Model) . . . . .	126

# Chapter 1

## Introduction

### 1.1 Background and Problem Statement

Considerable attention is now being applied to new solutions for improving transportation mobility and transportation-related energy consumption and air pollutant emissions due to emerging technology in connectivity and automation in recent years. Our daily transportation activities have not only been consuming a great amount of energy but also producing tailpipe emissions that contribute significantly to climate change and poor air quality. According to the latest report by the California Air Resource Board, surface transportation modes (such as passenger cars, trucks, buses and motorcycles) account for 41% of the total 429.4 MMT CO<sub>2</sub> California greenhouse gas (GHG) emissions in 2016 [1]. Meanwhile, in many areas, vehicle emissions have become the dominant source of air pollutants, including carbon monoxide (CO), volatile organic compounds (VOC), oxides of nitro-

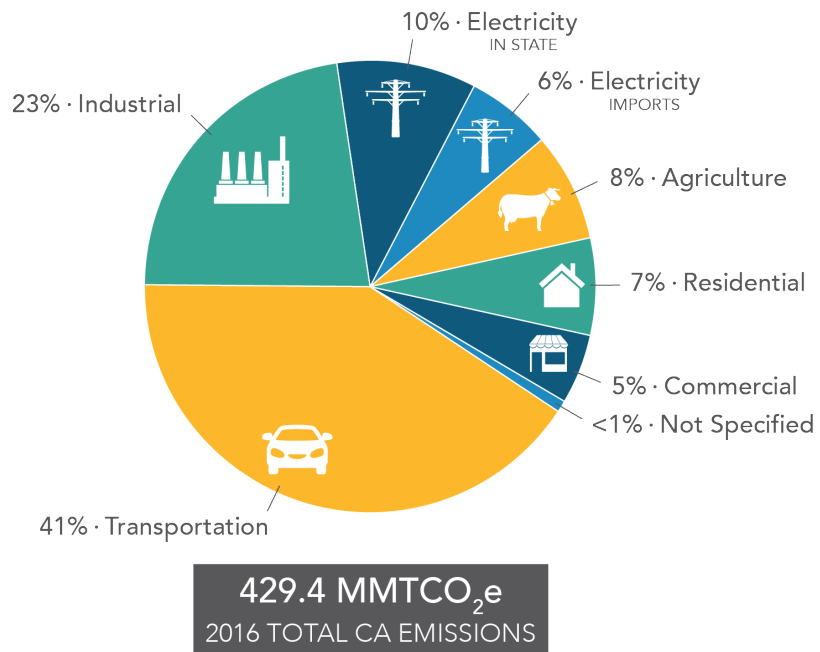
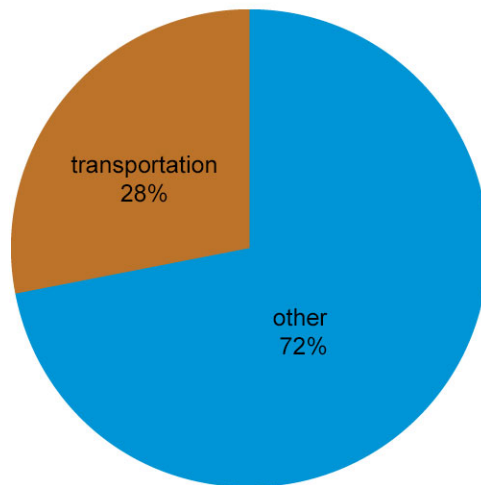


Figure 1.1: Total Green House Gas (GHG) emission in California by sector 2016 [1]

**Share of total U.S. energy used for transportation, 2018**



Source: U.S. Energy Information Administration, *Monthly Energy Review*, Table 2.1, April 2019, preliminary data 

Figure 1.2: Total U.S. Energy consumption by transportation sector 2018 (Source: [2])

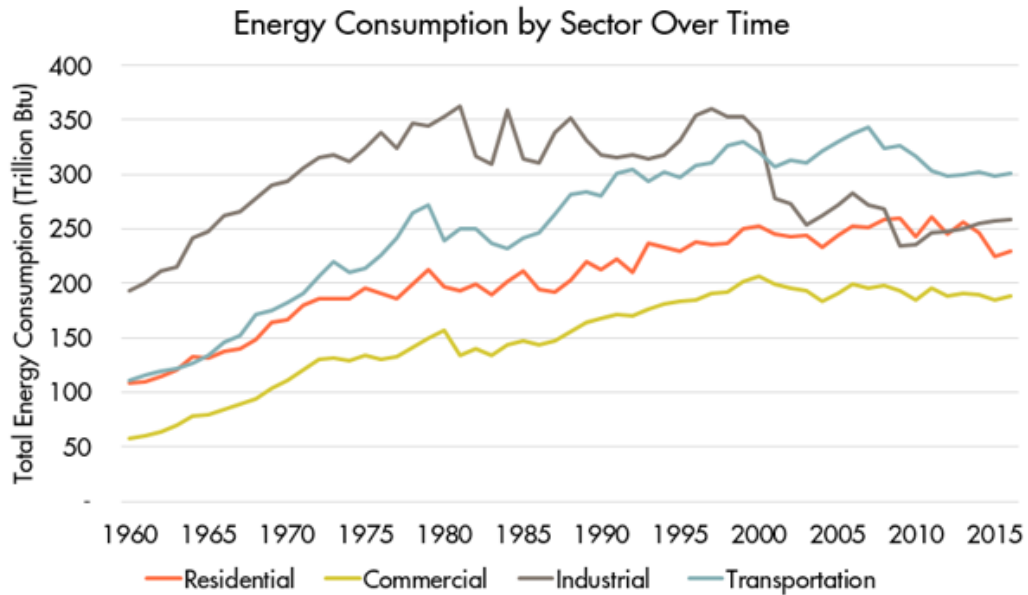


Figure 1.3: Energy consumption by sector, 1949-2018 (Source:[2])

gen ( $\text{NO}_x$ ), particulate matter (PM), and polycyclic aromatic hydrocarbons (PAH). In addition, the Monthly Energy Review from U.S. Energy Information Administration reports that the transportation sector accounts for 28% of the total U.S. energy consumption in 2018 [2]. As shown in Figure 1.3, energy consumption from the transportation sector increased by 200% from 1960 to 2015 and became the biggest source of energy consumption in the U.S. since 2000.

In recent years, many emerging technologies such as connected vehicles (CV), automated driving, transportation electrification, and edge computing have been stimulating increasingly dedicated efforts by engineers, researchers and policymakers to tackle these transportation-related energy and environmental problems. The rapid development in vehicle communication technologies has resulted in a variety of applications that promote energy savings and improved mobility aided by real-time crowdsourcing information shared between connected vehicles and infrastructure. To

enable various safety, mobility and environmental transportation applications, connected vehicle technology is being developed to achieve connectivity between vehicles (V2V), between vehicles and infrastructure (V2I, I2V) through the use of Dedicated Short Range Communication (DSRC) transceivers or cellular systems (e.g. 4G/LTE). DSRC is based on Wi-Fi radio adapted for vehicle communications. A number of messages can be sent in every 10 times/sec and the basic communication range is approximately 300m [3]. DSRC is preferred for connected vehicle safety applications since it is more reliable and has low latency compared to cellular network systems. DSRC might not be the only option when eco-driving algorithms are based on signal information from several upcoming intersections or for network-wide data collection. The basic protocol for obtaining information from a vehicle in a connected vehicle environment is the Basic Safety Message (BSM), which includes vehicle real-time position, speed, acceleration, heading, and many other things. This type of communication is valuable for improving energy efficiency and mobility in urban environments. Good examples were the Applications for the Environment: Real-Time Information Synthesis (AERIS) Program initiated by U.S. Department of Transportation [4], and the eCoMove Project funded by the European Commission [5]. A variety of environmentally-friendly CV applications, in particular those related to eco-driving strategies have been proposed, developed, and validated [6].

In addition, there are significant efforts devoted to developing autonomous vehicles (AVs, also referred to as the automated or self-driving vehicles) targeted for urban driving. AVs are being designed to drive themselves safely and navigate under various road conditions and environmental conditions based on on-board sensors with little driver input. As the pioneer and leading company of AVs, Google's self-driving cars have already driven over 10 million miles on real-world roads

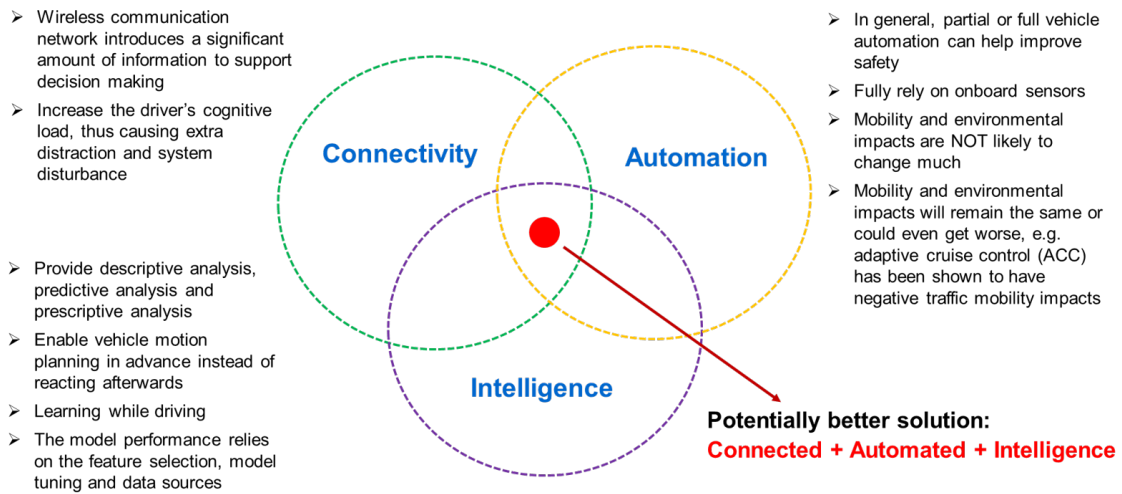


Figure 1.4: Overview of Connectivity, Automation, and Intelligence, the intersection of three is a potentially better solution

since 2009 [7] and numerous manufacturers have began testing their self-driving systems on the road including General Motors, Aptive, Mercedes-Benz, Nissan, Toyota, Volkswagen, etc. AVs fully rely on their observations from on-board sensors and operate in isolation from all the other vehicles and infrastructure. However, there exists some limitation on how far they can operate purely using sensors data. For instance, sensors usually have their its own limitations on detection range and measurement accuracy. Therefore, the current state-of-the-art autonomous driving is focused on safety critical control but do not consider much on mobility, energy efficiency, and environment aspects.

As show in Figure 1.4, combining connectivity, automation and artificial intelligence together can leverage compound benefits from all these technologies. Autonomous vehicles can help improve safety critical control but not so much for mobility and environmental improvement. In fact, studies

has shown the mobility and environmental impact remain the same or even get worse with some partial automation applications such as adaptive cruise control (ACC). Many of the mobility improvements and environment impacts depend not only on automated driving capabilities, but also on crowd-sourcing abilities through vehicle-to-vehicle (V2V) and vehicle-to-infrastructure (V2I) communications. Connected vehicle technology will very likely become standard on most vehicles before large-scale proliferation of AVs made throughout the U.S. vehicle fleet. Further, we are witnessing artificial intelligence as the "game changer" to help autonomous vehicles in object detection, classification, localization, scene understanding and others critical aspects to ensure safe self-driving. Recently, deep learning is expected to play a larger role for autonomous driving, especially in perception levels for complex environment scene understanding and even predictions of other traveler maneuvers. Perceptual predictions using machine learning and deep learning technology can enable vehicle decisions and plannings in advance instead of reacting afterwards which can significantly improve safety, mobility and reduce environment impacts.

The overall pipeline of connected and automated vehicles contains four major levels: Observation, Perception, Planning and Control as shown in Figure 1.5. Observations from onboard sensors are collected and fused to detect and track other travellers. Simultaneously, vehicle location, speed, heading, and signal phase and timing data can be transmitted with very low latency in real-time with nearby connected vehicles and the surrounding infrastructure via wireless communications including V2V, V2I/I2V and V2X. At the perception level, CAVs conduct surrounding object classification, environment/scene interpretation based on the observations from multiple sensors' measurements. Downstream traffic prediction and anomaly detection require longer effective range thus

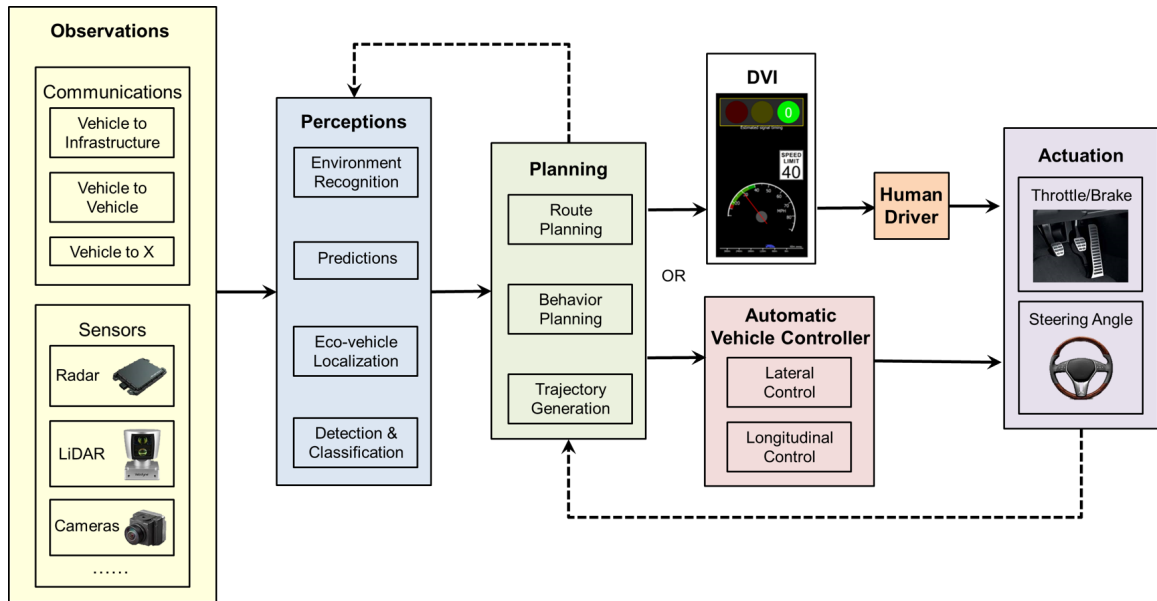


Figure 1.5: Connected and Automated System Structure

it rely on both sensor-based measurement and connected vehicle technologies. With the efficient and reliable estimation, classification, and prediction results, CAVs can regulate route planning, vehicle maneuvers and second-by-second speed trajectory in an optimum way depending on their priority concern. As shown in Figure 1.5, the computed optimal trajectory from the Planning Level is taken as the reference trajectory for the Control algorithms that follow. For the automated vehicle controller, the proper actuation in both longitudinal (i.e. throttle/brake) and lateral level (i.e. steering angle) are carried out based on some well established control schemes like model predictive control or even the simple PID control. For the driver assistant model, the proper Driver-Vehicle-Interface is designed to guide driver to follow a particular reference speed.

## 1.2 Related Work

More and more intriguing research and applications have been established to improve a vehicle's fuel economy and reduce their tail pipe emissions in a connected vehicle environment. For example, in Europe, the Energy Efficiency Intersection (EEI) service of the Compass4D project was implemented to reduce energy use and vehicle emissions at signalized intersections [8]. The eCo-Move project funded by the European Commission (EC) built a cooperative, efficient and ecological transportation system based on vehicle-to-vehicle (V2V) and vehicle-and-infrastructure (V2I/I2V) communication [5]. In the U.S., the Applications for the Environment: Real-Time Information Synthesis (AERIS) program investigated the eco-friendly transportation operations in Connected Vehicle (CV) environment [9].

Among all the programs listed above, eco-driving at signalized intersection is particularly promising for fuel saving and emission reduction in urban area, as drivers would effectively reduce stops and avoid unnecessary acceleration and deceleration by receiving real-time signal phase and timing (SPaT) information from the upcoming traffic signal. Connected eco-driving is also one of the most feasible pilot applications in the early stage of the Connected and Automated Vehicle (CAV) era, as it could show significant fuel economy improvements with a low penetration rate, even for a single vehicle that communicates with a signal controller. In the past decade, a variety of studies have been conducted on developing eco-driving applications, especially from the perspective of an isolated intersection.

Asadi and Vahidi [10] applied traffic signal information to design optimal cruise speeds for probe vehicles to minimize the probability of stopping at signals during red indications. A predictive cruise control system was utilized in this study to calculate a set speed for vehicle to achieve timely arrival at green lights with minimizing the idling time and stops at red lights as well as maintaining safe distance between vehicles. There are some limitation on this study based on their assumption and approach. In their proposed optimization-based control algorithm, instead of solving the optimization problem, the algorithm is simplified to find a proper target speed by some predefined logical rules and use model predictive controller to track this target speed. In this case, the proposed algorithm will provide a sub-optimal constant speed to cruise through signalized intersection. This simplification will have potential benefit in real-time application. Further, in their control algorithm, the signal phase and timing information from all the upcoming intersections are required to compute the proper target speed. However, this information may not be available due to the current limited wireless communication range. Another study conducted by Virginia Tech [11] designed an eco-cooperative adaptive cruise control (ECACC) system to compute the most fuel-efficient vehicle trajectory through a fixed signal intersection. In [12], authors developed a Green Light Optimized Speed Advisory (GLOSA) system whose goal was to minimize average fuel consumption and average stop delay at a traffic signal. By taking into account the queue discharging process, Chen et al. [13] developed an eco-driving algorithm for a vehicle approaching and leaving a signalized intersection to minimize a linear combination of emissions and travel time, without taking into account roadway grade information. Jin et al. [14] formulated a power-based optimal longitudinal connected eco-driving into a Binary Mixed Integer Linear Programming (MILP), which is applicable to signalized intersections, non-signalized intersections or freeways. The approach can take into

account road grade effect and powertrain dynamics, but has relatively low computational efficiency. Huang and Peng [15] adopted a simplified powertrain model and applied the Sequential Convex Optimization approach to optimize vehicle speed trajectory at signalized intersections, which aimed to keep a balance between the optimality and real-time performance.

Eco-Approach and Departure (EAD) was initially developed to address the problem that how to guide drivers to travel through (including to approach and to depart from) signalized intersections in an eco-friendly manner using signal phase and timing (SPaT) information from V2I/I2V communication. When considering the application of EAD system in a more realistic environment, many studies took a "reactive" approach to cope with the disturbance from the downstream traffic (e.g., switching to the car-following mode control if the subject vehicle was too close to its predecessor) or assumed traffic signals were running in fixed-time mode [16, 17]. To address these issues, some researchers specifically focused on tackling the queuing effects when planning the vehicle trajectory for fuel efficient driving [18]. Others dealt with uncertainties in traffic signal operation such as countdown information by improve the prediction of SPaT [19] or developing more robust eco-driving strategies [20].

Simultaneously, there have been rapid advances in machine learning and reinforcement learning techniques which can be used for learning-based approaches for eco-driving applications. Because of the nonlinear feature of traffic dynamics and vehicle behaviors, learning-based approaches can generally achieve better performance.

Modeling and predicting the driving behavior of conventional human-driven vehicles is essential for designing the motion behavior of CAVs in mixed traffic conditions. As the foundation of microscopic traffic models, car-following (CF) logic describes the longitudinal interactions between vehicles assuming there is no lane changing or overtaking. Over the past several decades, a considerable number of car-following models have been proposed and developed [21, 22]. For instance, Gipps model [23], Krauss model [24] and intelligent driver model (IDM) [25] are well-developed to address the speed adjustment according to the principle of collision avoidance between vehicles. A comprehensive comparative study of car-following models used in the state-of-the-art microscopic traffic simulators was conducted in [26]. More recently, to improve the traffic flow stability, an anticipation optimal velocity model (AOVM) was proposed by Peng *et al.* to consider the anticipation effect of optimal velocity [27]. Given that human factors play an essential role in driving behaviors especially under complex traffic conditions, notable efforts have been made to integrate human factors into the conventional CF model in order to achieve more realistic driving behavior [22]. Instead of assuming constant reaction time, Khodayari *et al.* proposed a artificial neural network (ANN) car-following model to estimate the following vehicle's acceleration based on variable reaction delay input [28]. In [29], a number of numerical tests showed that ANNs provide a good approximation of car following dynamics. Comparative studies and evaluation between major car-following models under mixed traffic conditions can be found in [30].

To describe the driving behavior in various traffic situations, some new methods have been proposed that use mathematical models and neural networks, such as Bayesian filtering and Recurrent Neural Network, to predict a driver's intended actions at different traffic scenarios [31, 32]. To in-

investigate the cause of stop-and-go pattern and estimate the vehicle behavior in traffic, Agamennoni *et al.* proposed a recursive Bayesian filtering approach to fulfill that purpose [31]. The problem of multi-agent inference was tackled by decoupling the joint inference to log-linear combinations of individual dependencies. Some other cutting-edge research involved studying the interaction between human driven vehicles and CAVs. To investigate the impact of AVs on traffic flow, the authors in [33] assumed both AVs and human-driven vehicles follow the well-known intelligent driver model (IDM) but with different parameters. Simulation studies on the interaction of a single AV and several human-driven vehicles showed that stabilization can be achieved with a single AV driving at an equilibrium speed [34]. In this work, a second-order car-following model (i.e. optimal-velocity-follow-the leader (OV-FTL) model) was applied to describe the AV and human-driven vehicles' behaviors. It is also demonstrated that by estimating vehicle behaviors and anticipating their future trajectories, more effective coordination between vehicles can be achieved in mixed traffic conditions.

As an essential component of Connected Eco-driving, the prediction of other participants and downstream traffic can be integrated to the vehicle trajectory planning, which is able to further improve the vehicle's energy efficiency, mobility, and safety in real-world traffic. In both urban arterials and highway networks, the interaction between vehicles, and between the vehicle and the infrastructure can improve the overall traffic performance in terms of safety, traffic capacity, and environmental sustainability. In this dissertation, predictive models are developed and integrated with various trajectory planning algorithms using machine learning and optimization techniques, which can promote traffic performance for both the "proactive" energy-efficient driving in a mixed connected

vehicle environment, as well as the group-wide driving strategy ensuring the optimal mobility and energy savings in a fully connected vehicle environment.

### **1.3 Contributions**

This dissertation introduces and develops various energy efficient driving tools (including algorithms and systems), and addresses concrete challenges in mixed traffic and anomaly traffic in connected vehicle environment. The main contributions of this dissertation include:

- Development of innovative electric vehicle energy consumption models using data-driven approach combined with physical concept modeling. These hybrid models can easily be integrated into eco-driving algorithm development with considering the regenerative braking effect. Statistical analyses using the real-world electric vehicle data indicate that the proposed hybrid models outperform both the knowledge-driven model by 89.3%-92.6% and the polynomial regression models by 75.5%-83.2% in terms of forecast accuracy.
- Development of machine learning algorithms to predict preceding vehicle's future trajectory and its future state in the queue at signalized intersections. Comparative study in terms of prediction accuracy and algorithm efficiency was conducted compared to some other commonly used time series prediction models including Gaussian Process and fully connected neural networks. Incorporation of real-time prediction of preceding vehicle's state into vehicle dynamic management (i.e. speed, acceleration) can enable energy efficient driving in real-world traffic and further reduce the energy consumption and emissions by 4%-42% under various driving scenarios.

- An advanced simulation study was conducted with integration of vehicle dynamic and powertrain operation optimization, off-line graph trajectory planning and online deep neural network, dynamic queue prediction model and interaction with real-world environment calibrated vehicular network.
- Develop and simulate an innovative agent-based, lane-level hazard prediction application called Lane Hazard Prediction (LHP) based on partially-available vehicle trajectories data collected from the V2V environment. The results of the research shows the potential for LHP to significantly improve the mobility and safety for both individual LHP users and the entire traffic system.
- A Bi-level Optimal Edge Computing (BOEC) methodology was developed to maximize both the vehicle mobility benefit and energy saving by optimizing the vehicle coordination and motion planning. With optimal scheduling and coordination of CAVs solved by BOEC algorithm, group-wide mobility benefits and energy savings can be achieved with 20.4%-21.2% travel time savings and 63.4%-66.8% energy savings. Another intriguing feature of the BOEC algorithm is the well balance of solution optimality and computational efficiency for online performance.

## **1.4 Organization**

The rest of this dissertation is organized as follows. Chapter 2 describes a hybrid approach to estimate electric vehicle energy consumption that leverages profound benefits from data-driven modeling and physical concept modeling. In Chapter 3, a Prediction-based Eco-Approach and Departure (PEAD) algorithm is developed to compute the optimum speed trajectory in the presence of preced-

ing vehicle and traffic. Machine learning techniques are applied to the snippet of preceding vehicle's trajectory to predict its future maneuvers. This information may help the subject vehicle better plan its trajectory for saving the energy consumption and reducing emissions. Chapter 4 presents an advanced simulation study of an integrated vehicle-powertrain eco-operation system for real-time operations of electric/plug-in hybrid electric buses. The two-layers vehicle dynamic control module consisting of a off-line graph trajectory planning algorithm and online deep neural network is developed to achieve real-time optimal performance. The proposed system can achieve a good balance between solution optimality and computational efficiency while interacting with preceding traffic. Chapter 5 describes a lane-level traffic anomaly detection model and its corresponding driver response model using sparse spatial-temporal vehicle trajectory data from partially connectivity vehicular network. Chapter 6 further develops a bi-level optimal edge computing model for on-ramp merging to maximize overall vehicle mobility benefits and energy saving while optimizing air pollutant emissions. Finally, Chapter 7 concludes the dissertation and presents directions of further work.

## **Chapter 2**

# **Data-Driven Modeling Combined with Physical Concept Modeling of Electric Vehicle Energy Consumption**

In this chapter, we propose a hybrid modeling approach to estimate electric vehicle energy consumption which features knowledge-driven variable selection and data-driven statistical synthesis. The proposed electric vehicle energy consumption model is developed based on real-world driving data which can be easily integrated into eco-driving algorithms and taking into account the regenerative braking effect. We then evaluate the model performance compared to some existing knowledge-based models and polynomial regression models. Results from statistical analysis indicate that our proposed hybrid model outperforms both the knowledge-driven model or the data-driven model in terms of forecast accuracy.

## 2.1 Background

At the heart of transportation electrification, the development of energy consumption estimation models of electric vehicles (EVs) has been an active topic within the realm of EV related research (see, e.g., [35–37]). According to the purpose for use, there are two major types of models: 1) those that estimate the instantaneous energy consumption rate (microscopic) [35, 38–40], which is also the focus of this chapter; and 2) those that estimate the energy consumption (macroscopic/mesoscopic) over unit distance [41]. From the modeling approach perspective, some studies propose knowledge-driven ("white-box") approaches which only rely on first principles (e.g., Newtonian equations) or detailed physical process of each module of an electric vehicle [35, 39, 41]. The others preferred data-driven ("black-box") approaches where the selection of variables does not necessarily take into account their physical meanings [36, 38, 40]. In many cases, the knowledge-driven models may be either too generic at the cost of significant estimation errors, or over-complex, being less attractive in real-time performance. On the other hand, the data-driven models may suffer from unsatisfactory predictability and extensibility since they are very likely to be customized by the features of specific training datasets (e.g., vehicle properties, route characteristics, driver behavior).

Recently, a good deal of effort has been devoted to develop estimation models for electric vehicles' energy consumption [35–42]. Several studies established EV energy consumption estimation models at different granularity for the purpose of eco-routing applications [42], assessment of different aggregation level influence on energy consumption [37] and eco-driving in urban arterials [36]. From the perspective of modeling methodology, the knowledge-driven ("white-box") approach ei-

Table 2.1: Related work on EV’s energy consumption.

	Year	Impact factors	Energy estimation model	Granularity
[35] Yang S.C <i>et al.</i>	2014	speed, acceleration, road grade	Physical/analytical model	Instantaneous
[36] Zhang R., <i>et al.</i>	2015	speed, acceleration, SOC	Polynomial regression	Instantaneous
[37] Baouche F., <i>et al.</i>	2013	average speed	VEHLIB consumption model	Trip-based
[38] Alvarex D., <i>et al.</i>	2014	statistic values of speed, acceleration and jerk	Artificial neural network	Instantaneous
Chang N. <i>et al.</i>	2014	speed, acceleration, road grade, cargo weight	Physical/ analytical model	Instantaneous
[40] Yao E., <i>et al.</i>	2014	speed, acceleration, VSP	Polynomial regression	Instantaneous
[41] Wu X.K., <i>et al.</i>	2015	speed, acceleration, road grade	Physical/analytical model	Instantaneous
[43] Felipe J., <i>et al.</i>	2015	speed, acceleration, jerk and road grade	Artificial neural network	Trip-based

ther considers the vehicle as a point-mass by applying Newton’s Laws (analytical model) or builds up a detailed physical process for each module in an electric vehicle [35, 39, 41]. Such an approach has the advantage of providing a direct link between vehicle or power train dynamics and the variables influential to energy consumption. However, the knowledge-driven models may be too generic without differentiating the powertrain type or overly complex in real-time implementation. For example, Wu *et al.* [41] used real-world measurements and established an instantaneous EV energy consumption model directly derived from the vehicle dynamics. All the parameters in their model are reduced to predetermined constants. In contrast, the data-driven (“black-box”) approach applies statistical techniques [36, 40] or machine learning algorithms [38] to the dataset collected from a vehicle test bed or real world driving. This approach may result in very accurate estimation results based on a customized dataset or a specific scenario. However, the applicability to another situation is questionable. In addition, the physical meanings of selected variables and interpretation of such models are not justifiable. In [40], the author proposed a purely statistical model whose variables include a complete list of combinations of speed and acceleration up to the 3<sup>rd</sup> order. The meaning of some variables is quite vague. Further, the results are validated only with data collected in an ideal environment without considering road grade effects. A summary of the prior works on EV’s energy consumption is provided in Table 2.1.

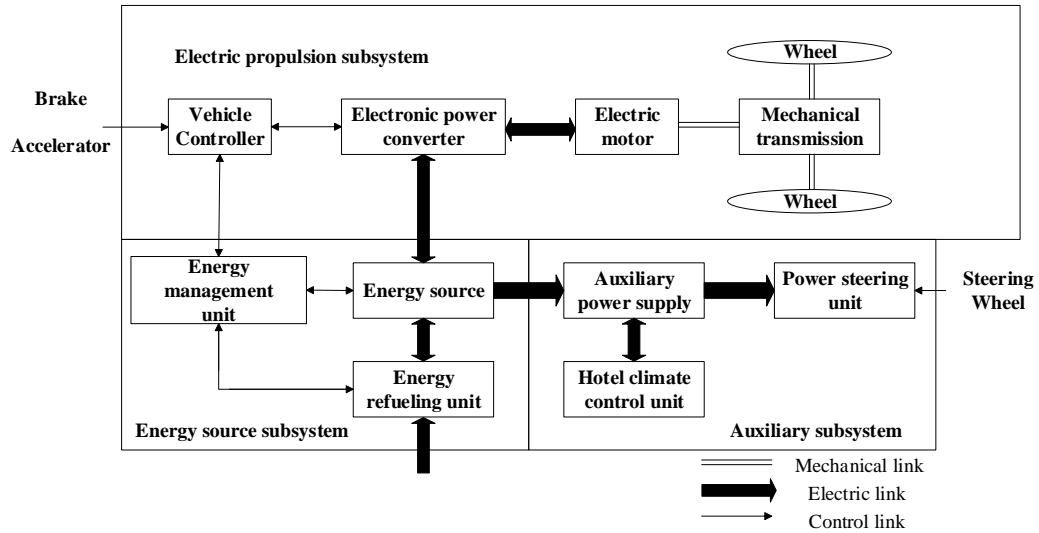


Figure 2.1: Schematic of EV's drivetrain [42].

This chapter describes a hybrid approach ("grey-box") that takes advantage of both knowledge-based and data-driven approaches, by calibrating the parameters in the model which captures the vehicle and powertrain dynamics. The proposed model is then validated using data from real-world driving, and compared with the knowledge-based model established by Wu *et al.* [41] and the data-driven model proposed by Yao *et al.* [40].

## 2.2 Electric Vehicle Drivetrain Configuration

A typical EV drivetrain configuration is conceptually illustrated in Figure 2.1 [42]. There are three major subsystems: electric propulsion subsystem, energy source subsystem and auxiliary subsystem. The vehicle controller sends control signals to an electronic power converter and energy management unit based on the control inputs from brake pedal and accelerator. The electric vehicle delivers power flow to the electronic power converter which is partially used for driving the electric



(a)



(b)

Figure 2.2: (a) CONSULT III plus kit to collect test vehicle's energy consumption and other vehicle activities data; and (b) GPS data logger.

motor and hence the wheels via mechanical transmissions. In the regeneration braking process, the electric motor acts as a generator, produces negative torque on wheels to convert the kinetic energy back into electric power, and restores it in the energy source subsystem. The energy management unit cooperates with the vehicle controller to manage power flows to satisfy the propulsion need and the auxiliary subsystem operation such as power steering, air conditioning, heater and radio.

### 2.3 Real-World Data Acquisition and Processing

In this section, we develop our models for energy consumption rate estimation based on driving data collected from a test electric vehicle (2013 NISSAN LEAF) in real world traffic.

### **2.3.1 Data Acquisition**

The field data collection was conducted during the period between March 2013 and July 2013. The test EV was equipped with two major data acquisition systems: CONSULT III plus kit and GPS data logger (see Figure 2.2), to access vehicle activities (e.g. instantaneous speed), energy related parameters (e.g., battery current and voltage), and real-time location information (i.e., latitude, longitude).

More specifically, the CONSULT III plus kit, which is designated for professional diagnostics of all NISSAN models (including NISSAN LEAF), is able to retrieve high resolution (up to 100 Hz) data from CAN bus, such as speed, current and voltage for each cell, A/C power, accessory power, and state of charge (SOC). On the other hand, the GPS data logger is able to report the latitude and longitude of test EV in real-time. Such information can be synchronized with existing geographic information system (GIS) to acquire the network-wide index and grade information of the road link on which the vehicle is traveling. We selected three typical routes near Riverside, California (USA) for real-world data collection: 1) SR 91 – Magnolia loop; 2) Riverside Plaza – Towngate loop; and 3) Columbia – Alessandro loop. Figure 2.3 presents the SR 91 – Magnolia loop which covers a major freeway (SR 91) and arterial (Magnolia Ave.), and a variety of traffic conditions and road grades. In total, more than 100 hours of vehicle driving data under real-world conditions were collected.

### **2.3.2 Data Processing**

Before the application of the aforementioned field test data for model development, we first combined the dataset from the CONSULT III plus kit with that from the GPS data logger. This data fusion is a two-step process:

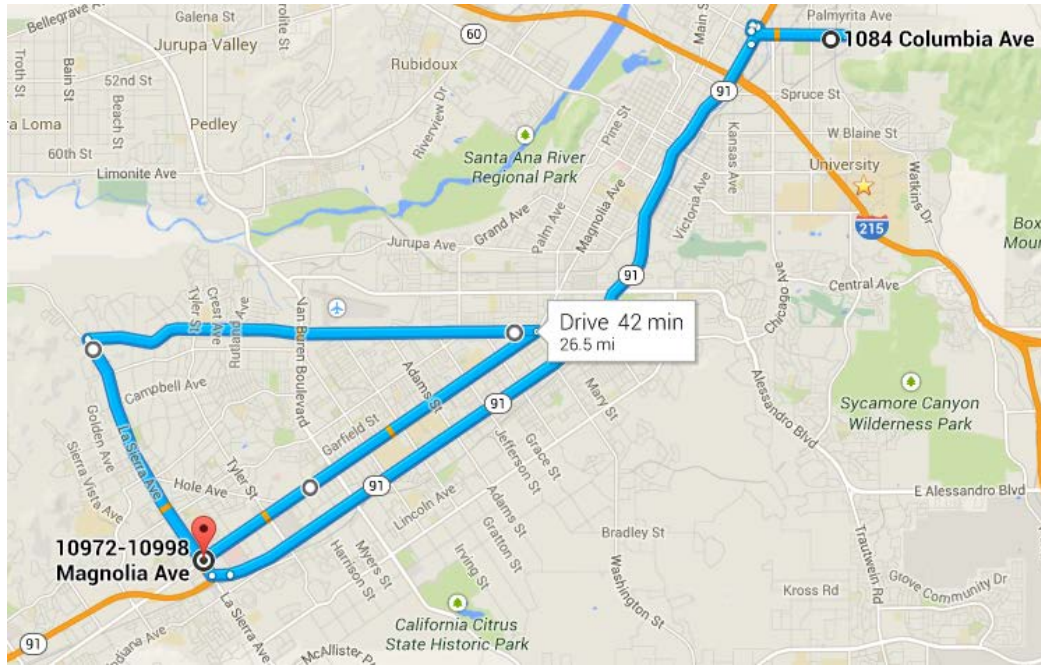


Figure 2.3: One of the field test loops consisting of SR-91 and Magnolia Ave., Riverside, California.

- 1) *Frequency realignment.* The frequency of raw GPS data was realigned into 1 Hz signal which is consistent with the data resolution from the CONSULT III plus kit and suitable for energy consumption estimation;
- 2) *Trip start time synchronization.* Unlike the GPS data logger, the CONSULT III plus kit uses a relative time stamp (i.e. each run always starts from time “0”) instead of a global time clock (i.e. Coordinated Universal Time). In order to synchronize these two datasets, we applied a cross-correlation technique [44] on vehicle speed which is common to both data sources.

## 2.4 Hybrid Modeling Approach

### 2.4.1 Power Flows at the Battery Terminal

The energy consumption of electric vehicle considered in this study is specified as an integration of output power of electric vehicle at the battery terminal. The equations of electric power for propulsion and regenerative braking at battery terminal are as follows [42].

$$P_{b-out} = v[mg(f \cos \alpha + \sin \alpha) + 0.5\rho C_D A_f v^2 + m\delta dv/dt]/\eta_t \eta_m \quad (2.1)$$

$$P_{b-in} = kv\eta_t \eta_m [mg(f \cos \alpha + \sin \alpha) + 0.5\rho C_D A_f v^2 + m\delta dv/dt] \quad (2.2)$$

Here,  $\eta_t$  stand for the transmission efficiency and  $\eta_m$  represents motor drive efficiency. These two parameters are commonly approximately by a constant value.  $m$  is EV's mass;  $f$  is the rolling resistance coefficient;  $g$  is the gravitational constant;  $\rho$  is the air density ( $\text{kg}/\text{m}^3$ );  $C_D$  is the aerodynamic drag coefficient;  $A_f$  is the EV's frontal area;  $\sigma$  is the coefficient that related to the EV's mass;  $v$  is the vehicle's speed (m/s);  $\alpha$  is the road grade (rad);  $k$  ( $0 < k < 1$ ) is the regenerative braking factor which indicates the percentage of the total braking energy that can be recovered by the electric motor. The regenerative braking factor is actually a complex and time-varying coefficient which will be discussed in detail in a later section.

Thus, the total power flows at the battery terminal can be defined as:

$$P_{\text{total}} = P_{b-out} + P_{b-in} \quad (2.3)$$

In the real-world test data, the accessory power and A/C power were also measured which turned out to be non-trivial and was therefore taken into account in the power estimation for the battery terminal.

## **2.4.2 Regenerative Braking Factor**

Regenerative braking power is one of the most distinct feature in electric vehicles that plays an important role in improving drivetrain efficiency. Compared to conventional internal combustion engine (ICE) vehicles, electric vehicles with regenerative braking have an advantage in energy efficiency, especially under stop-and-go driving scenarios. As described earlier, the regenerative braking factor,  $k$ , indicates the percentage of braking energy recovered back to charge the battery pack, implying the vehicle's recharging efficiency. The value of  $k$  is between 0 and 1 due to energy lost from battery internal resistance and cable resistance. Due to the complexity and time varying character of regenerative braking factor  $k$ , it is essential to find proper influential factors in order to model electric vehicles' regenerative braking energy. According to the literature review, there are two major approaches to model the regenerative braking effects: a piecewise linear function of vehicle's speed and a fuzzy logic model considering acceleration, jerk and road grade as input variables [35, 45]. The first approach was derived based on the assumption that the regenerative braking factor can be represented by regenerative braking force which is supposed to be linearly related to vehicle's speed (see Equation (2.4)). The second approach considers a more complex regenerative braking process with the measurement data available for by many factors (e.g., speed, acceleration,

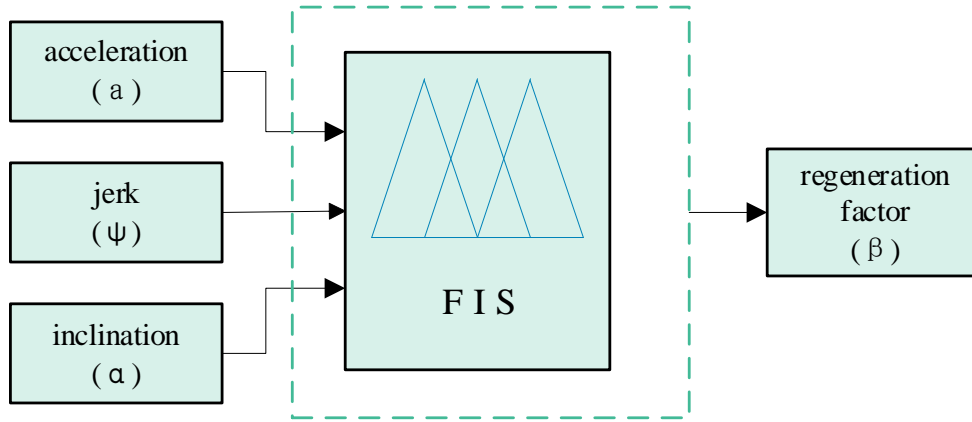


Figure 2.4: Structure of the fuzzy logic model of regenerative braking factor [45].

road grade) as shown in Figure 2.4.

$$k = \begin{cases} 0.5 \times v/5 & v < 5m/s \\ 0.5 + 0.3 \times (v - 5)/20 & v \geq 5m/s \end{cases} \quad (2.4)$$

### 2.4.3 Hybrid Approach for EV Energy Consumption Rate Estimation

In the proposed hybrid approach, the model variables are carefully selected based on the EV's physical model (as described in Section 2.4.1 and Section 2.4.2.) instead of blindly exhausting a long list of variables and their combination [40]. Then, a multi-linear regression (MLR) model is employed to calibrate the corresponding coefficients. On the other hand, the proposed approach excels in real-time performance but is more adaptive to different driving conditions without significantly compromising the model accuracy, when compared to the knowledge-based approach (e.g., [41]). The latter may require a large effort to measure the related parameters and calibrate the coefficients for the electric vehicle in a specific condition.

Based on the battery power equations (Equations (2.1) – (2.3)) and the characteristics of regenerative braking system discussed above, two types of “hybrid” regression models are proposed for EV energy consumption rate estimation. For simplicity, we assume the transmission efficiency  $\eta_t$  and motor efficiency  $\eta_m$  as constants.

A Type I hybrid energy consumption model is formulated as Equation (2.5), which simply considers the regenerative braking factor as a linear function of vehicle’s speed, or  $k \propto v$ . Therefore,

$$P_{est} = l_0 + l_1v \cos(\alpha) + l_2v \sin(\alpha) + l_3v^3 + l_4va + l_5v^2 \cos(\alpha) + l_6v^2 \sin(\alpha) + l_7v^4 + l_8v^2a \quad (2.5)$$

For comparison, we also applied the Type I hybrid energy consumption rate model to the subsets of data partitioned according to Equation (2.4), i.e.,  $v < 5 \text{ m/s}$  and  $v \leq 5 \text{ m/s}$ , and calibrated the coefficients, respectively. But it is noted that further investigation needs to be conducted to evaluate the impacts of the speed threshold.

In the Type II model, we considered the regenerative braking factor being related to not only vehicle’s speed but also other influential factors, including acceleration, road grade and jerk. Based on the fuzzy logic model provided by [46], we estimated the regeneration factor using our field driving data. Further dependency tests showed that jerk may not be a significant indicator. Therefore, the

type II MLR model includes all the variables as shown in Equation (2.6):

$$\begin{aligned}
P_{est} = & l_0 + l_1 v \cos(\alpha) + l_2 v \sin(\alpha) + l_3 v^3 + l_4 va + l_5 v^2 \cos(\alpha) + l_6 v^2 \sin(\alpha) \\
& + l_7 v^4 + l_8 v^2 a + l_9 va \cos(\alpha) + l_{10} va \sin(\alpha) + l_{11} v^3 a + l_{12} va^2 + l_{13} v\alpha \cos(\alpha) \\
& + l_{14} v\alpha \sin(\alpha) + l_{15} v^3 \alpha + l_{16} va\alpha
\end{aligned} \quad (2.6)$$

## 2.5 Experimental Setup and Results

We used the hybrid models proposed in the earlier section (i.e., Equation (2.5) and Equation (2.6)) as initial model and applied R software [47] to further variable selection (both forward and backward), parameter calibration and regression diagnosis. To quantify the predictive accuracy of the proposed models, we adopted the Mean Absolute Scaled Error (MASE) [46] as a metric in this chapter. Then, a comparison of key statistics was conducted between different EV energy consumption rate estimation models, including the proposed hybrid models, a polynomial regression model from Yao *et al.* [40] and a knowledge-based model proposed by Wu *et al.* [41].

### 2.5.1 Variable Selection and Model Calibration

Regression diagnosis tests have been conducted to detect outliers and assumption check including normality, co-linearity and heteroskedasticity. Prior to parameter calibration for the proposed models, both the Akaike Information Criterion (AIC) [48] and Bayes Information Criterion (BIC) [49] are applied to independent variable selection in order to avoid any redundant predictor and eliminate

Table 2.2: Parameter calibration results of Type I energy consumption rate with the entire dataset.

Variables	Type I hybrid energy consumption rate model coefficients	p-value
Intercept	-3.146	$< 2 \times 10^{-16}$
$v \cos(\alpha)$	-0.940	$< 2 \times 10^{-16}$
$v \sin(\alpha)$	-1.237	$< 2 \times 10^{-16}$
$v^3$	-	-
$va$	-1.521	$< 2 \times 10^{-16}$
$v^2 \cos(\alpha)$	$4.104 \times 10^{-2}$	$< 2 \times 10^{-16}$
$v^2 \sin(\alpha)$	$3.289 \times 10^{-2}$	$5.03 \times 10^{-11}$
$v^4$	$-4.4427 \times 10^{-5}$	$< 2 \times 10^{-16}$
$v^2a$	-	-
Adjusted $R^2$	0.677	

Table 2.3: Parameter calibration results of Type I energy consumption rate with the split datasets.

Variables	Type I model coefficients on subset $v < 5$ m/s (p-value)	Type I model coefficients on subset $v \geq 5$ m/s (p-value)
Intercept	-3.287 ( $< 2 \times 10^{-16}$ )	-8.176 ( $< 2 \times 10^{-16}$ )
$v \cos(\alpha)$	-	-
$v \sin(\alpha)$	-	-1.297 ( $< 2 \times 10^{-16}$ )
$v^3$	-0.013 ( $< 2 \times 10^{-16}$ )	-
$va$	-1.817 ( $< 2 \times 10^{-16}$ )	-1.575 ( $< 2 \times 10^{-16}$ )
$v^2 \cos(\alpha)$	-	-
$v^2 \sin(\alpha)$	-0.118 ( $< 1.47 \times 10^{-5}$ )	$3.593 \times 10^{-2}$ ( $1.36 \times 10^{-9}$ )
$v^4$	-	$2.653 \times 10^{-5}$ ( $< 2 \times 10^{-16}$ )
$v^2a$	-	-
Adjusted $R^2$	0.840	0.652

the multi-collinearity effect. The equations for AIC and BIC are presented in the following:

$$AIC = -2 \log(\text{likelihood}) + 2p \quad (2.7)$$

$$BIC = -2 \log(\text{likelihood}) + p \cdot \log(n) \quad (2.8)$$

Table 2.4: Parameter calibration results of Type II energy consumption rate with the entire dataset.

Variables	Type I hybrid energy consumption rate model coefficients	p-value
Intercept	-3.037	$< 2 \times 10^{-16}$
$v \cos(\alpha)$	-0.591	$3.32 \times 10^{-16}$
$v \sin(\alpha)$	–	–
$v^3$	$-1.047 \times 10^{-3}$	$3.32 \times 10^{-16}$
$va$	-1.403	$< 2 \times 10^{-16}$
$v^2 \cos(\alpha)$	$2.831 \times 10^{-2}$	$1.03 \times 10^{-10}$
$v^2 \sin(\alpha)$	–	–
$v^4$	–	–
$v^2a$	$-7.980 \times 10^{-2}$	$1.60 \times 10^{-5}$
$va \cos(\alpha)$	–	–
$va \sin(\alpha)$	-1.490	$1.13 \times 10^{-5}$
$v^3a$	$3.535 \times 10^{-3}$	$5.60 \times 10^{-9}$
$va^2$	-0.243	$< 2 \times 10^{-16}$
$v\alpha \cos(\alpha)$	-1.279	$< 2 \times 10^{-16}$
$v\alpha \sin(\alpha)$	–	–
$v^3\alpha$	$6.484 \times 10^{-4}$	$< 2 \times 10^{-16}$
$va\alpha$	0.998	$4.79 \times 10^{-4}$
Adjusted $R^2$	0.729	

where  $p$  is the model's degrees of freedom;  $n$  is the number of observations. We select those models that minimize these scores.

1) *For Type I hybrid energy consumption rate models:*

As described earlier, there are two forms of Type I hybrid energy consumption rate models developed that regard the regenerative braking factor as a linear function of instantaneous speed, with or without further splitting the dataset based on certain threshold of vehicle's speed (5 m/s in this study). The parameter calibration results for Type I hybrid energy consumption rate models in both forms are summarized in Table 2.2 and Table 2.3, respectively. As can be seen from both tables, the independent variables (including the intercept) after selection are all statistically significant at the significance level of 0.5.

2) *For Type II hybrid energy consumption rate models:*

The methodology of parameter calibration for Type II model is consistent with the one applied to Type I models, and the results are summarized in Table 2.4. Similar to Type I models, all the independent variables after selection are statistically significant (i.e., p-value is smaller than 5%)

### 2.5.2 Metrics for Model Accuracy Evaluation

In order to properly quantify the performance of the proposed energy consumption rate estimation model, the Mean Absolute Scaled Error (MASE) is adopted in this study to measure the forecast accuracy. The MASE was proposed by Hyndaman and Koehlers [46] as a generally applicable relative error measurement without the issues raised by the other measurements, e.g., the Mean Absolute Percentage Error (MAPE). Although MAPE has been widely used in many previous studies, it is not suitable for sample data whose value is close to zero. In this study, however, there are quite a few trivial samples which can be well handled by MASE as shown in Equation (2.9).

$$MASE = \frac{1}{n} \sum_{t=1}^n \left( \frac{|E_t - E'_t|}{\frac{1}{n-1} \sum_{i=2}^n |E_i - E_{i-1}|} \right) \quad (2.9)$$

where  $E_t$  is the measured energy consumption rate;  $E'_t$  is the estimated energy consumption rate; and  $n$  is the number of observations in the real-world data sample.

### 2.5.3 Comparative Results and Discussion

To better understand the performance of the proposed hybrid energy consumption rate estimation models, we select the polynomial regression model based on [40] and the knowledge-based model

Table 2.5: Comparison results of forecast accuracy between models.

Fitted model	Accuracy (MASE)
Type I hybrid energy consumption rate model	2.12
Type I separate hybrid energy consumption rate model on data subsets	1.46
Type II hybrid energy consumption rate model	1.75
Polynomial regression model	8.67
Wu <i>et al.</i> 's model	19.78

introduced by Wu *et al.* [41] for comparison. In order to ensure the consistency in comparison, all the procedures for statistical diagnoses and analyses are identical across different models. Based on the statistical results shown in Table 2.2 thru Table 2.4, the statistical results of our three proposed hybrid models all show better fitness for EV's energy consumption rate estimation in comparison to the pure polynomial regression model and Wu's model. More importantly, all the three proposed models largely improve the forecast accuracy in energy consumption rate estimation compared to other existing models (see Table 2.5). The MASE values of three proposed hybrid energy consumption rate model have 75.5%, 83.2% and 79.8% improvement respectively in forecasting accuracy in comparison to the purely polynomial regression approach proposed by Yao's model. There are 89.3%, 92.6% and 91.2% improvement respectively over Wu's model with the suggested vehicle's parameters values in [41].

## 2.6 Summary and Discussion

In this chapter, we developed a hybrid approach to estimate the energy consumption rate for EVs, which provides variables with actual physical meaning instead of exhaustive method used in conventional data-driven approaches. Compared to knowledge-driven models, the hybrid model needs less calibration and exhibit better real-time performance. The proposed two types of hybrid energy con-

sumption rate models are calibrated and validated with real-world driving data. Statistical analyses show that proposed hybrid models have better goodness of fit. More specifically, our approach can achieve approximately 70 – 80% higher accuracy in terms of MASE than the polynomial regression models with combinations of speed and acceleration up to the 3rd order each. Better performance (around 90% improvement) is witnessed when compared to the knowledge-based model.

## **Chapter 3**

# **Prediction-based Eco-Approach and Departure at Signalized Intersections**

In this chapter, we investigate three approaches for instantaneous vehicle speed prediction in urban intersections. A Prediction-based Eco-Approach and Departure (PEAD) is developed as a velocity advisory system that makes full use of activity information of preceding vehicle. Such information can be acquired via vehicle-to-vehicle (V2V) communication (if the preceding vehicle is a CV), onboard sensors (e.g., radar), or even infrastructure-based assistance (e.g., roadside camera). Using the approaching Signal Phase and Timing (SPaT) information and future states of the preceding vehicle predicted by Radial Basis Function Neural Network (RBF-NN) based forecasting model, the enhanced EAD algorithm provides an eco-friendly speed trajectory in the presence of preceding traffic and queues at intersections. The dataset from the Next Generation SIMulation (NGSIM) program [50] have been applied for model training and system performance evaluation.

### 3.1 Introduction

It is well known that vehicle fuel consumption and emissions are directly related to a vehicle's speed trajectory [16]. Unlike driving on freeways, traffic streams on arterial roads can be interrupted by traffic signals. The frequent stop-and-go maneuvers and associated accelerations in the arterial driving lead to excessive fuel consumption and GHG emissions. Such effects are more prominent when a vehicle approaches an intersection during a red phase and has to decelerate from cruising speed to a full stop, idle to wait for the green phase, and then accelerate to depart from the intersection. Knowledge of SPaT information has been proven to be significantly effective in terms of improving fuel economy for arterial driving [16, 51]. With the recent advances in Connected Vehicle (CV) technology, it is promising to develop advanced driving assistance systems (ADAS) such as EAD application to improve energy efficiency for traveling along signalized intersections. Asadi *et al.* [10] adopted a Model Predictive Control (MPC) approach to obtain a sub-optimal cruise speed to achieve timely arrival at green lights, thus minimizing the idling time and stops at red phase along a signalized corridor. Another study utilized dynamic programming (A-star algorithm) to find the most fuel-efficient speed trajectory through a fixed time control signalized intersection [52]. A multi-stage optimal control approach in [18] adds the estimated queue dissipation time and location at the intersection as constraints. Yang *et al.* [11] developed an ECO-CACC algorithm with considering queue effect to minimize the fuel consumption when vehicles proceed through signalized intersections. In [53], authors incorporated individual driver characteristics into the design of advanced driver assistance system for signalized intersections.

Eco-Approach and Departure (EAD) at signalized intersections was initially developed to take full advantage of signal phase and timing (SPaT) and Geometric Intersection Description (GID) information via wireless communications to provide eco-friendly driving suggestions (e.g., speed profiles) as vehicles approach signalized intersections. A series of EAD applications were designed in recent years for both fixed-time signals and actuated signals [20, 51, 54–56]. However, the aforementioned studies were applied and conducted real world experiments in traffic-free condition. Therefore, when considering the real-world deployment of the EAD application, it is beneficial to further explore the dynamic states from preceding vehicles and incorporate it into trajectory planning process. Forecasting vehicle speed trajectory in urban arterial is a challenge task as the vehicle’s maneuvers may be affected by various dynamic factors, e.g. signal status, traffic, driver’s experience, weather and etc. A number of recent effort has been made to incorporate the vehicle speed prediction to achieve optimal energy management strategy of hybrid electric vehicle [57–59].

## **3.2 Background**

### **3.2.1 Existing Eco-Approach and Departure Applications**

Eco-Approach and Departure (EAD) has been considered as a promising eco-driving strategy for vehicles traveling in an urban environment, where signal phase and timing (SPaT) information is well utilized to guide the vehicles passing through the intersection in a most energy efficient manner. The existing EAD applications have addressed the problem of a single vehicle approaches a fixed-timing signal whose phase sequence and duration are predetermined, and thus the advisory speed trajectory can be deterministically defined with the available SPaT and GID information. The

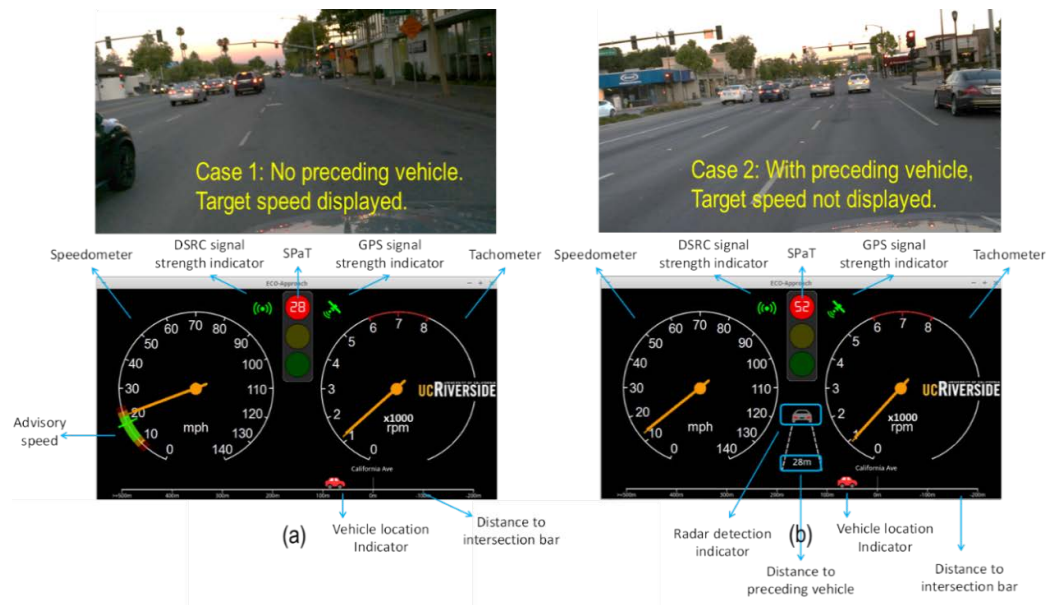


Figure 3.1: Human-machine interface for the EAD system without the predictive model at different traffic conditions: (a) no preceding vehicle, the interface displays the advisory speed, the SPaT information, and the distance to the approaching intersection; (b) with preceding vehicle, only displays the SPaT information and the distance to the approaching intersection, control is handed over to humans.

EAD application for fixed-time signals has shown 10% – 15% reduction on fuel consumption and emissions in microscopic simulation models [51] and 13% – 14% saving from real world testing [54]. An enhanced EAD application has shown satisfactory results for congested urban traffic conditions in a fully connected environment [55]. Extended efforts have been made to develop an EAD application for actuated signals [56]. Most of the existing EAD studies focused on the interaction between the subject vehicle and the traffic signals [20, 54–56]. Those applications work well under light traffic conditions, but are not effective in congested traffic, especially when there are preceding vehicles or queues. Figure 3.1 shows a rule-based strategy to deal with preceding vehicles. When there is no preceding vehicle ahead (within the detection range) in the same lane, the target speed estimated from the EAD algorithm is then displayed on the artificial dashboard. When radar detects a preceding vehicle in the near front, the display of target speed is turned off to avoid any distraction. With such a heuristic strategy, the EAD application may not work effectively in congested urban traffic, especially when there is often a preceding vehicle within the detection range. To address this issue, we need to consider both preceding traffic and signal information in the EAD application development in order to achieve desired system performance even under congested traffic conditions.

### **3.2.2 State-of-the-art Approaches for Vehicle Movement Prediction**

Accurate and reliable prediction of vehicle speed trajectory is an important component in many Intelligent Transportation Systems (ITS) applications, particularly for safety and environmental related applications. It is a challenging task as the vehicle speed trajectory may be affected by various dynamic factors, e.g. signal status, surrounding vehicles' maneuver, and perhaps interruption from pedestrians. In the literature, various approaches for vehicle speed prediction have been investigated and evaluated [60–67]. In general, the existing vehicle speed prediction strategies can be categorized

into two major classes: model-based approaches and data-driven approaches. The model-based approaches predict the vehicle speed trajectory based on pre-defined model structures such as Constant Speed Model (CS), Constant Acceleration Model (CA), Constant Yaw Rate and Acceleration Model (CYRA) [60]. However, the underlying dynamics of human cognition, decision making and execution of drivers and vehicle systems are extremely complex and these simplified models may not be applicable [61]. On the other hand, data-driven approaches have recently been well investigated since they show more flexibility and applicability in representing system dynamics. Good examples of effective data-driven approaches for vehicle speed trajectory prediction include Non-Parametric Regression (NPR), Gaussian Mixture Regression (GMR) and Artificial Neural Networks (ANNs) [62–65]. In [63], the defined maneuver recognition algorithm selected the best vehicle trajectory that minimizing a cost function by comparing the current maneuver to the pre-defined trajectory set in the highways. Considering the requirement for large sampled vehicle trajectories and complexity of maneuver recognition in urban areas, it is challenging to apply it in the real world urban traffic. Gaussian Mixture Regression (GMR) is another promising parametric method to approximate or predict vehicle trajectories by calculating a conditional probability density function that consists of a weighted linear combination of Gaussian component densities [64]. Artificial Neural Networks (ANNs) have been proven to be an effective method for accurately forecasting vehicle speed and position, due to their strong capability of capturing the complex and nonlinear dynamics [65–67]. A comparative study of major parametric and non-parametric approaches for vehicle speed prediction on highways indicates that ANNs outperform all the other methods in terms of both predictive accuracy and applicability [65].

### **3.3 Short-Term Vehicle Speed Trajectory Prediction**

#### **3.3.1 Learning-based Vehicle Speed Forecasting Models**

A reliable and accurate prediction on preceding vehicle's state is essential for efficiently applying EAD strategy in congested urban traffic conditions. As aforementioned, a number of studies have evaluated various time series prediction approaches for predicting segment/link-level vehicles' speeds or under the highway scenarios. However, to the best of our knowledge, none of them have discussed the prediction performance for microscopic urban driving. The real time prediction of vehicle second-by-second speed trajectory along the signalized corridors is much more challenging due to the various disturbances from signals, traffic queues and pedestrians. Other than the vehicle speed prediction at a macroscopic level using traffic condition, historical traffic data as inputs which are usually not applicable for real time implementation, we aim at developing a direct time series forecasting model with vehicle second-by-second speed trajectory detected by onboard sensor (i.e. radar) as inputs. The historical speed horizon of the input and forecasting horizon of the output are both three time steps (i.e., 3 seconds) for training and testing the speed forecasting models. In this study, we implement a Radial Basis Function Neural Network (RBF-NN) [68] for vehicle speed forecasting and compare its performance with other well-known nonlinear regression models like Gaussian Processes (GP) and Multi-Layer Perceptron Neural Network (MLP-NN) for different driving scenarios. The general RBF-NN based vehicle speed predictor has a feed-forward neural network framework with one hidden layer in which the nodes have radial transfer function as shown in Figure 3.2. The network input is a vector containing the preceding vehicle's historical speed trajectory of last 3 seconds, and the output is predicted speed trajectory within a 3-second horizon.

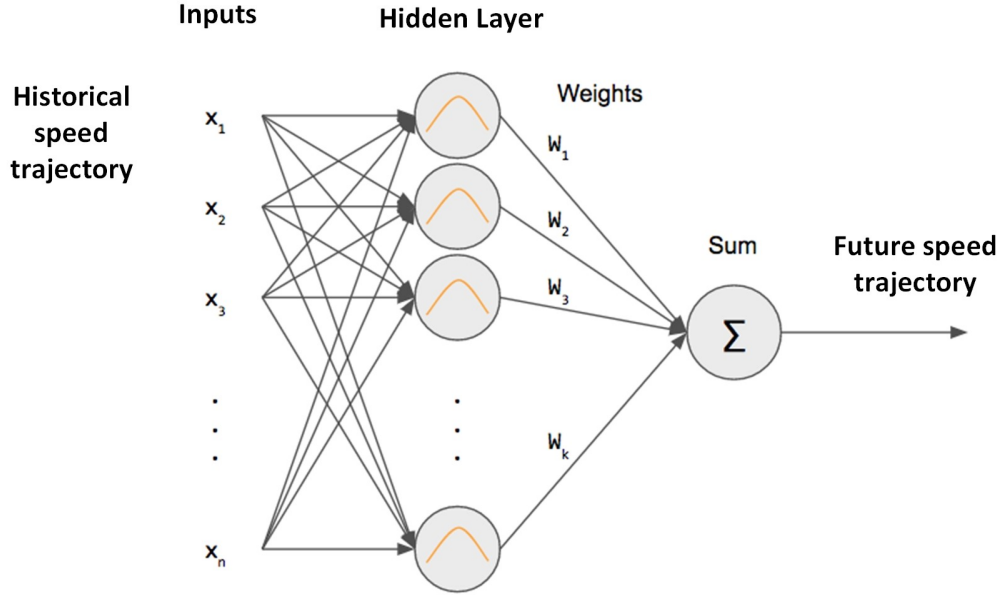


Figure 3.2: RBF-based vehicle speed predictor structure.

The implemented RBF-NN is a three-layer feed-forward networks with  $K$  hidden nodes. A radial basis function needs to be pre-defined for each hidden node to activate neurons in the hidden layer. Here, we apply Gaussian function as the activation function for the RBF-NN, formulated as:

$$\varphi_j(x) = \exp \left[ -(\bar{x} - \mu_j)^T \Sigma_j^{-1} (\bar{x} - \mu_j) \right] \quad (3.1)$$

$$y_k(x) = \sum_{j=1}^M w_{kj} \varphi_j(x) + b_{kj} \quad (3.2)$$

where  $\phi(j)$  is the activated function of node  $j$ ;  $\bar{x}$  is the input vector for node  $j$ ;  $w_{kj}$  is the output weights and  $b_{kj}$  is the constant bias;  $\mu_j$  and  $\Sigma_j$  are the mean vector and covariance matrix of the  $j^{th}$  Gaussian function. The mean  $\mu_j$  represents the center and  $\Sigma_j$  indicates the shape of the activation function. Finally, the output of each node at the RBF-NN's output layer is computed as a

linear combination of the outputs of the hidden nodes.

An advantage of RBF neural network compared to Gaussian Process and MLP neural network is that the efficiency on training based on two-stage procedure. The time complexity of training Gaussian Process for prediction are exponential growth with the sample size which is quite an issue when applied to large network in real time. MLP network could have more than one hidden layers and it uses iterative technique and work globally while RBF network has only one hidden layer and is based on non-iterative technique and acts as local approximation. Further, RBF network shows more robustness to adversarial noise and easier generalization compared to MLP neural network. In the first stage of RBF-NN training, the parameters of the basis function are set to model unconditional data density. The centers of our trained RBF network are determined by fitting a Gaussian mixture model with circular covariance using the Expectation-Maximization (EM) algorithm. The second stage of training determines the weights between the hidden layer and the output layer by using Moore-Penrose generalized pseudo-inverse which overcomes many issues in traditional gradient algorithms such as stopping criterion, learning rate, number of epochs and local minima. The structure of RBF-NN is optimized by pruning the network based on 5-fold cross validation in this study. Due to its shorter training time, forecasting accuracy and generalization ability, RBF-NN is our selected approach for real-time vehicle speed forecasting in urban driving.

### **3.3.2 Data Descriptions**

The NGSIM data collected from an arterial segment on Peachtree in Atlanta, Georgia are used for training and testing the vehicle speed forecasting models and evaluating the performance of the proposed Prediction-based EAD system. There are 5 lanes and 4 intersections in the study corridor.

The NGSIM Peachtree dataset includes the spatial and temporal information of all the vehicles as well as the traffic light information of four signalized intersections along the arterial segment from 12:45 p.m. to 1:00 p.m. and 4:00 p.m. to 4:15 p.m. on November 8, 2006 [50]. For data preparation, we randomly selected 70% of the real world data set for training and the rest 30% for testing. The SPaT information is also obtained for each signalized intersection based on the phase start/end time provided in the data. To develop accurate and reliable prediction of vehicle speed trajectory, we extract speed trajectory of each individual vehicle second by second by vehicle ID. Then, we utilized a sliding window to partition the time series dataset into a number of segment pairs with finite lengths. For each pair of segments, one is the past segment and the other is the future segment. This enables us to utilize the historical speed trajectory to predict the future speed trajectory within a pre-defined prediction horizon. The total sample size for training the vehicle speed forecasting model is 9878; and for testing is 4234. In addition, the traffic signal status and distance to the stop-bar jointly impact the driver behavior when approaching a signalized intersection. Therefore, we classify the predicted speed trajectories into three groups based on different driving scenarios. In Scenario 1, the vehicle is approaching the intersection far from the stop-bar with the red signal phase; In Scenario 2, the vehicle is close to the stop-bar but current signal phase is still red; In Scenario 3, vehicle approaching the intersection with green signal phase. The classified vehicle speed trajectories are used for developing and evaluating the vehicle speed forecasting models in each scenario, respectively.

### **3.3.3 RBF Model Architecture and Calibration**

The RBF network comprises a typical three layers: input, hidden and output. Each neuron of the hidden layer represents a kernel or basis function. Here, we apply Gaussian function as the basis

function to account for the non-linearity and the Gaussian function responds only to a small region of the input space where the Gaussian is centered. The key to a successful forecast vehicle speed trajectory based on RBF network is to find suitable centers for each Gaussian function, which is characterized by two parameters: center ( $\mu_j$ ) and peak width ( $\Sigma_j$ ) as shown in Equation (3.1). The output from the  $j^{th}$  Gaussian neuron for an input speed measurement  $x_i$  can be obtained by Equation (3.2). The RBF hidden layer is fully connected to the output layer by the size of the weight coefficient,  $w_{kj}$  and the constant bias  $b_{kj}$ . The weights  $w_{kj}$  are adjusted to minimize the mean square error of the forecasting outputs. There are two sets of parameters (the centers and the widths) in the hidden layer and a set of weights in output layer are adjusted, and the RBF neural network has a guaranteed learning procedure for convergence. The calibrated RBF network consists 15, 10, 15 neurons in hidden layer for each aforementioned driving scenario, respectively. For scenarios I and III, calibrated center is a 15 by 3 matrix, peak width is a vector with length 15, weights of hidden layer is a 15 by 3 matrix and bias is a 3 by 1 vector. For scenario II, calibrated center and weights' dimension are both 10 by 3, peak width is 10 by 1 and bias is 3 by 1. The details of calibrated parameters of the developed RBF-network can be accessed in the supplement material of this chapter.

To generate the short-term forecasting vehicle trajectory, one of the developed RBF networks is called based on the current driving scenario at each time step to provide a 3-sec vehicle future speed trajectory as illustrated in Figure 3.3. The solid black line is an example vehicle trajectory and the colored short lines represent our RBF-based short-term speed forecasting results over time. Figure 3.3 also shows the developed RBF-based vehicle speed forecasting model can provide reliable prediction based on the historical speed profile.

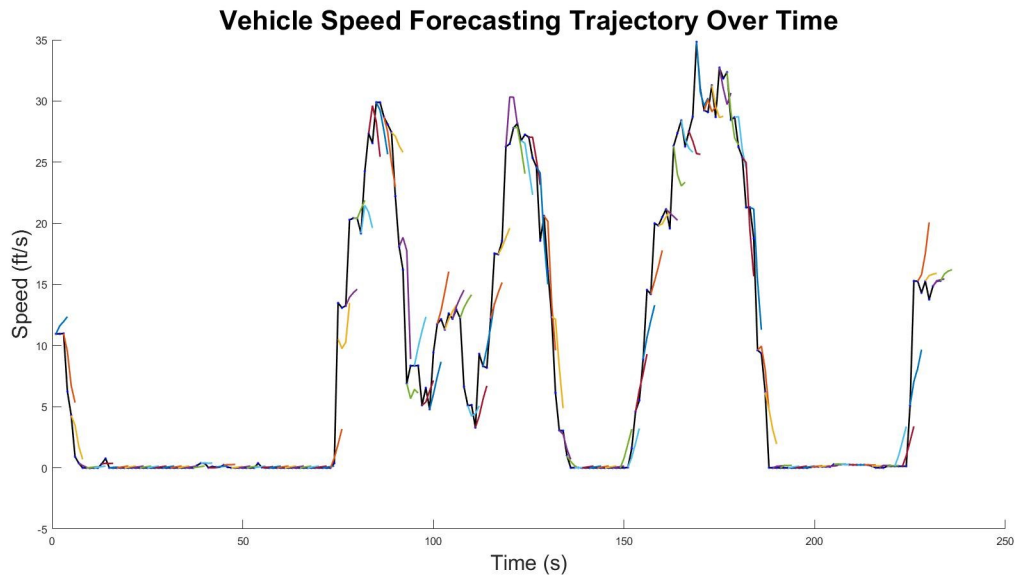


Figure 3.3: Vehicle speed forecasting results with 3 second prediction horizon using RBF-NN.

### 3.3.4 Evaluating the Performance of Vehicle Speed Forecasting Models

The evaluation and comparison of the vehicle speed forecasting models based on three different nonlinear regression methods (RBF network, MLP network, Gaussian Process) are conducted using real world driving data collected in urban traffic (NGSIM Peachtree data). The program was written in MATLAB and evaluated on a computer with i7 CPU @ 2.80GHz and 16 GB memory.

The parameters for nonlinear regression models were selected by  $K$ -fold ( $K = 5$ ) cross validation. For the MLP network, we selected the log-sigmoid function as the nonlinear activation function and trained by a back-propagation algorithm. The optimal network structure of MLP network includes two hidden layers with 20 neurons in the first hidden layers and 10 neurons in the second. The Root Mean Square Error (RMSE) is also adopted in this study to measure the time series forecasting

Table 3.1: Comparative results of vehicle speed forecasting models based on different methods

Performance		RBF-NN	MLP-NN	GP
RMSE (ft/s)	Scenario I	4.3	5.8	5.6
	Scenario II	1.7	3.7	3.2
	Scenario III	4.9	6.1	5.5
Training time (s)	Scenario I	0.03	1.6	0.9
	Scenario II	0.5	2.1	63.5
	Scenario III	0.3	1.7	22.6
Forecasting time cost (s)	Scenario I	1e-4	0.1	0.1
	Scenario II	1e-1	0.03	0.2
	Scenario III	1e-1	0.02	0.2

accuracy, defined as:

$$RMSE = \sqrt{\sum_N (y - \hat{y})^2 / N} \quad (3.3)$$

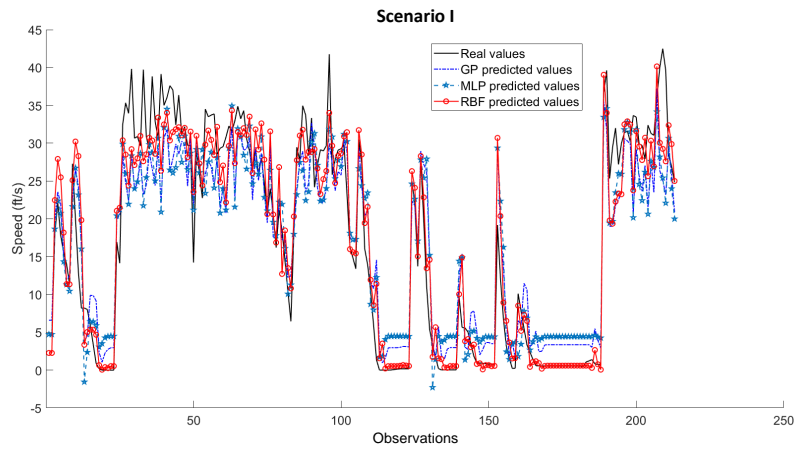
where  $N$  is the number of measurements,  $y$  and  $\hat{y}$  indicate the actual value and predicted value, respectively. A summary of the comparative results of vehicle speed forecasting models based on RBF-NN, MLP-NN and GP can be seen in Table 3.1 in terms of their forecasting accuracy and computational cost for both training and testing. RMSEs of the predicted vehicle speed trajectories based on RBF-NN with respect to the ground truth under three driving scenarios are 4.3 ft/s, 1.7 ft/s and 4.9 ft/s, respectively. For all three driving scenarios, RBF-NN speed forecasting model outperforms the other two approaches: MLP-NN and GP in terms of prediction accuracy. Although in scenario III, RMSE shows that GP and RBF-NN perform similarly well, it is quite time consuming on training a GP based forecasting model for large dataset. It is noted that the time cost for training GP is significantly higher than training MLP-NN or RBF-NN in Scenarios II and III, because it is cubically increased with respect to the size of the measurements. The forecasting speed represents for a given vehicle trajectory, how long it takes the trained vehicle speed forecasting model

to return the predicted results. As shown in Table 3.1, the forecasting time for RBF-NN is about  $10^{-3}$  to  $10^{-4}$  s; for MLP-NN is about  $10^{-1}$  to  $10^{-2}$  s and for GP is about 0.1 s. RBF network has the highest forecasting speed among the three forecasting models which makes it much more promising for real time applications. Therefore, we selected RBF-NN as our forecasting model to predict the preceding vehicle's speed trajectory which is applied to Prediction-based EAD system.

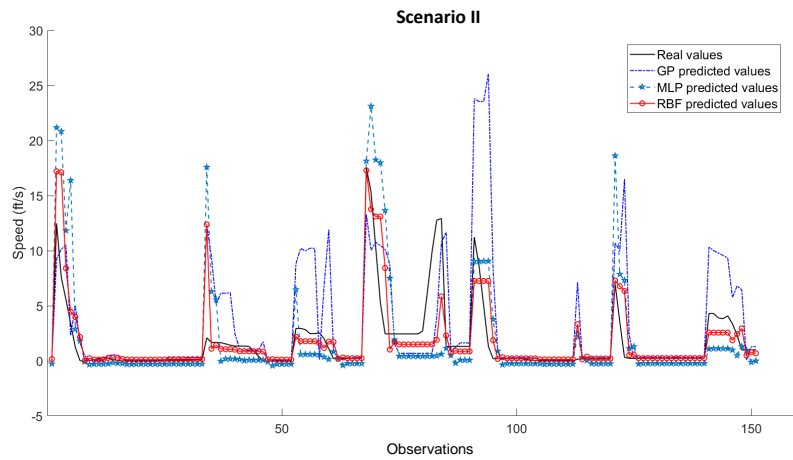
Figure 3.4 illustrates the predicted average speed within the prediction horizon of 3 seconds based on three different forecasting model vs. the ground truth under three driving scenarios, respectively. As shown in Figure 3.4, RBF-NN is able to provide reliable results with satisfactory prediction accuracy for each driving scenarios. Although all three forecasting models: RBF-NN, MLP-NN and GP show similar performance for Scenario III, RBF-NN has much better prediction results for Scenario I and II, compared to MLP-NN and GP.

### **3.3.5 Summary**

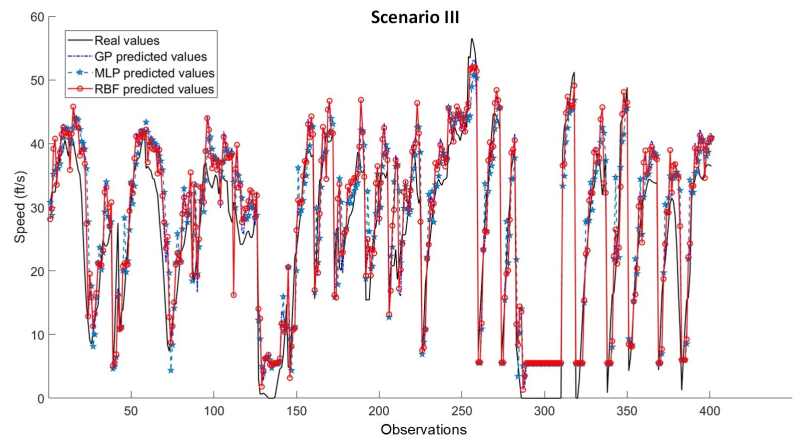
The comparative validation results in of short-term forecasting methods indicate that the proposed RBF-NN model outperforms MLP-NN and GP models in terms of accuracy and computation time for predicting preceding vehicle's speed trajectory under different scenarios. Based on SPaT and GID information as well as predicted states of preceding vehicle.



(a) Scenario 1: Red signal phase; Distance to intersection > threshold



(b) Scenario 2: Red signal phase; Distance to intersection < threshold



(c) Scenario 3: Green signal phase

Figure 3.4: Results of the predicted vehicle speed at different driving scenarios (black line: ground truth; red line: the predicted average speed within a 3-second horizon using RBF-NN; cyan starred line: prediction results from MLP-NN; and dark blue line: prediction results from GP).

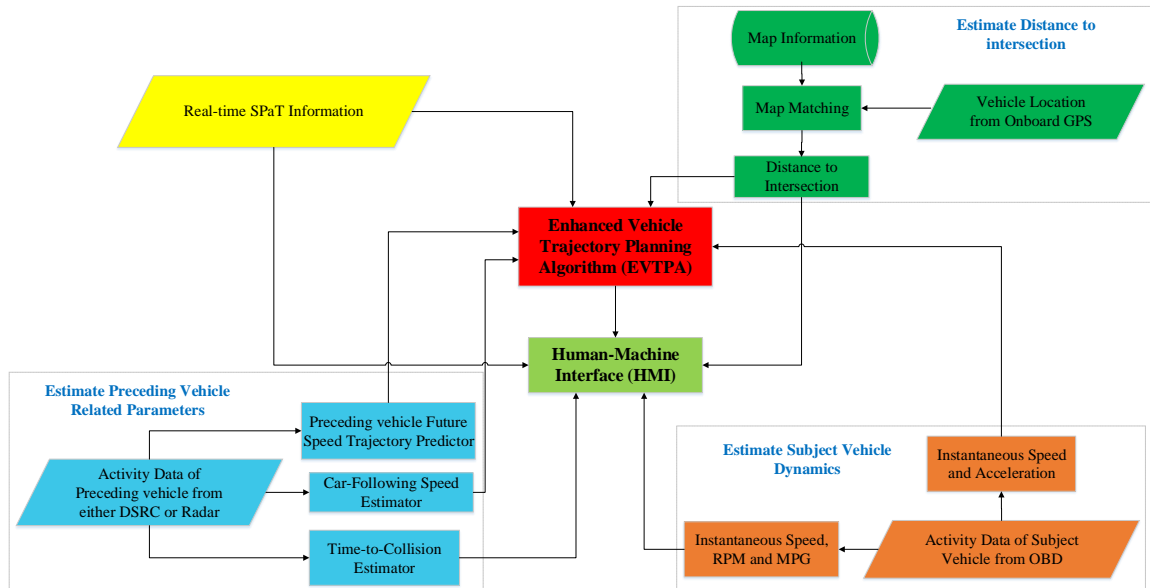


Figure 3.5: Prediction-based EAD system architecture.

### 3.4 Enhanced Trajectory Planning Algorithm (EVTPA) with the Consideration of Preceding Traffic

#### 3.4.1 System Architecture

In this section, our goal is to develop an enhanced EAD application that is applicable in relatively congested urban traffic. The overall architecture of the proposed Prediction-based EAD application is shown in Figure 3.5. The proposed system acquires various information from multiple data resources: SPaT and GID information from DSRC-equipped signal controller at the intersection, subject vehicle dynamics from on-board diagnostics (OBD) port, subject vehicle positions from on-board GPS receiver and activity data of preceding vehicle either from V2V communication if it is an DSRC-equipped vehicle or from on-board radar detection if it is an unequipped vehicle. In order to

get preceding vehicle's second-by-second future states within the prediction horizon, a RBF neural network forecasting model is developed considering its benefits in terms of predictive accuracy, efficiency and applicability for real time implementation. This Enhanced Vehicle Trajectory Planning Algorithm (EVTPA) is able to provide an eco-friendly speed trajectory in both light traffic and relatively congested traffic conditions based on the above acquired information and reliable prediction of preceding vehicle's future states. A Human-Machine Interface (HMI) is designed to inform driver a number of items such as vehicle's current speed, vehicle's revolutions per minute (RPM), SPaT information, vehicle's distance to intersection and the target speed calculated from EVTPA with the consideration of preceding traffic. As we highlighted in the flow chart, incorporation of real-time prediction of preceding vehicle's state into vehicle dynamic management (i.e. speed, acceleration) is the key contributions of this chapter.

### **3.4.2 Formulation of the Enhanced Trajectory Planning Algorithm (EVTPA) Model**

The EVTPA model was developed to address the situation where there exist mixed connected and conventional preceding vehicles. Two situations are considered in designing the desired trajectory for the subject vehicle in terms of both safety and fuel economy. If the vehicle is approaching the intersection during the red phase, the SPaT information and predicted preceding queue end location are utilized to design the optimal trajectory to avoid unnecessary idling and unnecessary acceleration/deceleration. If the preceding vehicle not in a queue or our subject vehicle approaching with a collision risk, we apply Gipps' model [23] as show in Equation (3.4) to conduct safe and

energy-efficient car following mode with smoothed trajectory.

$$v_n(t + \tau) = \min \left\{ \begin{array}{l} v_n(t) + 2.5a_n\tau \left(1 - \frac{v_n(t)}{v_n^d}\right) \sqrt{0.025 + \frac{v_n(t)}{v_n^d}} \\ b_n\tau + \sqrt{b_n^2\tau^2 - b_n [2(x_{n-1}(t) - s_{n-1} - x_n(t)) - v_n(t)\tau - v_{n-1}(t)^2/b]} \end{array} \right\} \quad (3.4)$$

Where  $\tau$  is the reaction time;  $v_n(t)$  and  $v_{n-1}(t)$  are the speed of the following vehicle  $n$  and the leading vehicle  $n - 1$  at time step  $t$ , respectively;  $v_n^d$  is the vehicle  $n$  desired speed;  $a_n$  is the vehicle  $n$ 's maximum acceleration;  $b_n$  and  $b$  are the most severe braking that the driver of vehicle  $n$  wishes to undertake and the expected leading vehicle maximum deceleration, respectively. The proposed EVTPA is illustrated by the overall flow diagram in Figure 3.6. When the proposed EAD system is triggered in relatively congested urban traffic, location of the end of queue with respect to the subject vehicle is estimated based on the predicted preceding vehicle trajectories. A virtual stop line is defined as a buffer space (i.e. length of vehicle) behind the preceding queue end.  $V_P$  and  $V_S$  are preceding vehicle speed and subject equipped vehicle speed, respectively. Further,  $d$  is the distance of the subject vehicle to the stop bar at the signalized intersection. To predict time delay and queue effect on the preceding vehicle, the first thing we need to estimate is whether the vehicle is going to join the queue or not. Figure 3.7 indicates the method we applied to determine whether or not the preceding vehicle will join the queue. The discharge process has been shown to be fairly stable compared to the arriving process. A vehicle's discharge pattern is observed to be close to uniformly distributed, leading to a relative constant discharge rate of the queue. Therefore, a queue dissipation rate  $w$  and vehicle spacing headway  $\Delta h_q$  were calibrated using the collected historical data. Based on the traffic counts  $k$  and the calibrated queue spacing, we could estimate the queue length  $\hat{y}_b$  in

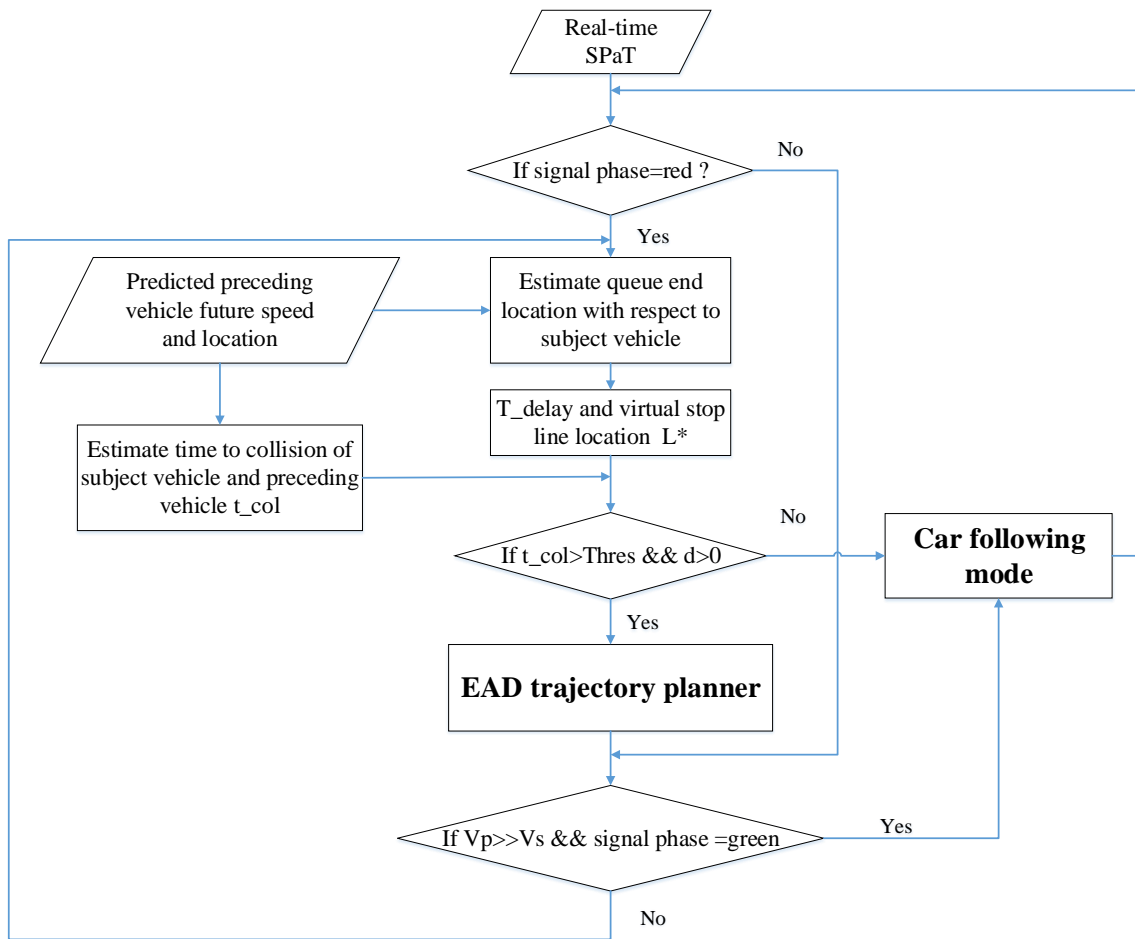


Figure 3.6: Prediction-based EAD system architecture.

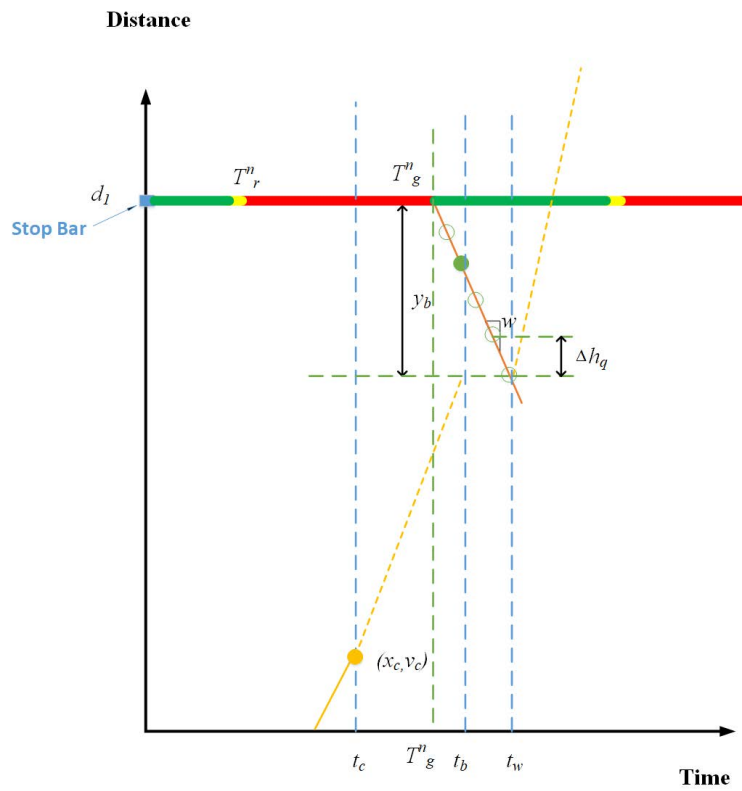


Figure 3.7: The proposed methodology for determining if the preceding vehicle will join the queue at the approaching intersection.

Equation (3.5). The travel time for the preceding vehicle and the dissipation shockwave  $w$  to reach the location could be obtained by Equations (3.6), (3.7), respectively.

$$\hat{y}_b = \mathbf{k} \times \Delta h_q \quad (3.5)$$

$$\bar{v}_{c:c+\Delta T} \cdot (t_b - t_c) = d_1 - x_c - \hat{y}_b \quad (3.6)$$

$$\mathbf{w} \cdot (t_w - T_g^n) = \hat{y}_b \quad (3.7)$$

where  $t_c$  represents the current time step,  $\bar{v}_{c:c+\Delta T}$  is the current average forecasting speed of the preceding vehicle in short time horizon  $\Delta T$ ,  $t_b$  is the time step when preceding vehicle reach the queue end location,  $t_w$  is the time step when dissipation shockwave reaches the queue end location.

As it is shown in Figure 3.7, if  $t_b < t_w$ , which indicates the preceding vehicle reach the queue end before the dissipation shockwave, then the preceding vehicle will be part of the queue in the current cycle. Otherwise, the dissipation shockwave reaches the location before the preceding vehicle indicates the queue will be discharged already at the time when preceding vehicle approaching the intersection. Therefore, we could predict the distance to the virtual stop bar  $L^*$  and  $T_{delay}$  for Prediction-based EAD to avoid preceding queue effect as follows:

$$L^* = x_c + v_c \times \Delta T + \frac{(v_{c+\Delta T} - v_c)}{2} \Delta T + \frac{v_{c+\Delta T}^2}{2d} + L_{\text{buffer}} \quad (3.8)$$

$$T_{\text{delay}} = T_g + \frac{d_1 - L^*}{w} \quad (3.9)$$

where,  $v_c$  is the current speed and  $v_{c+T}$  is the last forecasting speed within the time horizon;  $L_{\text{buffer}}$  is the distance buffer to the preceding queue end considering the physical length of a vehicle plus a safe margin in the car following model;  $d_1$  is the current distance to the actual stop bar.

The EAD trajectory planner takes the time delay ( $T_{\text{delay}}$ ) caused by the preceding queue and distance to the estimated virtual stop line ( $L^*$ ) as the inputs to generate a trajectory that minimizing the fuel consumption and emission. At each time step, the vehicle trajectory planning algorithm also predict the time to collision ( $t_{\text{col}}$ ) based on the preceding vehicle's movement to guarantee safety in the planned maneuver. If the subject vehicle is under the risk of collision in the near future, car following mode will take over to guide the driver through the intersection while keeping safety distance from the preceding vehicle. The transitions between EAD trajectory planner and car following mode enable the proposed EVTPA to maximize fuel savings and environmental benefits without compromising the safety. With the computed virtual stop line and time delay at the signalized intersection, we choose the optimal acceleration and deceleration based on Equations (3.10) – (5.3) that define a trigonometric function of the velocity with constraints of the vehicle traction power, preceding vehicle's states, and riding comfort. The developed EVTPA based on piecewise sinusoidal acceleration/deceleration profiles was proposed to ensure that the subject vehicle ensures that the subject vehicle reaches the virtual stop line after the time delay caused by the preceding vehicle in order to avoid any impact from the downstream queue

$$v = \begin{cases} \frac{v_m + v_c}{2} - \frac{v_m - v_c}{2} \cos(mt) & t \in [0, \frac{\pi}{m}) \\ v_m & t \in [\frac{\pi}{m}, \infty) \end{cases} \quad (3.10)$$

where  $v_c$  is the current speed and  $v_m$  is the speed limit from preceding traffic,  $m$  is the parameter that defines the acceleration and jerk profile. Equation (3.10) generates the proposed sinusoidal speed profile. In this study, the maximum acceleration ( $a_{max}$ ) is  $2.5 \text{ m/s}^2$  and a maximum jerk ( $j_{max}$ ) is  $10 \text{ m/s}^3$ . Then,  $m$  is selected as the maximum value that could meet the driving comfort and safety.

$$m = \min \left( \frac{2a_{max}}{v_m - v_c}, \sqrt{\frac{2j_{max}}{v_m - v_c}} \right) \quad (3.11)$$

The time length of the acceleration period is  $\pi/m$ , i.e., a half cycle. The distance  $d_a$  that the vehicle travels is:

$$d_a = \int_0^{\frac{\pi}{m}} \left[ \frac{v_m + v_c}{2} - \frac{v_m - v_c}{2} \cos(mt) \right] dt = \frac{\pi}{m} \cdot \frac{v_m + v_c}{2} \quad (3.12)$$

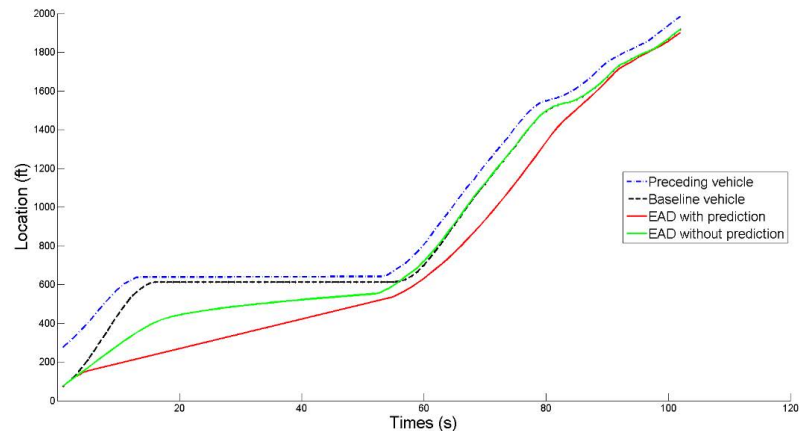
Therefore, the minimum travel time of subject vehicle to reach the virtual stop line (queue end) at the intersection is:

$$t_{min} = \frac{\pi}{m} + \frac{L^* - d_a}{v_m} \quad (3.13)$$

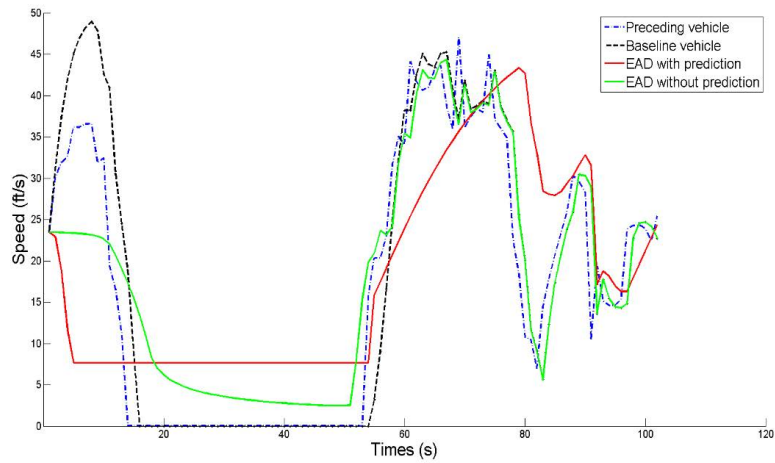
where  $L^*$  is the distance away from the virtual stop line.

### 3.4.3 Validation of the Trajectory Planning Algorithm with Traffic

In this study, we only consider the straight movement through the intersection. In this case, we take all the northbound through movement vehicles in the NGSIM Peachtree dataset as preceding vehicles (185 vehicles in total) after filtering out the trajectories on the side streets. Then, three different types of subject vehicles (baseline vehicle, EAD without prediction vehicle, EAD with prediction vehicle) are simulated as driving behind that preceding vehicle through signalized intersections for further comparison. More specifically, the baseline vehicle is the subject vehicle that is simulated



(a) Time-space trajectories



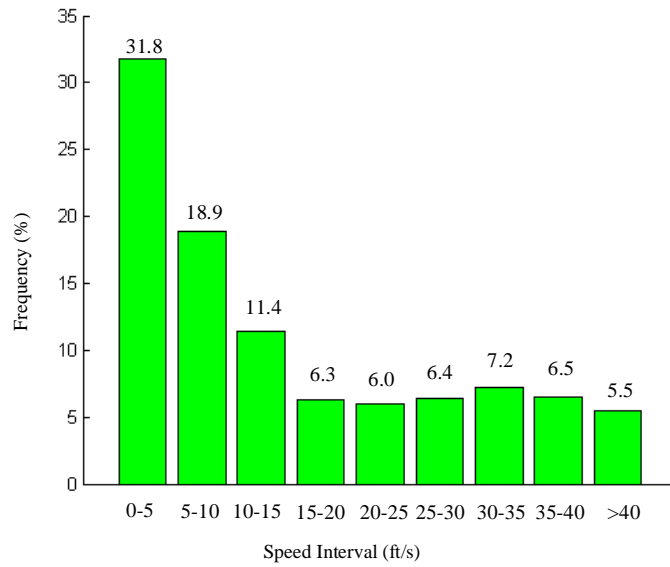
(b) Speed profiles

Figure 3.8: A comparison of different driving strategies.

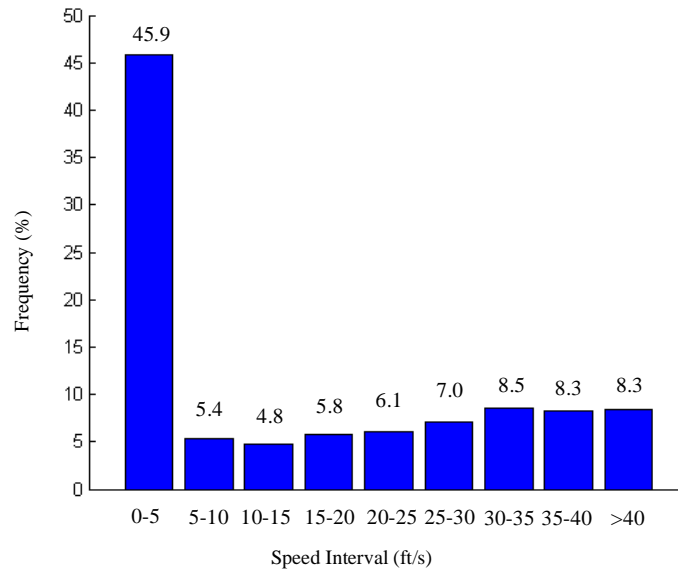
based on the car following strategy (i.e., Gipps's car following model in this study). For the EAD without prediction case, the vehicle switches from EAD to car following state if the relative distance to the preceding vehicle is less than a threshold (i.e., 70 ft) to guarantee safety. The EAD with prediction vehicle is the subject vehicle equipped with the proposed prediction-based EAD system. It is noted that the preceding vehicles' trajectories were generated from real world driving data in NGSIM and were used as the inputs to the proposed prediction method. Figure 3.8 compares the

estimated trajectories and speed profiles from different models in response to the trajectory of an example preceding vehicle. It illustrates how the proposed prediction-based EAD system reduces unnecessary idle time and speed oscillation, while keeping a safe distance from the preceding vehicle when driving through signalized corridors. As shown in Figure 3.8, the EAD system without prediction can reduce unnecessary acceleration and deceleration compared to the baseline when the subject vehicle is far from the preceding. However, without prediction of the preceding vehicle's activity, the subject vehicle may lead to a sudden deceleration to a very low speed (<5 ft/s) or even a full stop due to constraints from the preceding vehicle. In contrast, the prediction-based EAD system can enable the subject vehicle to drive through the signalized intersection in a much smoother maneuver based on the prediction of the preceding vehicle's activity and the queue end. This can significantly reduce the fuel consumption and emissions by avoiding unnecessary idling and further smoothing the speed profile. In Figure 3.9, we summarize the speed distributions of EAD with prediction vehicles and EAD without prediction vehicles over the total 185 test vehicle trajectories. There is a significant drop on the percentage of idling or low-speed (<5 ft/s) scenarios for vehicles with the prediction-based EAD system in Figure 3.9(a) compared to EAD without prediction vehicles in Figure 3.9(b). Meanwhile, the percentage of vehicles driving at high speed (i.e. speed larger than 40 ft/s) is significantly reduced. Those findings imply the proposed prediction-based EAD system is able to further reduce unnecessary idling, accelerations and decelerations even in the congested urban traffic.

To quantify the effectiveness of the proposed EAD system in terms of energy savings and emissions reduction, the U.S. Environmental Protection Agency's MOTO Vehicle Emission Simulator



(a) Speed distribution for EAD with prediction vehicles



(b) Speed distribution for EAD without prediction vehicles

Figure 3.9: Impact of the proposed prediction-based EAD system on vehicle speed distribution.

Table 3.2: Fuel consumption and pollutant emission comparison evaluation conducted using motor vehicle emission simulator (MOVES Model)

Vehicle Trajectory Planning	HC (g/mile)	CO (g/mile)	NO <sub>x</sub> (g/mile)	CO <sub>2</sub> (g/mile)	Energy (KJ/mile)	PM <sub>2.5</sub> (mg/mile)
Baseline Vehicle	0.44	8.08	1.14	689	9586	26.7
EAD without prediction	0.43	7.67	1.06	675	9384	23.3
EAD with prediction	0.41	6.85	0.81	662	9207	15.5
Saving in % (baseline)	5.2%	15.3%	28.3%	4.0%	4.0%	41.7%
Saving in % (EAD without prediction)	3.1%	10.8%	23.3%	1.9%	1.9%	33.4%

(MOVES) model [69] is applied. The MOVES model is the state of art emission simulator developed by the U.S. Environmental Protection Agency (USEPA). The model is designed to estimate energy consumption and emissions for mobile sources on a macroscale, mesoscale or microscale. The second-by-second Vehicle Specific Power (VSP) can firstly be calculated based on the vehicle's speed trajectory and road grade information. Then, the operating mode (OpMode) distribution over 23 bins for running exhaust emissions can be derived from a function of VSP, speed and acceleration values. Finally, with the OpMode distribution, the energy consumption and emissions of all the vehicle trajectories are estimated based on the emission factors from MOVES database. Based on the MOVES model, Table 3.2 shows the energy and environmental benefits of the total 185 vehicle trajectories generated by the proposed prediction-based EAD system, compared to the baseline and EAD without prediction, respectively. Results show that the subject vehicles equipped with proposed prediction-based EAD system has average 4.0% and 1.9% improvement in terms of energy savings with respect to baseline and EAD without prediction, respectively. In addition, significant reduction in air pollutant emissions of the prediction-based EAD-equipped vehicle can be observed from Table 3.2. The emissions of HC, CO, NO<sub>x</sub>, CO<sub>2</sub> and PM<sub>2.5</sub> per mile in the prediction-based EAD equipped vehicles are 5.2%, 15.3%, 28.3%, 4.0%, 4.0% and 41.7% less than the baseline vehicles, respectively. It turns out that the proposed prediction-based EAD system also

reduce of 3.1% HC, 10.8% of CO, 23.3% of NO<sub>x</sub>, 1.9% of CO<sub>2</sub> and 33.4% of PM<sub>2.5</sub> per mile compared to EAD without prediction. The prediction-based method also shows its advantage in safety performance. For the EAD without prediction system, the drivers may need to frequently switch from EAD mode to their own decision. This may lead to long perception/reception time and cause potential sharp braking or even accident. The prediction module would provide a smoother trajectory in the EAD-car following transition and enhance the safety.

### **3.5 Summary and Discussion**

This chapter describes a prediction-based EAD system for real-time implementation that enables the driver to travel through a signalized intersection in a safe and eco-friendly manner in urban traffic. The comparative validation results indicate that the proposed RBF-NN model outperforms MLP-NN and GP models in terms of accuracy and computation time for predicting preceding vehicle's speed trajectory under different scenarios. Based on SPaT and GID information as well as predicted states of preceding vehicle, the proposed EAD algorithm can provide a smooth and energy-efficient trajectory, considering the preceding traffic and possibly queues at intersections. Numerical simulation results show that the proposed system is able to save 4.0% of energy and reduce air pollutant emissions by 4.0% – 41.7% compared to conventional vehicles (simulated by Gipps' car-following model). It turns out that the prediction-based EAD system saves 1.9% energy and reduces 1.9% to 33.4% air pollutant emissions compared to EAD without prediction in congested traffic condition.

## **Chapter 4**

# **An Advanced Simulation Study of an**

# **Integrated Vehicle-Powertrain**

# **Eco-Operation System for Electric Buses**

In this chapter, a complete and novel simulation framework of integrated vehicle/powertrain eco-operation system for electric buses (Eco-bus) is designed and presented with embedded co-optimizing the vehicle dynamics and powertrain (VD&PT) controls. A comprehensive evaluation of the proposed system on mobility benefits and energy savings has been conducted at various traffic conditions. A deep neural network is developed to provide online optimal energy efficient trajectory with high computational efficiency and it can quickly react to dynamic changes in surrounding environment. Further, a dynamic queue prediction model is designed for improving the system performance when exists the downstream traffic. Simulation results are presented to showcase the superiority of the proposed simulation framework of the Eco-bus compared to the baseline

bus which is calibrated using real-world bus dataset, particularly in terms of mobility and energy efficiency aspects.

## **4.1 Introduction**

The advancement towards vehicle connectivity and autonomy offers many potentials and opportunities in developing innovative eco-driving systems and applications to leverage the energy efficiency. Specifically, a very promising example is eco-driving at signalized intersections, where the signal phase and timing (SPaT) information is shared with vehicles to optimize the vehicle dynamics, avoid the unnecessary or abrupt acceleration/deceleration, and reduce the idling period [12, 70, 71]. From a broader perspective, the positive impacts of eco-driving applications can be attributed to the highly predictable location and the high penetration of signalized intersections that may require vehicles to make complete stops.

Within this scope, the energy efficiency of transit buses have large potentials for improvement, as compared to standard passenger cars, since they are initially designed to make much more frequent and predictable stops, such as the loading/unloading of passengers at bus stops. In addition, the bus routes are commonly designed in densely populated areas, which also gives rise to a higher probability of encountering traffic jams. Therefore, a significant amount of energy savings can be anticipated with the connected eco-driving, provided that the operating state of the preceding vehicle can be shared and communicated to effectively optimize the vehicle dynamics. Moreover, electric vehicles (EV) generally have better energy efficiency in the urban areas than the rural areas thanks to the regenerative braking, which slows down the vehicle via an energy recovery mechanism

to convert the kinetic energy back to the electric energy. Therefore, an accurate and robust control of the EV powertrain can maximize the energy restored and further boost the energy efficiency. In this mechanism, the electric motor works in the generator mode to recover energy that would be otherwise lost to the brake discs as heat, and this excessive electric energy is used to recharge the battery pack, making electric vehicles better off in terms of energy efficiency, compared to those with combustion engines in the event of frequent deceleration and stops, such as a traffic jam.

However, early development and deployment of connected eco-driving technology mainly focused on optimizing vehicle dynamics (VD) [15, 17, 72, 73] and powertrain (PT) [74] operation independently, and therefore there exists untapped potential to further improve vehicle fuel efficiency through a simultaneous optimization of both VD&PT control. Therefore, this chapter describes an advanced simulation framework of an integrated vehicle-powertrain eco-operation solution for an electric bus with state-of-the-art Connected and Automated Vehicles (CAV) technologies, aiming at improving vehicle energy efficiency and reducing tailpipe emissions. The overall simulation framework incorporates a two-layer vehicle optimal trajectory planning module that seamlessly integrates a graph-based trajectory planning algorithm and a deep neural network, with the simulation settings and parameters calibrated using real-world electric bus data from Riverside Transit Agency (RTA) bus trajectories. The optimal trajectory can be generated with the proposed innovative VD&PT eco-operation control module embedded in a microscopic simulation tool – PTV VISSIM [75], and its energy-saving performance is validated with different test scenarios against the baseline driving strategies.

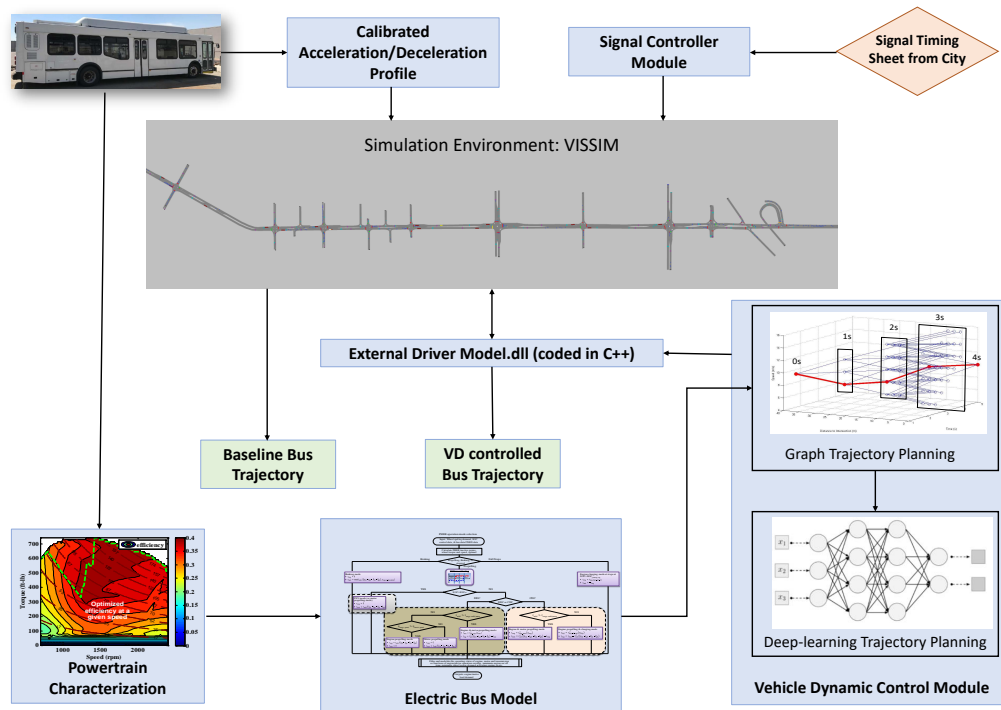


Figure 4.1: System framework

## 4.2 System Framework

Connected and automated vehicles (CAV) have the potential to excel at efficient driving because of their increased situational awareness and ability to execute more complex maneuvers more precisely [74]. In order to comprehensively optimize the operation maneuver of electric buses to improve the fuel efficiency, this chapter describes an advanced electric bus simulation framework integrating vehicle dynamics and powertrain operations. Specifically, this framework is established with real-time optimal trajectory planning under (VD&PT) control interacting with a calibrated environment using real-world data. The overall simulation framework develops traffic network modeling, embedded vehicle dynamic control, and real-world data calibration with PTV VISSIM. In the simulation en-

vironment, a programmable energy-efficient speed trajectory can be generated, optimizing with many parameters and data after the initial calibration process, including signal phase and timing (SPaT) information from upcoming intersections, the state variables of the preceding vehicle, and the vehicle's dynamics in the network. The optimized trajectory is generated with the innovative vehicle-powertrain eco-operation control module that we developed and embedded in a VISSIM application programming interface (API). A desirable energy-efficient speed trajectory through multiple signalized corridors can be optimized with many parameters and data after the calibration process, including the signal phase and timing (SPaT) information of the upcoming intersection, the state variables of the preceding vehicle and the Eco-bus itself in the network, etc. This trajectory is generated with the proposed innovative vehicle-powertrain eco-operation control module embedded in the VISSIM automated program interface (API).

Figure 4.1 illustrates the system framework of the advanced simulation framework for developing the connected Eco-Operation system for electric buses. In this framework, the baseline bus control is based on the embedded car-following logic in VISSIM, and its acceleration and deceleration behavior has been calibrated to match real-world acceleration/deceleration versus speed profiles of RTA bus trajectories. In addition, both the powertrain characteristics and the efficiency map are generated from the real-world testing data. To evaluate the specific energy consumption, a simplified electric bus model with a powertrain-related function of speed, acceleration and road grade is developed and applied to a built-in graph-based trajectory planning algorithm. This integrated mechanism will be used to evaluate the energy consumption of both the baseline bus trajectory and the integrated Eco-Bus trajectory. The simplified electric bus model which is a powertrain-related

function of the speed, acceleration and location-specific road grade is used to compute the energy consumption cost on the built graph of vehicle dynamic state transition.

In addition, a signal control module was developed to implement SPaT messages from signalized intersections along the simulation corridor based on the real-world signal timing sheet obtained from the City of Riverside. In the developed external driver model, the SPaT messages is obtained within the dedicated short-range communications (DSRC) range [3] and decoded into signal phase and countdown information. The vehicle dynamic control module contains a two-layer vehicle optimal trajectory planning: 1) a graph-based trajectory planning algorithm and 2) deep neural networks (DNN) [76]. Specifically, the first layer of trajectory planning algorithm is based on a graph model, which takes the energy consumption as the cost function to optimize the transit path. The second layer employs a DNN to expedite the calculation of the optimal target speed of an Eco-bus for the next time step. Then the output external driver model can effectively reinforce an energy-efficient trajectory for an electric bus. Similarly, this advanced simulation framework is able to generate the optimized output driver model for any user-specified traffic conditions and vehicle powertrain characteristics, which makes this framework very convenient to further evaluate any customized EV eco-operation system interfacing with the traffic network, via this integrated vehicle-powertrain approach.

## **4.3 Simulation Study**

### **4.3.1 Simulation Tools**

In this study, PTV VISSIM [75] is employed as a microscopic traffic simulation tool for traffic network modeling, bus characterization, External Driver Model.dll development with integrated vehicle-powertrain optimal trajectory planning using the VISSIM API, as well as Eco-bus mobility and energy performance evaluation. As a leading-edge microscopic traffic simulator, VISSIM is capable of modeling private transport, commodity transport and road- or rail-bound public transport down to pedestrians, simulating the wireless communication network, and calibrating with real-world data. In addition, VISSIM provides two types of add-on programming interface, namely the Component Object Model (COM) and the External Driver Model DLL. Specifically, COM interface is written in script that can be used to work as an Automation Server, modify the underlying simulation models, access the model outputs, and provide advisory longitudinal and lateral maneuvers. However, limitations exist on directly controlling the driving behavior in the simulation, as well as a high computation load while accessing a large scaled network with many vehicles under control. In this study, we used the External Driver Model DLL Interface of VISSIM to replace the inherent driving behavior model by a fully user-defined behavior embedded in the vehicle dynamic control module.

The External Driver Model DLL Interface of VISSIM is developed to access signal information and sensor measurements, it is also capable of integrating an innovative VD&PT control system to obtain the most energy efficient bus trajectory through multiple signalized intersections. The vehicle

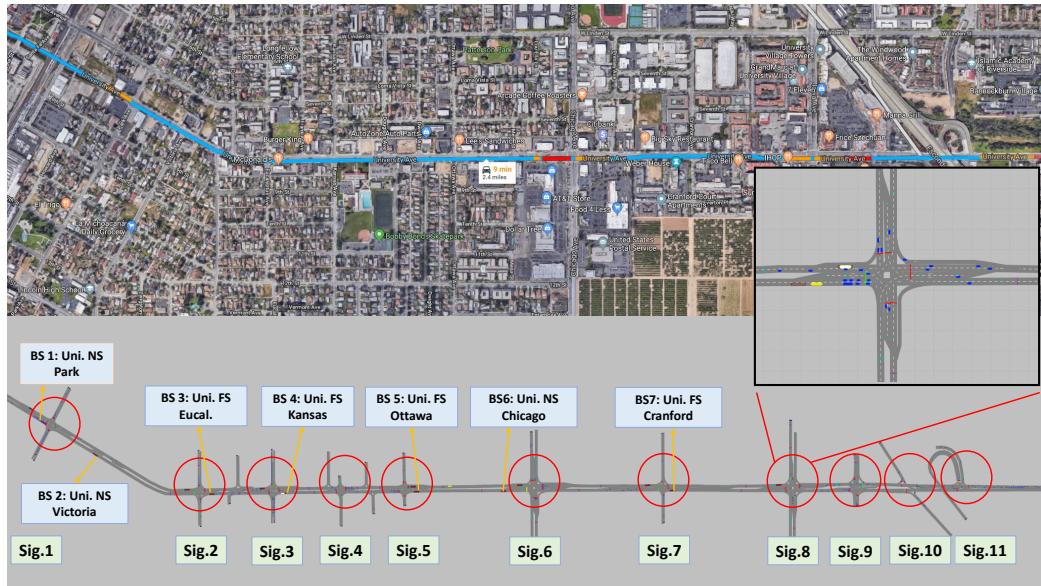


Figure 4.2: Simulated network on University Ave with signal control and bus stops.

dynamic control module, as shown in Figure 4.1, is implemented in a DLL written in C++. During a simulation execution, VISSIM calls the External Driver Model DLL code for the targeted electric bus in each simulation time step, which is able to obtain the current vehicle state, determine its next optimal speed, and then pass this updated vehicle state back to VISSIM.

### 4.3.2 Simulation Network Model

The real-world traffic network used in this study is a 3-mile signalized corridor along University Ave in Riverside, CA with its westbound beginning from the Riverside downtown and its eastbound ending in Canyon Crest Dr, as shown in Figure 4.2. The simulated network consists of eleven signalized intersections and seven bus stops on the eastbound bus route (see Figure 4.2). Based on the real-world signal timing sheets at each intersection from the city of Riverside, we decoded the information to design the Signal Controller with the consistent SPaT message. The transit buses

differ from the private vehicles or heavy-duty trucks in a sense that their trajectories are not only associated with the traffic light and the recurrent congestion, but they also need to comply with the specific bus stop schedule from Riverside Transit Agency (RTA). Therefore, the arrival time is estimated at each bus stop along the RTA bus EB route based on its specific schedule on two main stops. Then, the Public Transport module in VISSIM ID calibrated to match the assigned arrival time at each bus stop along the simulated network. In addition, the bus acceleration/deceleration profile in the simulation is also calibrated using real-world data from RTA bus trajectories. In summary, the network is well calibrated using the real-world signal controls, traffic inputs and bus trajectories data. Therefore, the results and observation from the proposed simulation framework should accurately represent the mobility and energy efficiency performance of an Eco-bus with the integrated VD&PT control.

### **4.3.3 Simulation Scenarios**

To gain an in-depth insight into the integrated vehicle dynamic and powertrain Eco-operation performance, a variety of traffic conditions were simulated under different system settings. Here, we used volume-to-capacity ( $v/c$ ) ratio to quantify the congestion level based on Highway Capacity Manual [77]. The traffic volume with the real-world traffic count is categorized as the Light Traffic condition with  $v/c$  ratio as 0.35. The other three traffic conditions are No Traffic, Moderate Traffic and Heavy Traffic condition with  $v/c$  ratio as 0.17, 0.7 and 1, respectively. Note that for Heavy Traffic case the actual traffic in the network is less than the input traffic demand in the OD matrix, as vehicles may be blocked out of the network at the first intersection due to over-saturation. For each simulation scenario, 10 runs were executed with a simulation duration of 3,600 seconds. All experiments are carried out using a computer with Intel i7 CPU with 2.80 GHz and 16 GB RAM.

## 4.4 Powertrain Model for EVs

In the energy consumption model for the electric bus powertrain, we assume the instantaneous vehicle speed is  $v$  and it is operating under the traction mode, then the motor speed  $\omega$  can be written as

$$\omega = n \cdot v \quad (4.1)$$

where  $n$  is the “lumped” gear ratio calibrated from the real world data.

Considering only a vehicle’s longitudinal motion governed by Newton’s second law of motion [74], the acceleration of the vehicle depends on the traction/brake force, the rolling resistance force impacted by road grade, and the aerodynamic drag

$$ma = F - \left( mg \sin \theta + \mu mg \cos \theta + \frac{1}{2} C_D \rho_a A v_i^2 \right) \quad (4.2)$$

where  $m$  is the vehicle mass ( $kg$ ),  $g$  is the gravity constant,  $\theta$  is the road slope ( $rad$ ),  $\mu$  is the rolling resistance coefficient,  $C_D$  is the aerodynamic drag coefficient,  $\rho_a$  is the air density ( $kg/m^3$ ) and  $A$  is the vehicle frontal area ( $m^2$ ).

The above equation also indicates the critical acceleration rate when the vehicle is coasting (i.e.

$F = 0$ ):

$$a_{coast} = -g \sin \theta - \mu g \cos \theta - \frac{1}{2m} C_D \rho_a A v_i^2 \quad (4.3)$$

When the vehicle is under coasting or braking mode, i.e.  $a \leq a_{coast}$ , we assume the fuel consumption rate is a constant  $Q_i$  which equals to the consumption rate while idling.

When the vehicle is under traction mode  $a > a_{coast}$ , the traction force based on motor torque  $\tau$  (in  $Nm$ ) is formulated as

$$F = \eta\tau n \quad (4.4)$$

where  $\eta$  is the overall efficiency of powertrain. We can derive the torque expression in the steady-state ( $a = 0$ ) in terms of speed and acceleration as:

$$\tau = \frac{1}{\eta n} \left( ma + mg \sin \theta + \mu mg \cos \theta + \frac{1}{2} C_D \rho_a A v^2 \right) \quad (4.5)$$

The energy consumption of the electrical motor can be derived based on the motor speed, torque and motor efficiency map.

As an electric vehicle is capable of converting kinetic energy into electric energy that can recharge the battery during braking, the regenerated braking power is formulated as

$$W_{reg} = \tau v \cdot \eta_{wh} \eta_{fd} \eta_{mot} \eta_{batt} \quad (4.6)$$

where  $\eta_{wh}$  is the wheel drive efficiency,  $\eta_{fd}$  is final drive efficiency,  $\eta_{mot}$  is motor efficiency, and  $\eta_{batt}$  is battery efficiency. The efficiency map is reconstructed from a real-world electric bus data from RTA.

## **4.5 Dynamic Queue Prediction**

### **4.5.1 Queue Location and Time Forecasting**

When driving at signalized arterials, the vehicle's motion trajectory is largely associated with the signal phase and timing but it is also very likely be constrained by its preceding vehicle's movement and the traffic ahead at the intersection, especially in the rush hours. Therefore, a reliable and accurate prediction on preceding vehicle's future state in the sense of both short-term speed profile as well as the its future state of position and time in the preceding queue are crucial for enabling the subject vehicle driving with minimum fuel cost in the real-world urban traffic. Although a number of approaches have been conducted to retrieve the queue length or time delay based on loop detectors or connected vehicle technologies and probe vehicles, it always be operated in a retrieving way. To estimate the queue length or delay of a cycle, they required certain measurements of the queue in that cycle such as queuing propagating and discharge time at the loop detector, the last vehicle in the queue position or the full trajectory of the probe vehicle. However, all these measurements may not be available for the upcoming cycle and these approaches ignore the fact that the subject vehicle and its preceding vehicle may also within the queue. In this sense, a reliable and real time forecast on the location and time of its preceding vehicle joins the queue and departure are critical from the subject vehicle motion planning perspective.

In this section, we introduced a lane-level queue forecasting model of location and time of a vehicle joins and discharge in the queue based on time headway measurements from advanced loop detectors and fitted discharge rate from the historical data. The forecasting accuracy could be largely

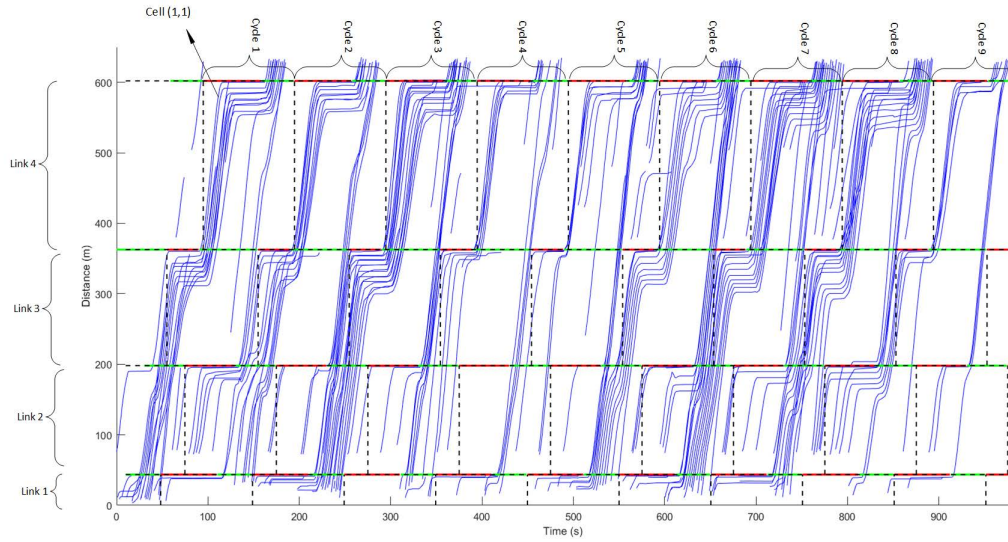


Figure 4.3: Time-distance discretized into cell regions, where each blue line represents a single vehicle trajectory traveling through signalized corridors, and the horizontal red and green line segments indicate the signal phase over time.

improved if there exists connected vehicle trajectory in the cycle which enables real time adjustments. The proposed forecasting model makes no prior assumptions on the uniform vehicle arrivals which is hardly the case for collected approaching trajectories at the signalized intersection from real world.

### Spatial-temporal partition

To develop accurate and reliable prediction of the location and time the vehicle joins the queue at a certain intersection during a single cycle, we need to specify the spatial and temporal region the forecasting model applied. The vehicles trajectories through four consecutive northbound signalized intersections are visualized in Figure 4.3. In this study, we focused on forecasting queue location and time of an approaching vehicle cycle by cycle. Therefore, overall studied spatial and temporal domain can be partitioned into several cell regions as show in Figure 4.3 (i.e. cell  $(i, j)$  represent



time of a vehicle meet the propagating queue (represented as red dots in Figure 4.4 as well as the location and time for that vehicle discharge from the queue (represented as green dots in Figure 4.4 are two critical points to determine the vehicle's approach and departure state at the queue. In this study, we considered a vehicle joining the queue from the moment it decelerates to under a specific idling speed threshold at its approaching process to an intersection. Here, we chose 5 feet/s as aforementioned speed threshold. Therefore, the first time step within the queue and its corresponding location defined as the Type I critical point  $(T_a, y_a)$ , which represents the state of the vehicle in queue at approaching process. The time step  $t_a$  of each individual vehicle is obtained by the following equation:

$$T_a = \min \{t | v_i(t) < v_{idl}, v_i(t - \Delta t) > v_{idl} \& y_a < d_1\} \quad (4.7)$$

Where  $v_i(t)$  is the instantaneous speed of the vehicle  $i$  at the time step  $t$ ,  $v_{idl}$  is the aforementioned idling speed threshold,  $\Delta t$  is the step size,  $y_a$  is the corresponding location at the moment of joining a queue at cycle  $n$ ,  $d_1$  is the location of the stop bar at the approaching intersection.

The Type II critical point of the departure process of a vehicle in the queue is defined as the moment when queue discharge propagating to the vehicle's idling position, represented as  $(T_b, y_b)$ . The time step  $t_b$  is accessible based on the following condition:

$$T_b = \max \{t | v_i(t) < v_{idl}, v_i(t + \Delta t) > v_{idl} \& y_b < d_1\} \quad (4.8)$$

Where  $y_b$  is the corresponding location at the moment vehicle  $i$  discharge from a queue in cycle  $n$ .

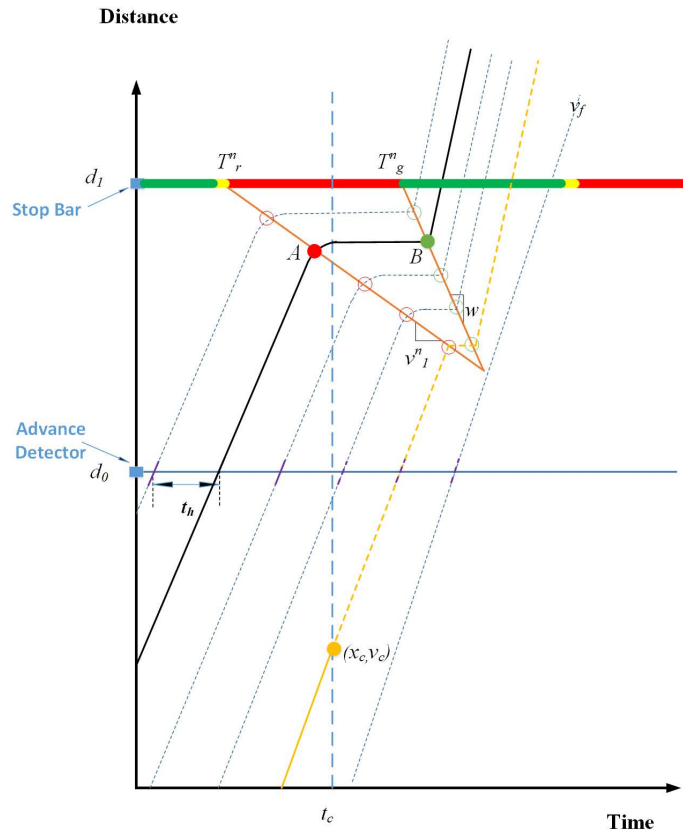


Figure 4.5: Schematic of proposed forecasting method.

## 4.5.2 Methodology Overview

Firstly, we introduced a forecasting model on the location (in terms of distance to the stop bar) and time of a vehicle joining the queue as well as its discharge time based on measurements only from advanced loop detectors and signal phase and timing (SPaT) information of the approaching intersection. As shown in Figure 4.5, the advanced loop detector was placed at the location  $d_0$  to collect the vehicle counts, vehicle instantaneous speed ( $v_0$ ) and the time headways ( $t_h$ ) between vehicles at the loop detector. In this study, we set the advanced loop detector for each lane at the distance 300 feet from the stop bar ( $d_1 - d_0 = 300 \text{ ft} \approx 91.5 \text{ m}$ ).

The formation of our proposed forecasting model is based on Lighthill-Whitham-Richards (LWR) shockwave theory. The shockwave formatting rate for cycle  $n$  is represented as  $v_1^n$  and the shockwave dissipation rate for cycle  $n$  is represented as  $w$ , as it is shown in Figure 4.5.

The discharge process has been shown to be fairly stable compared to the arriving process. Vehicle's discharge pattern is observed to be close to uniformly distributed, leading to a relative constant discharge rate of the queue. Therefore, a queue dissipation rate  $w$  and vehicle spacing headway  $\Delta h_q$  could be calibrated using the collected historical data. Based on the extracted Type II critical points and the start time of the green phase at the current cycle, the shockwave dissipation rate could be calculated based on the following equation:

$$w_n = \frac{(d_j - y_b)}{(T_b - T_g^n)} \quad (4.9)$$

$$\bar{w} = \frac{\sum_{i=1}^n w_i}{n} \quad (4.10)$$

Where  $w_n$  is the shockwave dissipation rate for cycle  $n$ ,  $d_j$  is the location of the stop bar of the intersection  $j$ ,  $y_b$  is the location of the vehicle at the Type II critical point at cycle  $n$ .

Therefore, we could compute the discharge time for a vehicle in the queue as follows:

$$\hat{y}_b = d_j - n \times \Delta h_q \quad (4.11)$$

$$\hat{T}_b = T_g + \frac{d_j - \hat{y}_b}{w} \quad (4.12)$$

We assumed for the current time step, the number of vehicles queuing at the approaching intersection is available. Between vehicle spacing at the queue  $\Delta h_q$  was calibrated using the collected historical data in order to indicate the position of the queue end respect to the subject vehicle.

Since the free flow speed for urban driving is usually much less than on the freeway and it is also very relevant to configuration and location-dependent speed rules. Therefore, we calibrated the free speed  $v_f$  at Peachtree using the trajectories from all the vehicle's traveling from northbound. To predict the trajectory of the preceding vehicle, first thing we need to estimate is whether the vehicle is going to join to queue or not. The strategy is the same as indicated in Figure 3.7 , which we presented earlier in the last chapter. Based on the traffic counts and the calibrated queue spacing, we could estimate the location of the preceding vehicle in the queue  $\hat{y}_b$  according to Equation (4.11). The travel time for the preceding vehicle and the dissipation shockwave  $w$  to reach the location could be obtained by Equations (4.13), (4.14), respectively.

$$v_c \cdot (t_b - t_c) = \hat{y}_b \quad (4.13)$$

$$\mathbf{w} \cdot (t_w - t_c) = \hat{y}_b \quad (4.14)$$

where  $t_c$  represents the current time step,  $v_c$  is the current speed of the preceding vehicle,  $t_b$  is the time step when preceding vehicle reach the queue end location,  $t_w$  is the time step when dissipation shockwave reaches the queue end location.

As it is shown in Figure 3.7, if  $t_b < t_w$ , which indicates the preceding vehicle reach the queue end before the dissipation shockwave, then the preceding vehicle will be part of the queue in the current cycle. Otherwise, the dissipation shockwave reaches the location before the preceding vehicle indicates the queue will be discharged already at the time when preceding vehicle approaching the intersection.

The limitation of the fixed location sensor is that it only provides the aggregate information and temporal information such as vehicle counts, time headways. The lack of spatial information from the measurements may sometimes lead to unsatisfactory performance of the forecasting model. With the recent advent of connected vehicle technologies, a connected vehicle could also serve as a mobile sensor as it provides detailed trajectories at the signalized intersection. Therefore, a precision measurement on critical points of connected vehicle could correct the predicted shockwave rates and time headways, resulting in a reduction in the forecasting error of critical points state for vehicles cycle by cycle in real time.

In Figure 4.5, the connected vehicle's trajectory is represented as solid black lines and the conventional vehicle's trajectory is represented as dashed blue ones. We could extract accurate measurements of the critical points A and B (see Figure 4.5) from the connected vehicles which could correct the shockwave propagation rate and disperse rate and spacing to make better forecasting results. At the situation that there is no input from connected vehicles, we then assumed a constant shockwave speed  $v_1$  which was calculated as based on the average headway from previous cycle and traffic counts so far at the current cycle.

Assume the current time step is  $t_c$  and our subject vehicle is following a preceding vehicle whose trajectory is represented in yellow shown in Figure 4.5. The aim of our proposed forecasting model is to provide a prediction on the Type I and Type II critical points of the preceding vehicle based on the onboard sensor measurements, road side unit measurements and SPaT from I2V communication. The onboard radar sensor could detect the preceding vehicle's speed and location and our developed vehicle speed profile predictor could predict its future movement with the confidential 5 secs time window. Considering the case that the preceding vehicle is approaching a signalized intersection with a distance to the loop detector as shown in Figure 4.5. In Figure 4.5, the yellow line represents the preceding vehicle's trajectory. The solid part is the trajectory detected by the onboard radar sensors. Assume the current time step is  $t_c$  and the current position and speed of the preceding vehicle measured by our onboard radar detection is  $(x_c, v_c)$ . We used the average speed in the prediction window and its distance to the loop detector to forecast its arriving time at the loop detector based on the Equation (4.15).

$$t_l = \frac{d_0 - x_c}{\bar{v}_{c+5}} + t_c \quad (4.15)$$

where  $t_l$  is the forecasted time the preceding vehicle passing the advanced loop detector.  $\bar{v}_{(c+5)}$  is the average speed of the future 5 seconds speed trajectory from the speed predictor we developed in (Fei et al 2017). Based on the time gap between the predicted arriving time of the preceding vehicle and the current time step, we could roughly estimate the number of vehicles between the

loop detector and the preceding vehicle based on the assumption of uniform arrival rate.

$$n_2 = \frac{t_l - t_c}{\overline{\Delta t_h}} + t_c \quad (4.16)$$

Where  $\overline{\Delta t_h}$  is the average time headway from the previous cycle. Then, we could predict the position of the preceding vehicle based on the number of vehicles in queue ahead of it.

We observed there exists a short time deceleration period before the vehicle joining the end of queue. We assume that deceleration time period before joining the queue is  $\Delta T = 3$  s and the vehicle has a constant deceleration rate  $a$ . Based on the measurement of the time headway and vehicle count, we did a briefly measurement of the

$$\hat{y}_a = \hat{y}_{a-1} - \Delta h_d \quad (4.17)$$

$$v_c \cdot T + \frac{1}{2}a\Delta T^2 = \hat{y}_a \quad (4.18)$$

$$\hat{T}_a = t_c + T \quad (4.19)$$

Where  $\hat{y}(a - 1)$  is the position of the last vehicle ahead in the queue,  $\Delta h_d$  is the average spacing between vehicles joining the queue,  $\Delta T$  is the deceleration period and  $v_c$  is the current speed of the preceding vehicle,  $t_c$  is the current time step,  $\hat{T}_a$  is the forecasted time for vehicle joining the queue.

The dynamic queue prediction accuracy can be further improved with at least one present CV in the same cycle. The effect of connected vehicles for improving the performance of the proposed

Table 4.1: Performance of the proposed queue location and time forecasting model

Accuracy	Time joining queue (second)		Location joining queue (feet)		Time departure (second)		Location departure (feet)	
	Lane 1	Lane 2	Lane 1	Lane 2	Lane 1	Lane 2	Lane 1	Lane 2
Without CAVs	1.68	1.98	5.66	6.05	2.21	2.15	5.02	6.42
With CAVs	1.59	1.71	3.85	3.41	1.40	2.14	3.69	3.16
Improvement	5.4%	13.6%	32.0%	43.6%	36.7%	0.5%	26.5%	50.8%

queue forecasting model is further investigated in the simulation results. Here, 100% penetration rate is not a necessary requirement for our proposed approach.

### 4.5.3 Numerical Experiments

#### Evaluation on Queue Location and Time Forecasting Model

The performance of the vehicle queue state forecasting model was tested based on real world field test data (NGSIM Peachtree data). The lane-level vehicle queue state forecasting was conducted for the two through movement lanes in the northbound.

The accuracy of the proposed forecasting model is measured by the mean absolute error (MAE) of forecasted location and time of vehicle joining the queue and discharge location and time compared to the observations, which is defined as

$$MAE = \frac{\sum_{i=1}^N |\hat{y} - y|}{N} \quad (4.20)$$

where  $N$  is the number of observations,  $\hat{y}$  is the predicted value and  $y$  is the observed value. Table 4.1 summarizes the results of the proposed vehicle queue state forecasting model. In Table 4.1, we also compared the performance of the forecasting model with only loop detector measurements and

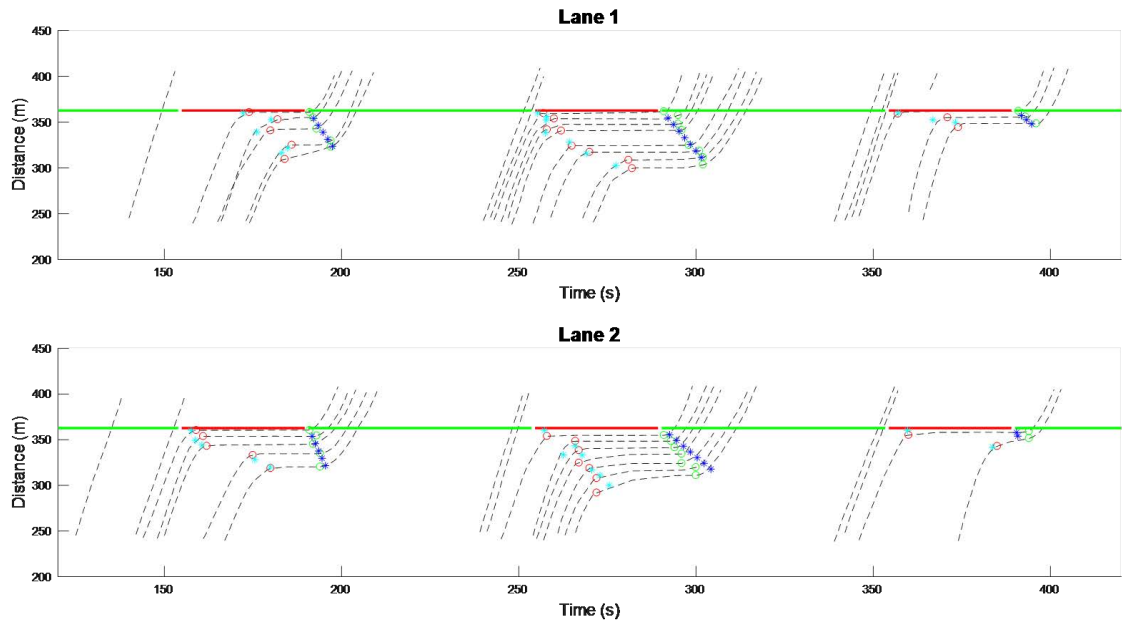


Figure 4.6: Detailed view of the forecasted and the observed vehicle states in the queue (red circle: ground truth of the vehicle states joining the queue; green circle: dissipation states of vehicles in the queue; blue star: prediction results of vehicles joining and departing the queue)

the model with corrections from CAVs. MAE of the forecasted results at the distance of 300 feet without CAVs for each lane are around 1.7 – 2.2 sec for time and around 5 – 6 feet for location. And the forecasting results with the correction from CAVs are around 1.4 – 2.1 sec for time and around 3.2 – 3.9 feet for location. Regarding the improvement from CAV correction, the forecasting accuracy could achieve 0.5% – 36.7% improvement on time and 26.5% – 50.8% on location.

Figure 4.6 gives a detailed view of the forecasted results from this proposed model. The red circle is the ground truth of the Type I critical points of vehicle that indicates the state when vehicle joining the propagation queue and green circle is the ground truth of the Type II critical points that implies the dissipation state of vehicle in queue. And the star is our forecasting results for both Type I and Type II critical points. It has been showed the proposed queue forecasting model

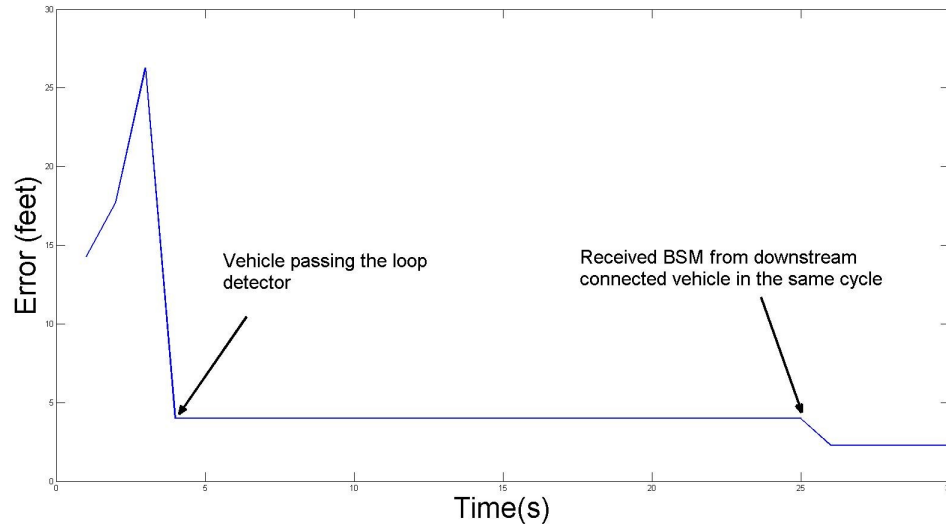


Figure 4.7: Queue end forecasting error of a vehicle approaching the intersection

could provide reliable results with satisfying prediction accuracy for various driving condition and arrival rate.

As shown in Figure 4.7, when the preceding vehicle approaches the signalized intersection, the prediction of its queue states (time and location of vehicle joining and departure of the queue) can get dynamically improved with the updated information. We dynamically update the queue end prediction per second based on the loop detector measurements and potential connected vehicle trajectories via wireless communications. The forecasting accuracy of queue end state respect to our host vehicle is dependent on the calibrated departure rate and spacing as well as forecasting result on preceding vehicle future position in queue. Before the preceding vehicle passes the loop detector, the arrival rate before the preceding vehicle is estimated under the assumption of uniform distribution. The estimated queue end state of the preceding vehicle converges after it passes through the loop detector until a connected vehicle's queue state further correct it afterwards.

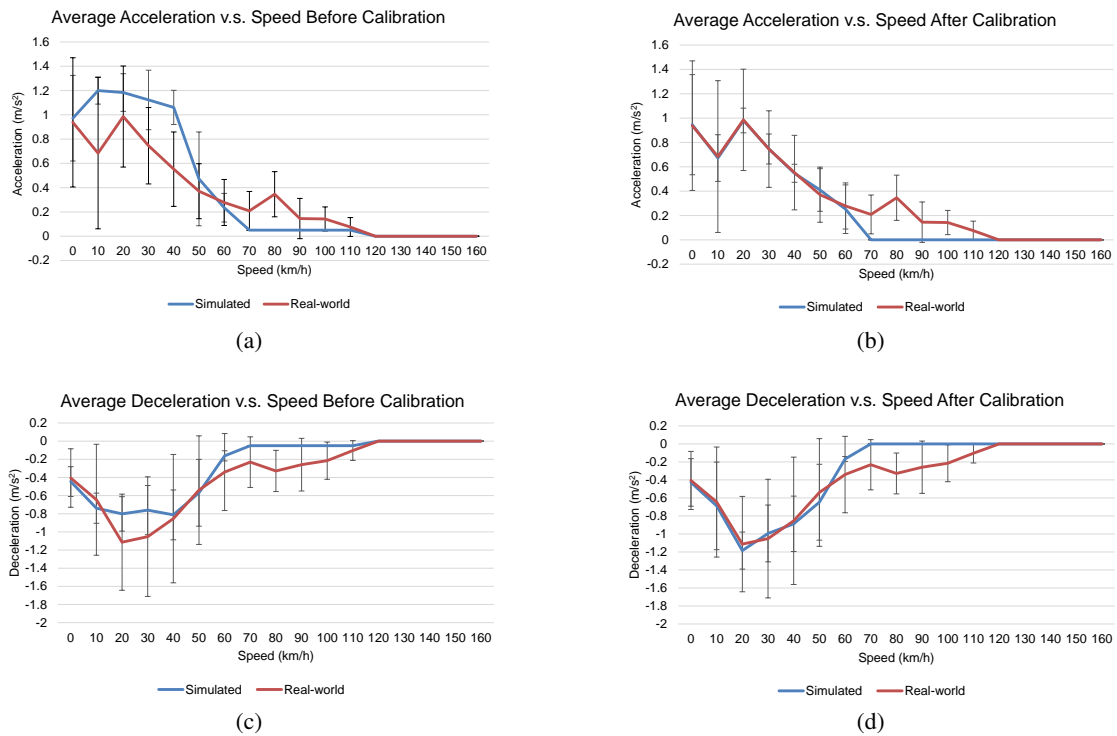


Figure 4.8: Average acceleration and deceleration before and after calibration.

## 4.6 Simulation Evaluation and Analysis

This subsection presents results of the default bus acceleration/deceleration profile, the bus schedule calibration, and the sensitivity analysis of the VD&PT controlled Eco-Bus performance in terms of mobility and energy savings under various traffic conditions.

### 4.6.1 Calibration Results

Figure 4.8 compare the bus average acceleration and deceleration profile over speed, before and after performing calibration with real-world RTA bus data. It is demonstrated that the simulated acceleration/deceleration profile under the default bus characteristics in VISSIM pretty much violates

Table 4.2: Route 14 EB stops along the University Avenue.

Stop Name	Latitude	Longitude	Estimated Arrival Time	Estimated Departure Time	Distance from Previous Stop (m)	Simulated Arrival Time
University FS Brockton				07:28:00 (Actual)		
East University NS Lemon	33.980889	-117.372455	7:30:44	7:30:54	660	
University NS Park	33.977343	-117.364859	7:34:02	7:34:12	804	7:31:47
University NS Victoria	33.976519	-117.363105	7:34:55	7:35:05	182	7:33:14
University FS Eucalyptus	33.975493	-117.364859	7:36:35	7:36:45	384	7:34:18
University FS Kansas	33.975538	-117.356839	7:37:36	7:37:46	220	7:35:32
University FS Ottawa	33.875565	-117.349528	7:39:20	7:39:30	404	7:38:00
University NS Chicago	33.975545	-117.349528	7:40:34	7:40:44	276	7:38:46
University FS Cranford	33.975603	-117.343839	7:42:47	7:42:57	528	7:40:40
Iowa FS Blaine			7:48:00 (Actual)		1240	
Route travel time			0:08:45			0:08:53
Route travel time (min)	8.8					8.9
Percentage Difference						1.5%

the real-world conditions. After fitting the bus characteristics settings in an iterative manner, much more acceleration/deceleration profile can be generated comparing to the real-world bus.

Based on the RTA Route 14 time table available on [78], we first identified the Time Points (i.e., key bus stop for planning the schedule) that bracket our test route, which are University @ Brockton (western) and Iowa @ Blaine (eastern). By looking up the time table, we realized the scheduled arrival times at these two Time Points are 07:28 a.m. and 07:48 a.m., respectively, for the simulation period (i.e., between 07:00 a.m. and 08:00 a.m.). The bus departure time and average speed (or total route travel time) were then calibrated to match with the associated bus schedule. Table 4.2 summarizes the calibration results where the difference in departure time is 10 second and the total route travel time is off by only 1.5%, which is considered to be acceptable.

## 4.6.2 Energy Consumption Evaluation

The energy consumption factor (EF, energy consumption in unit distance, KJ/mile) can be obtained by:

$$EF = \frac{\sum_{i=1}^n \sum_{t=1}^{T_i} energy_{i,t}}{\sum_{i=1}^n \sum_{t=1}^{T_i} VMT_{i,t}} \quad (4.21)$$

where  $energy_{i,t}$  is the energy consumption rate for vehicle  $i$  at time  $t$ , in KJ, and  $VMT_{i,t}$  is the vehicle miles traveled for vehicle  $i$  at time  $t$ .

The boxplot and error bars of the average energy consumption of baseline bus and Integrated Vehicle-Powertrain Eco-bus (VPEO-bus) over different traffic congestion levels are shown in Figure 4.9(a). It illustrates the energy consumption of the VPEO-bus are significant lower than baseline bus in all the traffic conditions. The average energy consumption of VPEO-bus are 878 KJ/mile, 881 KJ/mile, 887 KJ/mile and 942 KJ/mile in no traffic, light traffic, moderate traffic and heavy traffic condition, respectively. However, the average energy consumption of the baseline bus are all above 1200 across different traffic conditions.

## 4.6.3 Mobility Analysis

The mobility benefits are quantified by average speed of vehicle, provided as

$$\bar{v} = \frac{\sum_{i=1}^n \sum_{t=1}^{T_i} VMT_{i,t}}{\sum_{i=1}^n \sum_{t=1}^{T_i} VHT_{i,t}} \quad (4.22)$$

where,  $VMT_{i,t}$  = vehicle miles traveled for vehicle  $i$  at timestep  $t$ ;

$VHT_{i,t}$  = vehicle hours traveled for vehicle  $i$  at timestep  $t$  According to Figure 4.9(b), as the

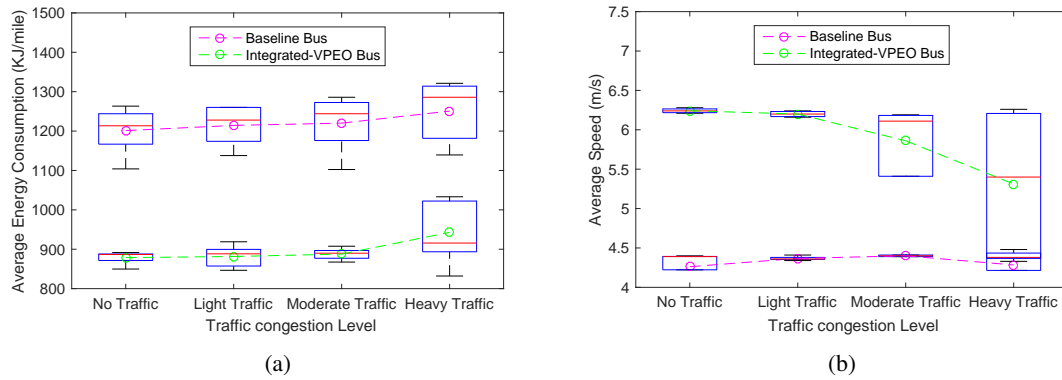


Figure 4.9: Comparative results of the VPEO bus and the baseline bus at various traffic conditions including no traffic ( $v/c$ : 0.17), light traffic ( $v/c$ : 0.35), moderate traffic ( $v/c$ : 0.7), and heavy traffic ( $v/c$ : 1.0): (a) the average energy consumption, and (b) the average speed.

traffic congestion level increases, average speed of the Eco-bus is decreasing with a larger variance. Overall, the average speed of Eco-bus is higher than the baseline bus with higher mobility benefits when traffic condition is lighter.

#### 4.6.4 Improvements

A summary of the energy efficiency improvements of VPEO-bus under VD&PT control with dynamic queue prediction is shown in Table 4.3. In Table 4.3, we can see that the Percentage Energy Savings (column 3) between the VPEO-bus and the baseline is in the range of 18% to 27%, under various traffic conditions and the penetration rate of CAVs in the traffic stream. The improvements on energy efficiency are kept within a stable range of around 19% to 24% with no other CAVs presented, showcasing the its robust performance and good adaptability under all traffic conditions. With presenting 20% penetration rate of CAVs in the traffic stream, there are additional 2.0% to 8.2% of energy savings resulting from improved performance of queue dynamic prediction.

Table 4.3: Comparative Results on Energy Savings for VPEO-bus

Traffic level (volume-to-capacity (v/c) ratio)	Penetration rate (PR) of CAVs	% savings	CAV extra improvement (%)
No traffic (0.17)	0% CAVs	21.7	3.3
	20% CAVs	25.0	
Light traffic (0.35)	0% CAVs	20.6	5.7
	20% CAVs	26.3	
Moderate traffic (0.7)	0% CAVs	18.7	8.2
	20% CAVs	26.9	
Heavy traffic (1.0)	0% CAVs	24.0	2.0
	20% CAVs	26.0	

## 4.7 Summary and Discussion

This chapter describes an advanced simulation framework of the integrated vehicle/powertrain eco-operation system for an Eco-bus. The comprehensive results under different traffic scenarios showcase the superiority of the proposed Eco-bus simulation framework compared to a conventional bus, particularly in terms of increased mobility and energy efficiency.

## **Chapter 5**

# **Anomaly Detection in Traffic with Partial Connectivity**

The research presented in this chapter aims to develop and simulate an innovative agent-based, lane-level hazard prediction application called Lane Hazard Prediction (LHP) based on partially-available vehicle trajectories data collected from an V2V environment. In addition, the corresponding driver response model was simulated to estimate the effectiveness of the LHP application under various penetration rates. The results of the research shows the potential for LHP to significantly improve the mobility and safety for both individual LHP users and the entire traffic system. The LHP application identifies the position of a downstream lane-level hazard based on a spatial and temporal data mining and machine learning technique. It then guides the application-equipped vehicles with suggestions for proper lateral maneuvers far ahead of the hazard to avoid a traffic jam. This guidance provides the vehicle driver with a suggestion to either change lanes (out of the hazard lane) or maintain the current lane to avoid getting into the hazard lane.

## 5.1 Introduction

Traffic accidents have been increasing over the past two years and are one of the leading causes of non-natural fatalities in the United States [79]. The conventional method of detecting an accident or hazard is based on either fixed-location sensors (such as loop detectors), crowdsourced roadway data, or vehicle onboard sensors (e.g. radar, LiDAR). However, these approaches may not be effective in reducing traffic congestion and potential collision risks, due to their constrained detection range in space and time, or the fact that they only provide partial/road-level information regarding the hazard. In recent years, connected vehicle (CV) technology has been rapidly emerging worldwide as a method to enhance roadway users' safety and mobility, while reducing fuel consumption and emissions. For example, several V2V applications have already been identified by the U.S. National Highway Traffic Safety Administration (NHTSA) as possible candidates to improve roadway safety [80]. Nevertheless, most of these applications require a certain level of market penetration to be effective. A variety of V2V-based applications have been proposed and developed in various projects. Examples of such efforts in the U.S. including:

- Connected Vehicle Reference Implementation Architecture (CVRIA) [6], which summarizes a large number of CV applications developed under the U.S. Department of Transportation (USDOT);
- Safety Pilot model deployment program [81];
- Dynamic Mobility Application (DMA) program [82];
- Applications for the Environment: Real-time Information Synthesis (AERIS) program [4].

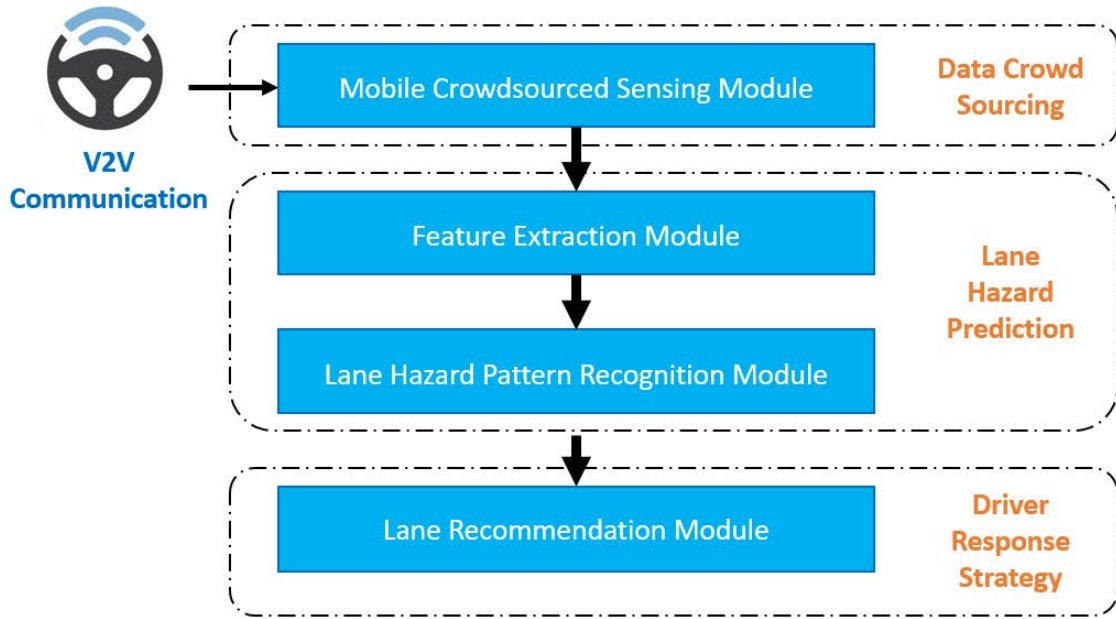


Figure 5.1: Framework of lane hazard prediction application

In addition to V2V activities in the U.S., the European Union, Japan, and other countries have also been actively supporting research on V2V technology [83–85]. To date, a few research efforts have been conducted using simulation to evaluate the effectiveness of V2V and V2I warnings/alerts about an event or hazard information on the highways in the assumption of the hazard message can be directly accessed through V2V and V2I communication [86, 87]. Liu *et al.* [88] discussed the potential of using variations of instantaneous driving decisions to understand the occurrence of extreme event such as crash or hazard. Given the partial availability of vehicle trajectory information, a reliable hazard prediction model is needed to enable the safety and mobility benefits when a hazard occurs.

## 5.2 Framework

The framework of the proposed LHP application is shown in Figure 5.1. The developed LHP application contains four major modules:

- *Mobile Crowdsourced Sensing*: This module obtains the position, speed, and direction information of CVs downstream within the communication range, with respect to the host application-equipped vehicle through V2V network communication. It then partitions the spatial and temporal domain in the traffic network into lane-level longitudinal segment cells and time slices, performing integration over multiple time steps.
- *Feature Extraction*: Using the cell-based CVs' information in the spatial and temporal domain, this module identifies the key factors that are deemed to be representative and critical for detecting a potential downstream hazard or abnormality in traffic.
- *Lane Hazard Pattern Recognition*: This module runs locally for each partitioned cell and outputs a binary hazard flag (1: hazard exists, 0: no hazard) every 20 seconds. The lane hazard pattern recognition module provides prediction on a lane-level hazard position and its associated longitudinal bound with a resolution of 30 meters, which is the longitudinal segment length for each cell.
- *Lane Recommendation*: Based on the lane-level hazard prediction results, this module suggests a lane change out of the hazard lane for LHP-equipped vehicles. Alternatively, it suggests that the vehicle keep moving in the current, non-hazard lane when approaching the hazard location to avoid joining the associated queue behind it.

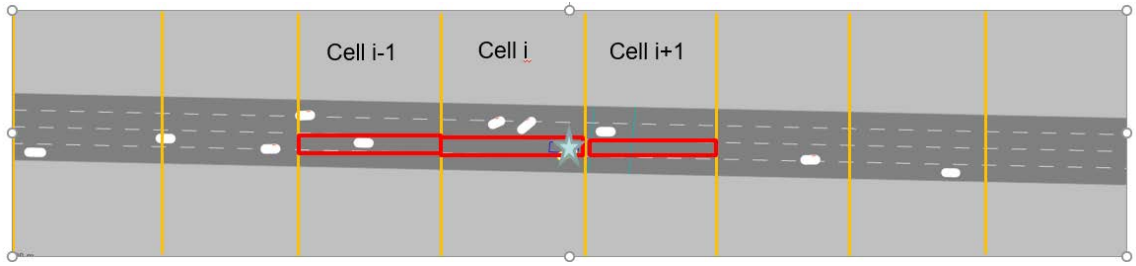


Figure 5.2: Illustration of scaling and partitioning on an example network

### 5.3 Lane Hazard Prediction Model

To perform lane-level hazard prediction, the traffic network was partitioned into spatial lane-level cells (30 meters long). The data integration and temporal resolution for the developed LHP application was 20 seconds. The information (e.g. lane-level position, speed, and direction) obtained from CVs over the V2V network were accumulated at a rate of 0.05 Hz, integrating over 20 seconds at each cell. The binary hazard predictor ran locally for each cell, which facilitated its adaptability to different geographic locations and the scalability to a larger scope. Patterns were observed that could potentially identify unusual collective behaviors for vehicles approaching the hazard location. By combining the knowledge of traffic engineering with a data-driven approach, a total of eight features were identified as input variables for the binary logistic regression-based LHP model. For each cell  $(i, j)$  in the traffic network (where  $i$  represents the longitudinal position, and  $j$  indicates the lane number), measurements were considered from the ego-cell as well as its adjacent cells in both the upstream and downstream segments, as shown in Figure 5.2.

The vehicle maneuvers within a cell were categorized into five classes:

- M1 – Through maneuver including both entry and exit

- M2 – left lane change out of the cell
- M3 – right lane change out of the cell
- M4 – right lane change into the cell
- M5 – left lane change into the cell

The input features considered for the algorithm included:

- The average speed of all vehicle travel across the cell during the 20-second time interval, calculated by the ratio of vehicle miles traveled to vehicle hours traveled
- The average speed ratio between the cell and across all the lanes at the same/upstream adjacent/downstream adjacent longitudinal segment
- The percentage of through maneuvers in the cell and lane changes into and out of the cell
- The entropy of vehicle maneuvers, which captured the diversity of all maneuvers in the cell. The entropy attained its minimum value of zero when all the vehicle maneuvers were from the same category, and its maximum value when all the vehicle maneuvers were uniformly distributed over different categories.

The log *it* function constrains the values of landslide susceptibility index of the model in the range [0, 1] (the index threshold was set as 0.75). The logistic regression-based LHP model is described in Equation (5.1):

$$\begin{aligned} \log it (P_{ij}) = \ln \left( \frac{P_{ij}}{1 - P_{ij}} \right) = & \beta_0 + \beta_1 \times \bar{V}_{ij} + \beta_2 \times \frac{\bar{v}_{ij}}{\bar{v}_i} + \beta_3 \times \bar{v}_{ij} + \beta_4 \times \bar{v}_{ij} \\ & + \beta_5 \times \frac{m_1}{m} + \beta_6 \times \frac{m_2 + m_3}{m} + \beta_7 \times \frac{m_4 + m_5}{m} + \beta_8 \times \sum_{i=1}^n \frac{m_i}{m} \log \left( \frac{m_i}{m} \right) \end{aligned} \quad (5.1)$$

Table 5.1: Parameters calibration results of the LHP model

Variable	$\beta_0$	$\beta_1$	$\beta_2$	$\beta_3$	$\beta_4$	$\beta_5$	$\beta_6$	$\beta_7$	$\beta_8$
Coefficient	-2.43	-2.24	-2.21	-2.23	-2.25	-1.90	0.88	-0.03	-0.17

Therefore, the probability of a hazard in cell  $(i, j)$  can be obtained by

$$P_{ij} = \frac{1}{1 + \exp(-\text{logit}(P_{ij}))} \quad (5.2)$$

Where,

$\bar{V}_{ij}$  is the average speed of cell  $(i, j)$ ;

$\bar{V}_i$  is the average speed across all the lanes of longitudinal segment  $i$ ;

$\bar{V}_{i-1}$  is the average speed across all the lanes of upstream adjacent longitudinal segment  $i - 1$ ;

$\bar{V}_{i+1}$  is the average speed across all the lanes of downstream adjacent longitudinal segment  $i + 1$ ;

$\bar{m}_i$  is the number of maneuvers at cell  $(i, j)$ , belonging to predefined maneuver type  $i$ ;

$m$  is the total number of maneuvers at cell  $(i, j)$ ;

$n$  is the number of maneuver types;

$\beta_k$  is the parameters' coefficients.

The parameters calibration results of the proposed Lane Hazard Prediction model based on logistic regression approach is shown in Table 5.1.

## **5.4 Lateral Driver Response Model**

Using the output of the LHP algorithm, the lateral, lane selection, and driver behavior of LHP-equipped vehicles could be modified to avoid a hazard. This guidance is performed when a hazard flag is activated downstream of the ego-vehicle's current position in the same lane, within the V2V communication range (assumed in this work to be 2,000 meters). In addition, the upstream LHP-equipped vehicles in the other lanes would be guided to stay in the current non-hazard lane until they passed the hazard position.

## **5.5 Prediction Evaluation and Simulation Setup**

This section introduces the method for prediction evaluation, simulation tools, network model, and scenarios for a comprehensive analysis of the LHP application.

### **5.5.1 Lane Hazard Prediction Evaluation**

The LHP evaluation was conducted with respect to prediction accuracy, efficiency, and application effect on safety and mobility. The LHP application provided a lateral maneuver decision based on the results of a lane-level hazard prediction model. Both effectiveness and efficiency of the proposed LHP application were evaluated under different levels of penetration rate and traffic conditions.

In this study, the receiver-operating characteristic (ROC) curve and the area under the curve (AUC) were used to evaluate the performance of the developed LHP model [89]. The ROC curve illustrated the tradeoff between the true positive rate and the false positive rate of the binary logistic

regression-based LHP model. The closer the ROC curve got to the top left corner of the graph, with a larger AUC number, the better the LHP model performed in terms of predicting a hazard, with limited false positives. The AUC for random guessing was 0.5 with the ROC curve following the diagonal. The reaction time of the LHP model, defined as the time in seconds from the point when the hazard occurred to the point when the first accurate prediction was triggered, was used as a measure of efficiency. In addition to evaluating the performance of the hazard prediction model, the LHP application's effectiveness in terms of safety and mobility were also assessed. The safety performance of LHP-equipped vehicles, unequipped vehicles, and the overall traffic was analyzed using a conflict frequency measure of effectiveness. The average speed measure of effectiveness was used to evaluate the mobility performance, provided as Equation (4.22):

### **5.5.2 Simulation Tools**

PTV VISSIM [75] was used in this study as the microscopic traffic simulation tool for traffic network modeling, development of the LHP application using an application programming interface (API), and evaluation of individual vehicles and the overall traffic system performance. As a state-of-the-art microscopic, timestep-oriented, and behavior-based traffic simulation tool, VISSIM is capable of simulating a large-scale road network and wireless communication network and calibrating the traffic flow and speed with real-world data. In addition, VISSIM provides an add-on programming interface, Component Object Model (COM), which was used in this study to modify the underlying simulation models, access model outputs, and override default vehicle behaviors.

For safety performance evaluation, the Surrogate Safety Assessment Model (SSAM) [90] was used as a post-processing model to perform safety evaluation by analyzing vehicle trajectory data (.trj

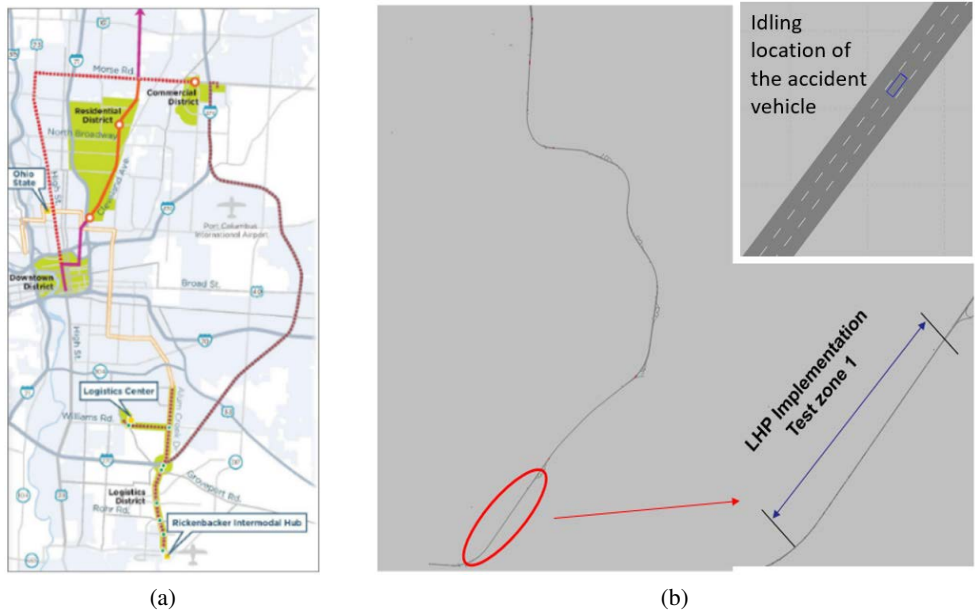


Figure 5.3: Road network of I-270N in real world and VISSIM.

files) generated from VISSIM. In SSAM, the safety performance was assessed through measured conflict potentials, considering both the risk of longitudinal collisions (rear-end conflicts) and lateral collisions (lane change conflicts).

### 5.5.3 Simulation Network Model

The real-world network used in this study was a 17-mile stretch of Interstate 270 (I-270) North, in Ohio, with seven on-ramp/off-ramp pairs (see Figure 5.3). The longest segment located between the second on-ramp/off-ramp pair was selected, and an accident event was created to test LHP performance. The speed limit on I-270N is 70 mph, and the traffic demands are well calibrated with real-world data from the Traffic Count Database System (TCDS) by the Ohio Department of Transportation [91].

#### **5.5.4 Simulation Scenarios**

To gain in-depth insight into the developed LHP application performance, simulation tests were conducted under various V2V penetration rates. V2V market penetration rate is expected to take several years to achieve a significant level. A full penetration rate (i.e., 100%) enables the LHP application to attain the most accurate traffic measurements, leading to higher prediction accuracy and shorter reaction times. However, since 100% penetration is not currently available, the sensitivity analysis over different penetration rates is meaningful. The application provides solid performance, even at lower penetration rates, as discussed in the results section.

The simulation test was performed on a three-mile stretch of road, and the simulation duration was 1,800 seconds. The LHP-equipped vehicle percentage was set to 9% out of the total V2V-equipped vehicles. This percentage corresponds to Honda's market share. Therefore, three types of vehicles ran in the simulation network: 1) LHP- and V2V-equipped vehicles; 2) V2V-equipped vehicles; and 3) conventional vehicles. Conventional vehicles do not have V2V communications capability, and their behavior follows VISSIM default lane change and car following models. V2V-only vehicles exchange real-time information (e.g., speed, lane-level position, etc.) with other V2V vehicles without the onboard application. LHP-equipped vehicles exchange information via V2V, perform hazard predictions, and change (or maintain current) lanes to avoid hazards downstream. Seven levels of penetration rate (0, 5%, 10%, 20%, 50%, 80%, and 100%) V2V-equipped vehicles were evaluated (in which LHP-equipped vehicles accounted for 9% of the above penetration rate levels). Both user benefits and system benefits were evaluated in terms of mobility (average speed difference) and safety (conflict frequency difference) under different penetration rate. Ten simulation runs for each

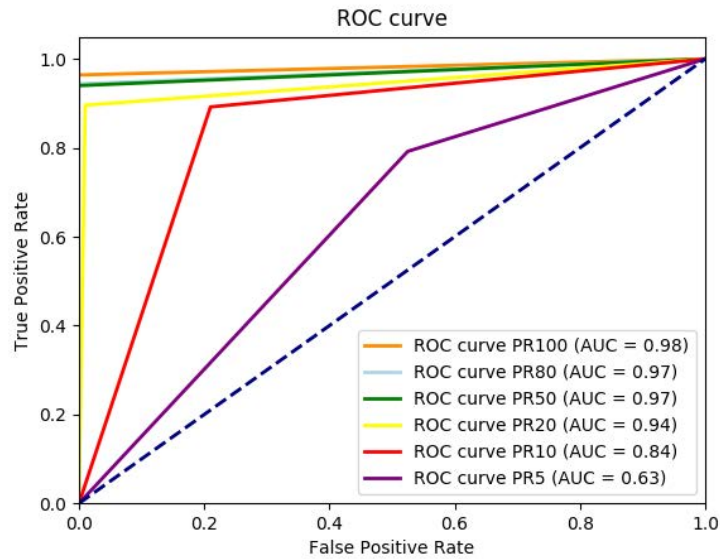


Figure 5.4: ROC curve of LHP under different penetration rates.

simulation setting were conducted.

## 5.6 Results and Discussion

This section presents the evaluation of LHP application from three aspects:

- 1) Prediction analysis in terms of accuracy and efficiency of the developed LHP model
- 2) Safety analysis of LHP-equipped and unequipped vehicles
- 3) Mobility analysis of LHP-equipped and unequipped vehicles

### 5.6.1 Prediction Performance

As previously described, ROC curves and associated AUC values were used to assess the accuracy of the developed lane hazard predictor. In addition, the reaction time of LHP was used as the key

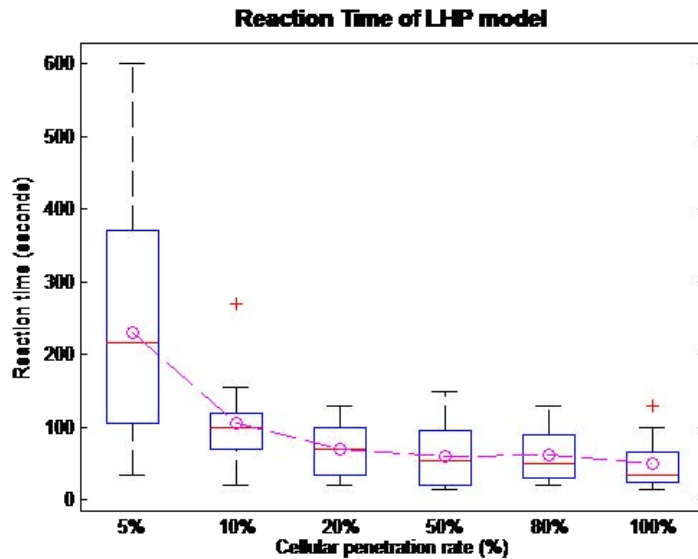
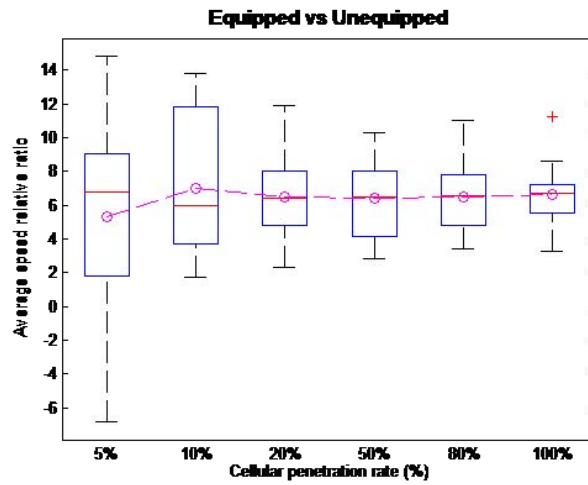


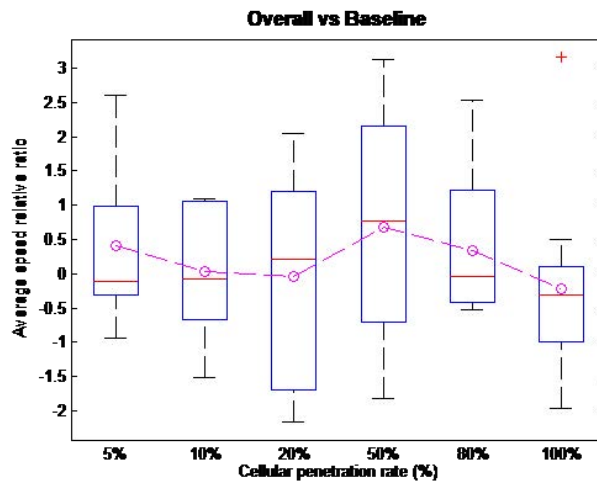
Figure 5.5: Reaction time of LHP under different penetration rates.

index to evaluate the algorithm efficiency. The results of sensitivity analysis for different levels of penetration rate are shown in Figure 5.4 and Figure 5.5. With a 100% penetration rate of connected vehicles, the LHP algorithm provided the best performance with 0.98 AUC. Other results were as follows (see Figure 5.4):

As for the application efficiency, the average reaction time of LHP was less than 60 seconds across the penetration rates between 20% and 100% (see Figure 5.5). However, there was a rapid increase in reaction time at the 5% penetration rate, with larger variation. This result may be caused by a noisy measurement due to the low number of vehicles equipped with LHP at the 5% penetration rate. Therefore, LHP was proven to be highly efficient and reliable at a penetration rate as low as 20%. At lower penetration rates, such as 5% or 10%, the LHP application can be considered a lane advisory system.



(a)



(b)

Figure 5.6: Sensitivity analysis of penetration rate on mobility benefits: (a) user benefits and (b) system benefits.

## 5.6.2 Mobility Performance

Mobility performance was quantified by the average speed, which was calculated using Equation (4.22). The comparative results in terms of user benefits and system benefits were obtained using

the average speed relative ratio (%), as denoted in Equations (5.3) and (5.4), respectively.

$$\frac{MOE_e - MOE_{us}}{MOE_{us}} \times 100\% \quad (5.3)$$

where  $MOE_e$  is the metric of equipped vehicles (i.e. average speed of equipped vehicles);  $MOE_{us}$  is the metric of unequipped vehicles (i.e. average speed of unequipped vehicles)

$$\frac{MOE_{oa} - MOE_{bl}}{MOE_{bl}} \times 100\% \quad (5.4)$$

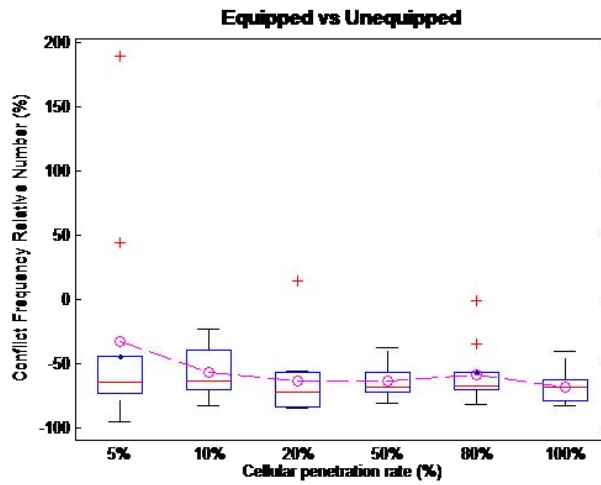
where  $MOE_{oa}$  is the metric of overall vehicles with LHP scenarios;  $MOE_{bl}$  is the metric of overall vehicles with 0 penetration rate as the baseline.

The boxplot and error bars of the average speed relative ratio in terms of V2V penetration rates are shown in Figure 5.6. According to Figure 5.6, average speed improvements (up to 7%) for LHP-equipped vehicles were witnessed across all penetration rates. When the penetration rate was high enough (i.e., greater than 10%), the improvement tended to be stable, with much less variation. Considering the system mobility benefits, the average speed relative ratio of overall vehicles compared to the baseline (penetration rate of 0) varied between -0.2% and 0.7%. Overall, the applied LHP model had negligible effects on the system-level mobility, regardless of the penetration rates.

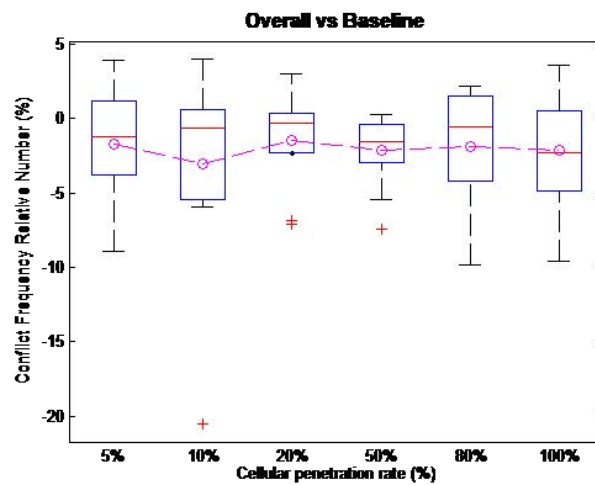
### 5.6.3 Safety Performance

The rear end and lane change conflict frequency were selected to assess vehicle safety performance.

The decrease in conflict frequency implied an improved safety performance. The comparison of



(a)



(b)

Figure 5.7: Sensitivity analysis of penetration rate on safety benefits: (a) user benefits and (b) system benefits.

LHP-equipped and unequipped vehicles was quantified with a rear end conflict frequency relative number, as denoted in Equations (5.3) and (5.4). As shown in Figure 5.7, significant user benefits in terms of safety could be achieved across all simulated penetration rates.

The average conflict frequency difference was decreased by a factor of 32.8% – 68.1%. The user benefits in terms of safety achieved the highest point at a penetration rate of 100% and the lowest at a 5% penetration rate. The results were more stable at higher penetration rates. As indicated in Figure 5.7, positive effects on system benefits in terms of safety were also witnessed across all penetration rate levels. The average conflict frequency ratio varied between -1.4% and 3.0%. The conflict frequency was significantly reduced from both user and system perspectives under different penetration rate. The significant improvement in safety performance may have resulted from the fact that the LHP application enabled equipped vehicles to avoid sharp speed drops upstream in the hazard lane and encouraged lane change behavior earlier and in a smoother manner.

## **5.7 Summary and Conclusions**

In this chapter, an innovative V2V-based lane-level hazard prediction algorithm and corresponding driver response model called Lane Hazard Prediction (LHP) was developed and evaluated. Results of a comprehensive simulation study showed that the LHP application could provide highly accurate lane-level prediction of a downstream hazard within tenths of seconds after it occurred, by crowdsourcing V2V communications information. The LHP application provided lateral maneuver guidance to LHP-equipped vehicles. A detailed simulation study was performed to assess the effectiveness of the proposed LHP application in terms of safety and mobility benefits. Results demonstrate that LHP-equipped vehicles may gain significant mobility and safety benefits without compromising the mobility and safety performance of the overall traffic. An attractive feature of the proposed LHP application is that accurate prediction within seconds and noticeable benefits in safety and mobility can be achieved, even under a relatively low V2V penetration rate.

## **Chapter 6**

# **Bi-Level Optimal Edge Computing**

## **Model in Connected Vehicle**

### **Environment**

This chapter describes a Bi-level Optimal Edge Computing (BOEC) methodology to maximize both the vehicle mobility benefit and energy saving without compromising safety perspective. We first develop an optimal merge sequence and merge time scheduling model by crowd sourcing initial state of vehicles, clustering vehicles based on their potential conflict at the merge point and solving a Mixed-Integer Linear Program (MILP). We evaluate the effectiveness of the proposed MILP-based optimal scheduling model by comparing it with the existing rule-based FIFO model in terms of mobility and sustainability. We then determine the optimal vehicle trajectories to guarantee vehicles meet the assigned merge time with the lowest energy cost. For the vehicle trajectory planning, we propose three different approaches (a closed-form heuristic model, a quadratic programming model

and a graph based model) on energy consumption map based on the trade off between computation efficiency and optimality.

## **6.1 Background**

The increasing transportation activities and traffic jam have led to significant effect on social and economic issue. In 2014, congestion caused urban Americans to travel an extra 6.9 billion hours and purchase an extra 3.1 billion gallons of fuel for a congestion cost of \$160 billion [92]. The bottlenecks such as ramp merging and intersections in the transportation system not only lead to huge economic and mobility cost, but also have side effect on increasing air pollutant emissions, energy consumption and the risk of collision. Intersection coordination control receives a lot of research interest. In recent years, research effort has been made to develop centralized management system to coordinate vehicles [93]. In [94], a reservation-based intersection coordinator is proposed that uses the multi-agent pair of vehicles on a collision course and decides actions for assigning a particular time interval when vehicles approach the intersection. With vehicle pre-defined paths at the intersection, [95] and [96] transform the nonlinear and non-convex problem into a linear programming formulation accounting for signal-free autonomous intersection control in terms of conflict free and capacity of the intersection. However, the energy saving and air pollutant emission reduction are not mentioned in these coordination systems.

On-ramp merging is another topic that attracts significant research attention. On-ramp merging has been approached by designing cooperative ramp metering [97, 98] and local cooperative maneuver when vehicles approach the merge zone [93, 99, 100]. Ramp metering has been widely used in

California to regulate the traffic flow of on-ramp vehicles when they merge into the highway. Other than the traditional pre-timed ramp metering algorithm based on historic traffic data [101], some advanced ramp metering algorithms have been developed using the vehicle connectivity. A cooperative ramp metering is proposed in [97] to take the advantage of the enabled cooperation among vehicles to form a platoon in the CAVs environment. Yang *et al.* [98] presents a ramp metering control based on reinforcement Q-learning to enhance the capacity of merging section. However, with the ramp metering approaches, the undesirable idling at on-ramp merge point is still not fully avoidable. The stop-and-go pattern at the ramp metering results in large air pollutant emissions and energy consumption and have the side effect on vehicle safety due to the speed gap between the highway vehicle and on-ramp vehicle when on-ramp vehicle starts off from the ramp metering. The existing traffic management is mainly cloud-based system [102]. However, cloud computing may not always be the best strategy for real-time applications such as cooperative on-ramp merging. To address the real time on-ramp merging control, we leverage the edge computing approach [103] that can efficiently access and process resources at the particular point/location in the vehicular network, e.g., roadside unit (RSU).

## **6.2 System Framework**

In this section, we present the proposed BOEC architecture for on-ramp merging coordination and eco-driving. Figure 6.1 illustrates the framework and overall structure of the proposed BOEC model, which consists of a vehicle crowd sourcing module and a bi-level edge computing module. We partition section of the road within V2I communication range into two zones: the sequencing zone and the control zone.

Bi-level optimization for vehicle mobility and fuel consumption based on a hierarchical structure

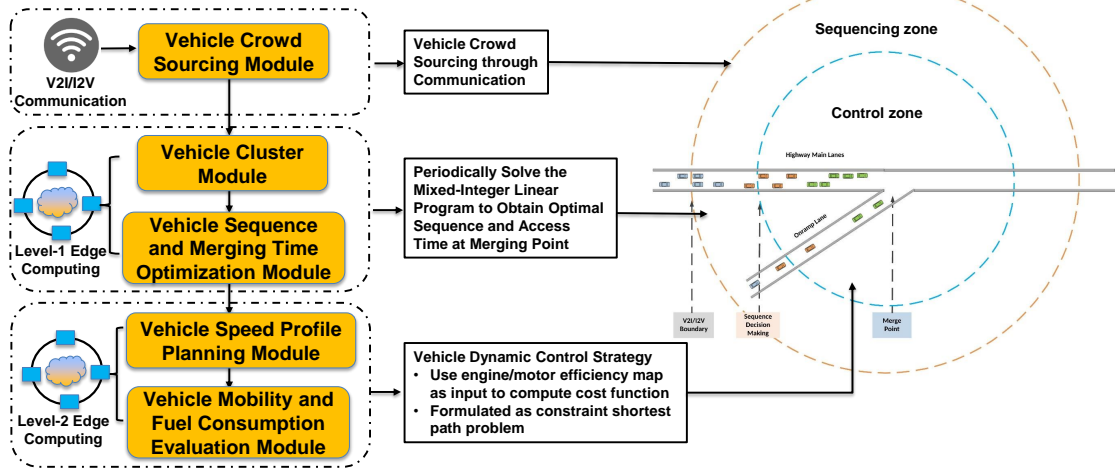


Figure 6.1: Flow diagram and framework of bi-level optimal edge computing for on-ramp merging

The first-level edge computing, i.e., the first level optimization, takes place in the sequencing zone to cluster the connected vehicles into groups and to obtain optimal merge sequence and merge time. First, we use RSU to collect vehicle information including position, speed, heading, lane information upstream with respect to the merge point. We then assign each vehicle into an associated cluster group based on its state and potential conflict at the merge point. We formulate the problem of on-ramp merging scheduling as a Mixed-Integer Linear Program (MILP) [104]. The formulated optimization problem is periodically solved for the clustered vehicles in the sequencing zone using IBM CPLEX solver [105]. The corresponding outputs (vehicle merge sequence and assigned merge time) are used in the second-level edge computing.

The second-level edge computing, i.e., the second level optimization, is realized in the control zone following merge sequence and merge time assignments to compute the optimal speed trajec-

tory for the connected vehicles in terms of energy efficiency and air pollutant emission reduction. In the second-level edge computing, we propose three different approaches: a closed-form heuristic model, a quadratic programming model and graph-based shortest path model. In the control zone, vehicles travel with the optimal energy-efficient trajectory following the merge sequence and merge time.

### **6.3 Optimal Vehicle Merge Scheduling by Edge Computing**

In this section, we describe our proposed Mixed-Integer Linear Programming model for optimal scheduling and a simple reservation-based first-in-first-out (FIFO) policy approach for performance comparison.

The reservation-based FIFO policy approach takes initial state of the connected vehicles when they enter the sequencing zone and calculates the earliest estimated arrival time at the merge point. This approach then dynamically adjusts vehicle merge time by filling up a reservation table scaling by the safety headway before vehicle enters the control zone. The reservation management is based on FIFO policy. Although this approach can reduce the conflicts at the merge point with low computational cost, it limits the potential of maximizing the vehicle throughput at the merge point and enlarges the transmission burden in the V2I communication network.

To obtain optimal merge sequence and merge time for the clustered vehicles to further improve the travel throughput and maximize the mobility benefit, we formulate the problem as a Mixed Integer Linear Program (MILP) [104] to minimize total travel time for both mainline vehicles and

on-ramp vehicles. As described in Equation (6.1), the attributes of each connected vehicle  $CV_i$  ( $1 \leq i \leq n$ ) contains vehicle ID, vehicle position, vehicle speed, speed limit, distance to the merge point, lane number, the time vehicle entering to the sequencing zone and the earliest merge time at the merge point calculated based on the speed limit.

1) *Vehicle Attributes:*

$$CV_i = \{i, x_i, v_i, v_{max}, d_i, l_i, t_{0,i}, t_{merge,min,i}\} \quad (6.1)$$

2) *Decision Variables:* Optimal merge time of the vehicle at merging point

$$t_{merge,i}, t_{merge,j}, i \in \{1, 2, \dots, n_1\}, j \in \{1, 2, \dots, n_2\} \quad (6.2)$$

3) *Objective function and optimization problem:*

$$\min J = \min \sum_{i=1}^{n_1} (t_{merge,i} - t_{0,i}) + \sum_{j=1}^{n_2} (t_{merge,j} - t_{0,j}) \quad (6.3)$$

4) *Constraints:*

$$t_{merge,k} > t_{merge,min,k} \quad (6.4)$$

$$t_{merge,k1} - t_{merge,k2} \geq t_{headway1} \quad (6.5)$$

$$t_{merge,i} - t_{merge,j} \geq t_{headway2} \quad (6.6)$$

$$\text{or } t_{merge,j} - t_{merge,i} \geq t_{headway2}$$

where  $n_1$  and  $n_2$  are the number of the mainlane vehicles and the number of on-ramp vehicles, respectively;  $t_{0,i}$  is the time mainline vehicle  $i$  entering to the sequencing zone;  $t_{0,j}$  is the time on-ramp vehicle  $j$  entering to the sequencing zone;  $k \in \{1, 2, \dots, n_1\}$  or  $k \in \{1, 2, \dots, n_2\}$ ;  $k_1, k_2 \in \{1, 2, \dots, n_1\}$  or  $k_1, k_2 \in \{1, 2, \dots, n_2\}$ ;  $t_{headway1}$  is the time headway between the adjacent merging vehicles on same lane and can be different for the mainlane vehicles and the on-ramp vehicles;  $t_{headway2}$  is the time headway between adjacent merging vehicles on different lanes. The constraints assure the safety and the traffic rule as well as vehicle acceleration/deceleration capability. The first constraint (Equation (6.4)) ensures that vehicle will not violate the speed limit through the merge zone. The other two constraints (Equation (6.5) and Equation (6.6)) are based on the assumption that no overtaking is allowed for vehicles in the same lane and ensure the safety headway for both vehicles on the same lane and vehicles between the mainlane and the on-ramp. We choose different headway based on whether vehicles are traveling on the same lane or not. For the same lane vehicles, they can potentially formulate a platoon with much shorter headway that is taken into consideration in our optimization problem.

The formulated problem intends to provide the optimal merge time  $t_{merge,i}$  for the involved mainline vehicle and the optimal merge time  $t_{merge,j}$  for the involved on-ramp vehicle to minimize their travel time through the merge zone. Therefore, the objective of the MILP problem is to minimize the total travel time for all the involved vehicles through the merge zone. The optimal merge sequence and merge time of the connected vehicles at the merge point guarantee the overall difference between the sequencing zone entering time and the assigned merge time is minimized without compromising any safety perspective or the traffic rule.

To mathematically interpret and solve the discontinuity in the last constraint (Equation (6.6)), additional binary variables have been introduced, which we refer to the big-M method [106]. We can transform the last constraint into a 0-1 binary linear programming problem such that if one of these two inequalities is true the other one is always redundant. For this purpose, we introduce new binary variable  $B_{i,j}$  and a constant  $M$ . Then, the Equation (6.6) can be converted to Equation (6.7):

$$\begin{aligned} t_{merge,i} - t_{merge,j} + MB_{i,j} &\geq t_{headway2} \\ t_{merge,j} - t_{merge,i} + M(1 - B_{i,j}) &\geq t_{headway2} \end{aligned} \quad (6.7)$$

where  $B_{i,j}$  is either 0 or 1, and  $M$  is a large enough constant to make the  $t_{headway2} + |t_{merge,i} - t_{merge,j}|$  negligible compared to it. We set  $M$  to 2000 in our formulated optimization problem.

$$v_n(t + \tau) = \min \left\{ v_n(t) + 2.5a_n\tau \left( 1 - \frac{v_n(t)}{v_n^d} \right) \sqrt{0.025 + \frac{v_n(t)}{v_n^d}}, \right. \\ \left. b_n\tau + \sqrt{b_n^2\tau^2 - b_n[2(x_{n-1}(t) - s_{n-1} - x_n(t)) - v_n(t)\tau - v_{n-1}^2(t)]} \right\} \quad (6.8)$$

## 6.4 Optimal Vehicle Trajectory Planning

Once the optimal merge sequence and the optimal merge time become available, we need to efficiently plan vehicle speed trajectory online in order to assure the assigned merging time at the merge point while minimizing the overall energy consumption. In this section, we propose three different planning approaches to obtain vehicle trajectory through the control zone. Different approaches can be applied under different scenarios or for different goals according to the trade off

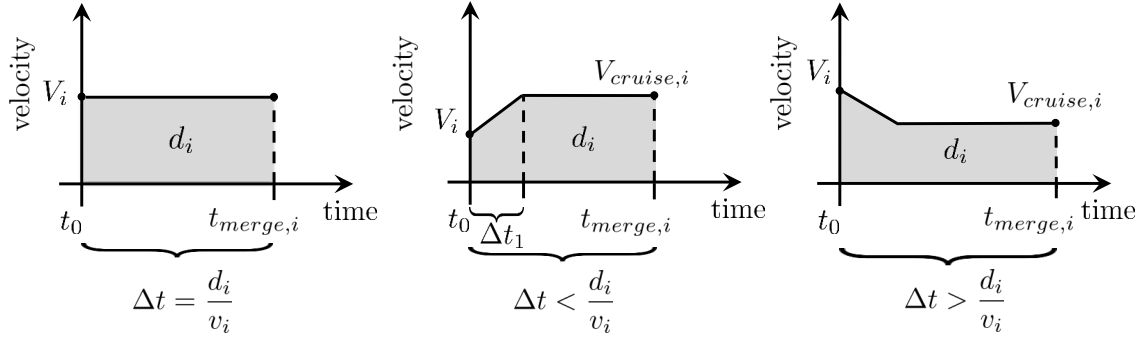


Figure 6.2: Heuristic vehicle speed trajectory planning

between computation efficiency and optimality. The first vehicle trajectory planner is based on a closed-form heuristic model combined with the Gipps' car-following model (see Equation (6.8)) to constrain the vehicle headway relative to its preceding vehicle. The second trajectory planner is formulated as a quadratic programming (QP) optimization problem to minimize the  $L^2$ -norm of the control input (acceleration/deceleration rate). Finally, we propose a Graph-based optimization approach using Dijkstra's algorithm to find the minimum energy cost path with constraints that directly optimize energy consumption while following the assigned merge sequence and merging time from the first-level edge computing without compromising safety.

#### 6.4.1 Heuristic Vehicle Trajectory Planning

Once the merging time is assigned to each vehicle, we determine whether a vehicle can keep the current speed  $v_i$  or needs a acceleration/deceleration to follow the assignment based on its current state attributes. If the arrival time at the merge point using current speed is larger than the remaining time to the assigned merging time, vehicle needs to accelerate to meet the goal and vice versa. We assume vehicles have the constant acceleration/deceleration rate till they reach their desired cruise speed that enables their remaining travel time to the merge point equal to the time difference be-

tween their merging time to the merge point  $t_{merge,i}$  and the current time  $t_0$  as shown in Figure 6.2.

A closed-form analytical vehicle trajectory solution can be obtained as follows:

$$\text{Vehicle attribute: } CV_i = \{i, v_i, v_{lim}, d_i, t_{0,i}, a_{min}, a_{max}, t_{merge,i}\}$$

Using Figure 6.2, we can obtain

$$\begin{cases} v_{cruise,i} = v_i + a\Delta t_1 \\ v_i\Delta t_1 + \frac{1}{2}a\Delta t_1^2 = d_{in} \\ v_{cruise,i}(\Delta t - \Delta t_1) = d_i - d_{in} \end{cases} \quad (6.9)$$

which can further derive

$$\Delta t_1 = \frac{a\Delta t \pm \sqrt{a^2\Delta t^2 - 2a(-v_i\Delta t + d_i)}}{a} \quad (6.10)$$

where  $\Delta t = t_{merge,i} - t_{0,i}$ ;  $\Delta t_1$  is the acceleration time from the initial speed  $v_i$  to the cruise speed  $v_{cruise,i}$ ;  $d_{in}$  is the travel distance within the acceleration period  $\Delta t_1$ ;  $a = a_{max}$  or  $a_{min}$  is the constant acceleration rate or deceleration rate.

Therefore, the cruise speed for both acceleration-cruise pattern and deceleration-cruise pattern can be obtained from Equation (6.9) and Equation (6.10) as follows:

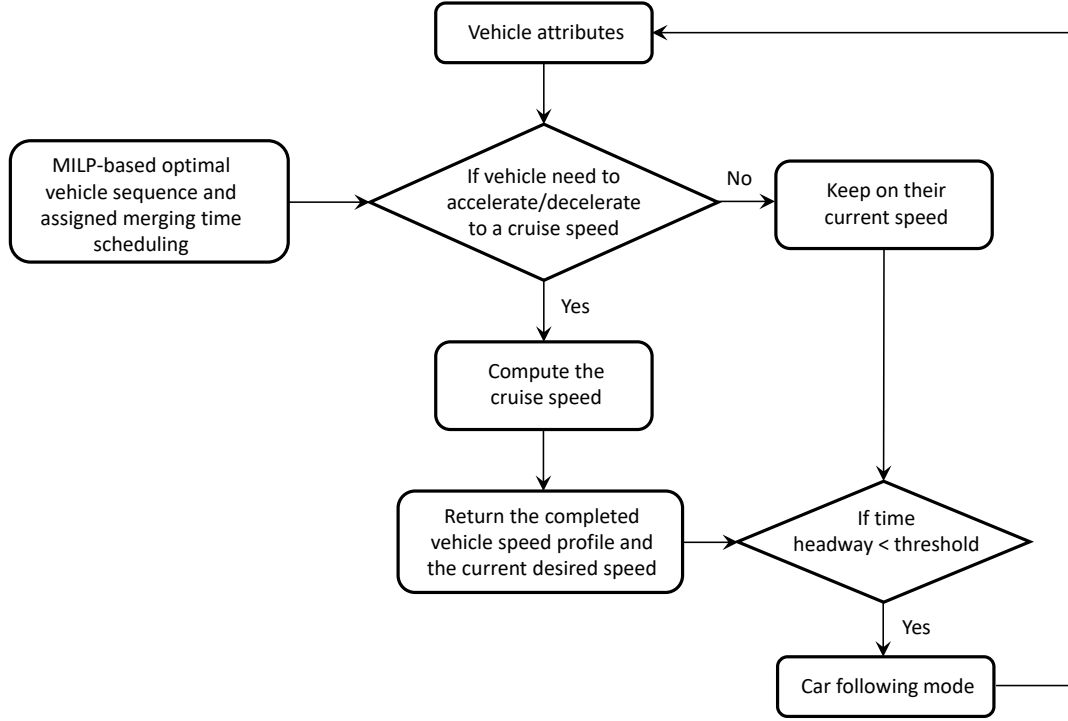


Figure 6.3: Flow diagram of heuristic vehicle trajectory planner

Acceleration-cruise pattern, if  $t_{merge,i} < t_0 + \frac{d_i}{v_i}$ :

$$v_{cruise,i} = v_i + a\Delta t - \sqrt{a^2\Delta t^2 - 2a(-v_i\Delta t + d_i)} \quad (6.11)$$

Deceleration-cruise pattern, if  $t_{merge,i} > t_0 + \frac{d_i}{v_i}$ :

$$v_{cruise,i} = v_i + a\Delta t + \sqrt{a^2\Delta t^2 - 2a(-v_i\Delta t + d_i)} \quad (6.12)$$

The flow diagram of the heuristic vehicle trajectory planner is shown in Figure 6.3. Given the optimal sequence and merge time from the first-level edge computing and vehicle's current attribute,

vehicle can keep its current speed  $v_i$  as cruise speed to the merge point if  $t_{merge,i} = t_0 + \frac{d_i}{v_i}$ . Otherwise, we determine vehicle's driving pattern and compute the vehicle speed trajectory based on Equation (6.11) or Equation (6.12).

The Gipps' car following model [23] is applied as a subsystem to guarantee safety perspective as described in Equation (6.8), where  $\tau$  is the reaction time (can be very small);  $v_n(t)$  and  $v_{n-1}(t)$  are the speed of the following vehicle  $n$  and the leading vehicle  $n - 1$  at time step  $t$ , respectively;  $v_n^d$  and  $a_n$  are the desired speed and the maximum acceleration of vehicle  $n$ ;  $b_n$  and  $b$  are the most severe braking that the driver of vehicle  $n$  wishes to undertake and the expected leading vehicle maximum deceleration, respectively.

## 6.4.2 QP-Based Optimal Trajectory Planning

It has been proven that the vehicle energy consumption highly relies on the acceleration/deceleration and speed profile [107]. The optimization problem becomes a constrained nonlinear programming problem. Solving that constrained nonlinear programming problem using energy consumption model as the objective function is quite challenge. The nonconvexity and high nonlinearity usually lead to great computational cost and hardly feasible for real-time microscopic vehicle maneuver application. Therefore, in this study, we formulate the problem as minimizing the  $L^2$ -norm of the control input (acceleration/deceleration rate) to provide a feasible trajectory based on quadratic programming method.

Vehicle dynamic equations are as follows:

$$\begin{cases} x_i(t_{k+1}) = x_i(t_k) + \frac{v_i(t_{k+1}) + v_i(t_k)}{2} \Delta t \\ v_i(t_{k+1}) = v_i(t_k) + a_i(t_k) \Delta t \end{cases} \quad (6.13)$$

The convex objective function can be expressed by setting  $H$  as positive definite matrix and  $f$  as zero vector in general form:

$$\min \Sigma a_i^T H a_i + f a_i \quad (6.14)$$

subject to

$$x_i(t_{merge,i}) = d_i \quad (6.15)$$

$$0 \leq v_i(t_k) \leq v_{lim} \quad (6.16)$$

$$a_{min} \leq a_i(t_k) \leq a_{max} \quad (6.17)$$

$$|x_i(t_k) - x_j(t_k)| \geq d_{headway} \quad (6.18)$$

$$x_i(t_0) = x_{ini,i} \quad (6.19)$$

$$v_i(t_0) = v_{ini,i} \quad (6.20)$$

where  $a_i$  is the control input (acceleration/deceleration rate);  $d_i$  is the current distance to the merging point;  $t_{merge,i}$  is the optimal merge time at the merge point;  $\Delta t$  is time step;  $x_{ini,i}$  and  $v_{ini,i}$  represent the vehicle's initial state;  $d_{headway}$  is the safety distance between vehicles;  $v_{lim}$  is the road speed limit;  $a_{min}$  and  $a_{max}$  are vehicle minimum acceleration rate and maximum acceleration rate, respectively.

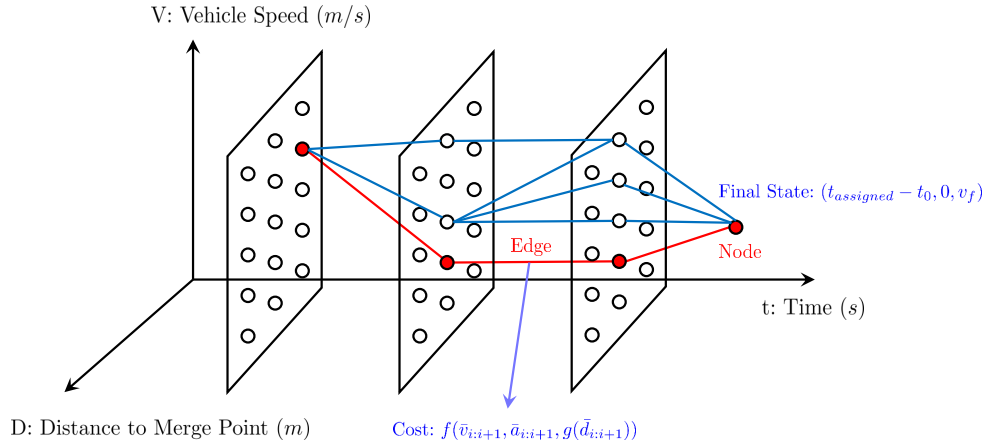


Figure 6.4: Graph-based optimal trajectory planner illustration

### 6.4.3 Graph-Based Optimal Trajectory Planning

As described earlier, the object of the proposed second-level edge computing is to minimize vehicle energy consumption through control zone till they reach the merge point with their assigned merge time. The energy consumption is a nonlinear function that mainly depends on vehicle type, speed, acceleration/deceleration and road grade. Solving that constrained nonlinear programming problem using energy consumption model as the objective function is quite challenge and hardly feasible for a real-time vehicle microscopic maneuver application. To enable optimization of the energy consumption model while enhancing the computation efficiency, we propose a graph-based optimal trajectory planning approach with constraints on total travel time, total travel distance, maximum capable acceleration/deceleration rate and final speed at the merge point. To formulate this graph-based model, we first discretize the system states, e.g., 0.5 sec time step and 0.5 m/s speed resolution, and balance the data resolution against the computation cost. The state transition diagram is illustrated in Figure 6.4. At each node of the proposed directed graph  $G = (V, E)$ , we assign a

unique 3-D coordinate  $(t, x, v)$  that describes the dynamic state of the vehicle, where  $t \in [t_0, t_{merge}]$  is the time (in second),  $x \in [0, d]$  is the distance to the merge point (in meter) and  $v \in [0, v_l]$  is the speed (in m/s), where  $v_l$  is the speed limit in this graph. For each time step, the feasible nodes for the next state is determined by the current state and constraints from speed limit, maximum power and capability of braking system. There is an edge transit from the state  $(t_i, x_i, v_i)$  to state  $(t_{i+1}, x_{i+1}, v_{i+1})$  with a cost as the energy consumption during this state transition process. We assume the road grade satisfies a predefined function of distance  $g(d_{i:i+1})$  as shown in Equation 6.21.

$$\theta = g(d_{i:i+1}) = \arcsin \frac{2(d_{i+1} - d_i)}{(v_{i+1} + v_i) \cdot \delta t} \quad (6.21)$$

where  $d_i$  is the distance to the merge point at time step  $i$ ;  $\delta t$  is the time step scaling factor.

At this point, the fuel consumption minimization problem is converted into a problem to find the shortest path from the source node  $N(0, X, V_s)$  to the destination node  $N(t_{merge}, 0, V_f)$  in the directed graph  $G = (V, E)$ . We apply Dijkstra's algorithm to solve this single-source shortest path problem with non-negative cost. Figure 6.4 illustrates an example of the optimal speed transit trajectory in terms of energy consumption through the control zone while satisfying all exogenous and endogenous constraints. The proposed algorithm is able to deal with more complicated problem with longer time period/distance and higher time/location resolution efficiently, as the time complexity of Dijkstra's algorithm is  $\mathcal{O}(\log(N) \cdot E)$ , where  $N$  is the source node number and  $E$  is the number of edges.

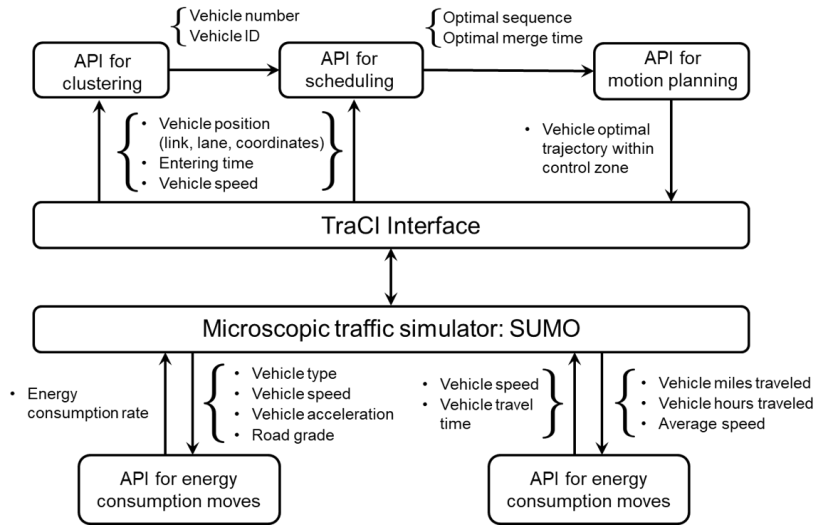


Figure 6.5: Simulation software components and interface block diagram

## 6.5 Experiment Setup and Test Scenario

This section describes experiment design setups and test scenarios.

### 6.5.1 Simulation Setup

In this section, the microscopic traffic simulation SUMO (Simulation of Urban Mobility) [108] is used to evaluate the performance of the proposed BOEC model by interfacing with the movement of each individual vehicle. Figure 6.5 illustrates the interaction among the traffic simulator SUMO, the developed BOEC model and the energy consumption simulator MOVES [69]. We assume that the penetration rate of connectivity is 100%. We access the connected vehicle information in the network and develop three advanced API modules (vehicle clustering, vehicle optimal scheduling and vehicle optimal trajectory planning) to achieve optimal on-ramp merge coordination in connected vehicle environment through the Traffic Control Interface (TraCI) in SUMO. These API modules

acquire vehicle information such as speed, position, acceleration/deceleration and entering time to determine the clustered group for coordination maneuver. Then, the optimal merge sequence and merge time for the involved vehicles are periodically computed using CPLEX optimization solver before vehicles enter the control zone. The API for motion planning provides the energy efficient vehicle trajectory in the control zone following the assigned merge sequence and merge time without compromising safety. These control inputs are sent back to SUMO to model each individual vehicle movement through on-ramp merging. In the simulation, we assume the speed limit on the highway is 108 km/h and on the on-ramp is 72 km/h. The maximum acceleration or deceleration are  $2.5m/s^2$ ,  $-2.5m/s^2$ , respectively. In addition, vehicle trajectories and road elevation map generated by SUMO are used as inputs to MOVES model to evaluate the energy consumption and air pollutant emissions. The mobility benefits are quantified by average travel time and average speed of the vehicles which is the same format as provided in Equation (4.22). All experiments are carried out using a computer with Intel i7 CPU with 2.80 GHz and 16 GB RAM.

### 6.5.2 Energy Consumption Model and Evaluation Metrics

The MOVES model is utilized here to estimate energy consumption and emissions. The evaluation metrics chosen for effectiveness analysis on the environmental influences includes emissions of  $HC$ ,  $CO$ ,  $CO_2$ ,  $NO_X$ ,  $PM_{2.5}$  and energy consumption. The energy consumption factor (EF, energy consumption in unit distance, KJ/mile) can be obtained by:

$$EF = \frac{\sum_{i=1}^n \sum_{t=1}^{T_i} energy_{i,t}}{\sum_{i=1}^n \sum_{t=1}^{T_i} VHT_{i,t}} \quad (6.22)$$

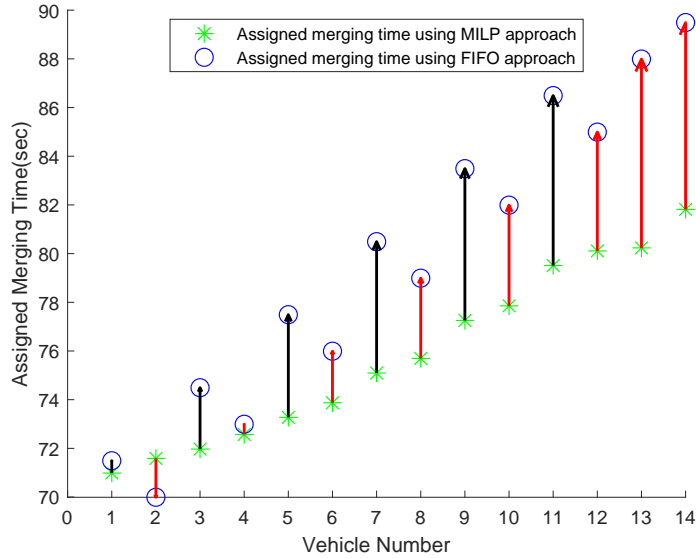


Figure 6.6: An example of the assigned merge time difference using the MILP-based model and the FIFO-based model

where  $energy_{i,t}$  = is the energy consumption rate for vehicle  $i$  at time step  $t$ , in KJ.  $VHT_{i,t}$  = is the vehicle hours traveled for vehicle  $i$  at time step  $t$ .

## 6.6 Experimental Results and Performance Comparison

In this Section, we first compare our proposed MILP-based optimal scheduling algorithm with the traditional FIFO-based approach in terms of vehicle mobility benefit. We then evaluate the overall energy consumption and air pollutant emissions by using three different vehicle trajectory planning algorithms. Total 290 vehicles and 207 vehicles have been released from west bound of the highway and the on-ramp, respectively.

Table 6.1: Performance comparison between the optimal MILP-Based scheduling model and the FIFO-based approach

	Average through time on mainline (sec)	Standard Deviation	Average through time on-ramp (sec)	Standard Deviation
FIFO-based	13.03	1.12	12.67	0.94
MILP-based	10.27	0.48	10.09	0.13
Relative improvement (%)	21.2%		20.4%	

### 6.6.1 Simulation Validation of the Proposed MILP-based Optimal Scheduling

Figure 6.6 shows an example of a clustered vehicles with the merge time and merge sequence differences assigned by the MILP-based model and the FIFO-based model. The blue dots indicate the assigned merge time for each individual vehicle using FIFO-based reservation table and the green stars show the assigned optimal merge time by the proposed MILP-based method. The arrows indicate the time assignment difference with red for mainline vehicles and black for on-ramp vehicles. It is obviously observed that the merge sequence of vehicles using MILP-based model is different from that using FIFO-based model with some vehicles on the mainline sacrifice their merge time to achieve the group travel time saving and mobility benefits. The statistical comparison analysis of the MILP-based optimal scheduling model and the FIFO-based model is shown in Table 6.1. The average travel time on the mainline by the MILP-based model is 10.27 sec that achieves 21.2% improvement compared with FIFO-based reservation model. On-ramp vehicles can also improve their throughput time by 20.4% using the proposed MILP-based optimal scheduling model. In addition, the standard deviation of the MILP-based model is much smaller compared with FIFO-based model, which leads to more reliable performance.

Table 6.2: Fuel consumption and pollutant emission comparison evaluation conducted using motor vehicle emission simulator (MOVES Model)

Vehicle Trajectory Planning	HC (g/mile)	CO (g/mile)	NO <sub>x</sub> (g/mile)	CO <sub>2</sub> (g/mile)	Energy (KJ/mile)	PM <sub>2.5</sub> (mg/mile)	Ave Time cost (sec)
Graph Based Method	0.029	0.86	0.11	53.4	743.34	2.9	4.6
Quadratic Programming Based Method	0.025	0.54	0.13	58.8	818.33	1.6	0.01
Analytical Solution (Baseline)	0.079	2.43	0.38	106.88	2238.42	7.7	0.00014
Improvement (%) of Graph Based Method	62.6%	64.4%	71.7%	66.8%	66.8%	61.5%	
Improvement (%) of QP Based Method	68.7%	77.6%	65.3%	63.4%	63.4%	79.4%	

### 6.6.2 Simulation Validation of the Proposed Vehicle Trajectory Planner

Based on the MOVES model, Table 6.2 shows the energy and environmental benefits of the total 497 vehicle trajectories generated by three trajectory planning approaches proposed. It is obvious that both QP-based and graph-based optimal trajectory methods can significantly improve the energy saving and air pollutant emissions. Compared with the baseline analytical solution, QP-based optimal solution and graph-based optimal solution improve average energy saving by 63.4% and 66.8%, respectively. In addition, significant air pollutant emission reduction can be observed from Table 6.2. The emissions of HC, CO, NO<sub>x</sub>, CO<sub>2</sub> and PM<sub>2.5</sub> per mile using QP-based model are 68.7%, 77.6%, 65.3%, 63.4% and 79.4% less than the baseline model, respectively. Table II also shows that the proposed graph-based optimal trajectory model can reduce 62.6% of HC, 64.4% of CO, 71.7% of NO<sub>x</sub>, 66.8% of CO<sub>2</sub> and 61.5% of PM<sub>2.5</sub> per mile compared with the baseline analytical model. The average computation cost for a 400 meter trajectory planning using Graph-based model, QP-based model and a heuristic solution are 4.6 sec, 0.01 sec and 0.1 mili-sec, respectively.

## 6.7 Summary and Discussion

In this chapter, we described a Bi-level Optimal Edge Computing (BOEC) model for on-ramp merging to maximize overall vehicle mobility benefits and energy saving while optimizing air pollutant emissions. Our key contributions are: 1) developing an edge computing scheme based on V2I/I2V communication; 2) improving vehicle throughput and average speed by grouping vehicles and periodic mixed-integer linear program optimization; 3) updating the heuristic vehicle trajectory planning approach by introducing a sub-system of car-following model; 4) developing a quadratic programming based optimal trajectory model that guides vehicle merging coordination with the minimum air pollutant emissions; and 5) developing a graph based optimal trajectory model that guides vehicle merging coordination with the minimum energy consumption. Microscopic simulation results demonstrate that the proposed MILP-based optimal merge sequence and merge time scheduling can save the travel time on both mainline and on-ramp by 21.2% and 20.4%, respectively, compared to the FIFO-based reservation approach. The comparative validation results of vehicle trajectory planning algorithms indicate that the proposed QP-based trajectory model and graph-based optimal trajectory model outperform the heuristic baseline model in terms of energy saving by 63.4% and 66.8%, respectively. Both QP-based and graph-based trajectory planning models can reduce air pollutant emissions by 61.5% – 79.4% compared to the baseline approach. It turns out that the computational cost of these three vehicle trajectory planning approaches can satisfy the objective of the real time performance.

## **Chapter 7**

# **Conclusions and Future Work**

### **7.1 Conclusions**

This dissertation has presented a variety of connected eco-driving technologies with learning, prediction and anomaly detection models in a connected vehicle environment with advanced machine learning algorithms. It involves the development of innovative electric vehicle energy consumption estimation models, vehicle speed trajectory prediction algorithms, integrated vehicle dynamic-powertrain-environment prediction systems for energy efficient trajectory planning, lane hazard prediction algorithms and their corresponding lane selection models, as well as optimal edge computing on cooperative on-ramp merging techniques. These proposed technologies have been evaluated using either microscopic traffic simulations or data from the real world.

With the advancement of vehicle connectivity and autonomy, connected eco-driving techniques with prediction, learning and edge computing provide new opportunities for real-world energy efficient

semi-autonomous driving. In both urban arterials and highway networks, vehicles and infrastructures that interact in both a mixed or a fully connected vehicular network can significantly improve the overall traffic performance in terms of safety, mobility and environmental sustainability, thanks to the optimal scheduling and the group-wide coordination.

In Chapter 2, an innovative electric vehicle energy consumption model has been developed for enabling the real-time eco-driving algorithm for electric vehicles considering the regenerative braking effect. By introducing a hybrid modeling approach that provides variables with actual physical definition instead of the exhaustive method used in the conventional data-driven approaches, the knowledge-driven variable selection and the data-driven statistical methods are synthesized together to further improve the estimation accuracy. The proposed energy consumption models can be easily integrated into eco-driving algorithms while taking the regenerative braking effect into account.

The work in Chapter 3 fills the gap in many of the existing eco-driving algorithms, including the conventional EAD algorithms which are not flexible enough to handle interactions with other traffic, road grade, and downstream vehicles. Machine learning techniques are applied to predict the future trajectories of preceding vehicle given its historical trajectories and some scene context. By integrating the prediction results into the trajectory planner, the developed Prediction-based EAD algorithm provides an eco-friendly speed trajectory, which also takes the presence of preceding traffic and queues at intersections into account. The trajectory obtained with the proposed prediction algorithm is able to offer an additional 2–34% energy savings and emission reduction when compared to the EAD algorithm without prediction.

Chapter 4 has presented a complete and novel simulation framework of an integrated vehicle/powertrain co-operation system for electric buses (Eco-bus), which performs a co-optimization on the vehicle dynamics and powertrain (VD&PT) controls. Specifically, the overall simulation framework incorporates a two-layer vehicle optimal trajectory planning module that seamlessly integrates a graph-based trajectory planning algorithm and a deep learning based trajectory planning algorithm. This optimal trajectory planning module is able to interact with the environment calibrated using real-world data from the city of Riverside and the Riverside Transit Agency (RTA). It is shown that the deep learning based EAD algorithm can achieve a good balance between solution optimality and computational efficiency. Furthermore, a dynamic queue prediction algorithm in the connected vehicle environment is developed to better plan the bus trajectory for energy savings. A comprehensive evaluation of the proposed system on mobility benefits and energy savings has been conducted across various traffic conditions.

Chapter 5 has showcased a Lane-Hazard Prediction (LHP) application that can detect lane-level hazards effectively and efficiently. LHP can also assist drivers to take a lane change if the vehicle is approaching a detected hazard. Specifically, a machine learning approach is proposed and perform feature extraction in the spatial-temporal domain, which achieves a sustainable and highly accurate lane-level prediction of a downstream hazard within tenths of seconds. The LHP application then guides the vehicle with suggestions for proper lateral maneuvers far ahead of the hazard to avoid a traffic jam. Results demonstrate that LHP-equipped vehicles enjoy significant mobility and safety benefits without compromising the mobility and safety performance of the overall traffic.

Chapter 6 has investigated the edge computing technology for the group-wide vehicle coordination. A Bi-Level Optimal Edge Computing (BOEC) methodology is developed to maximize the vehicle mobility and the energy saving benefit by optimizing the vehicle coordination and motion planning methodologies. For the on-ramp scenario, the first-level edge computing is applied to the road side unit (RSU) that collects data from the connected vehicle. Additionally, this first-level edge computing can dynamically assign each vehicle an associated cluster group based on its state and potential merging conflict, and it also periodically solves their optimal scheduling sequence and arrival time at the merge bottleneck for the clustered vehicles. Once the clustered vehicles receive their assigned arrival time at the merge point, the second-level edge computing determines the optimal vehicle trajectory to guarantee vehicles meet the assigned arrival time with the minimum energy cost. It is shown that the computational cost of vehicle trajectory planning approaches can satisfy the objective of the real time performance and can significantly reduce energy consumption and average travel time.

## 7.2 Selected Paper and Patent Coverage

The research work presented in this dissertation has resulted in the following publications:

1. **F. Ye**, P. Hao, X. Qi, G. Wu, K. Boriboonsomsin, and M. J. Barth, "Prediction-based Eco-approach and departure at signalized intersections with speed forecasting on preceding vehicles," *IEEE Trans. Intell. Transp. Syst.*, no.4, vol.20, pp.1378-1389, 2019.
2. **F. Ye**, J. Guo, K.-J. Kim, P. Orlik, H.-J. Ahn, S. D. Cairano, and M. J. Barth, "Bi-level Optimal Edge Computing Model for On-ramp Merging in Connected Vehicle Environment," in *Proc.*

- 30th IEEE Intell. Vehicles Symp. (IV'19)*, Paris, France, 2019.
3. **F. Ye**, P. Hao, G. Wu, K. Boriboonsomsin, and M. J. Barth, "An Advanced Simulation Framework of an Integrated Vehicle-Powertrain Eco-Operation System for Electric Buses," in *Proc. 30th IEEE Intell. Vehicles Symp. (IV'19)*, Paris, France, 2019.
  4. G. Wu, **F. Ye**, P. Hao, D. Esaid, K. Boriboonsomsin, and M. J. Barth, "Deep Learning-based Eco-driving System for Battery Electric Vehicles," in *the National Center for Sustainable Transportation Publications*, May 2019.
  5. Z. Zhao, Z. Wang, G. Wu, **F. Ye**, and M. J. Barth, "The State-of-the-Art of Coordinated Ramp Control with Mixed Traffic Conditions," in *Proc. 22st Int. IEEE Conf. Intell. Transp. Syst. (ITSC)*, Auckland, New Zealand, 2019, *under review*.
  6. **F. Ye**, G. Wu, K. Boriboonsomsin, Matthew J. Barth, S. Rajab, S. Bai, "Development and evaluation of lane hazard prediction application for connected and automated vehicles (CAVs)," in *Proc. 21st Int. IEEE Conf. Intell. Transp. Syst. (ITSC)*, Maui, HI, 2018, pp. 2872–2877.
  7. **F. Ye**, P. Hao, X. Qi, G. Wu, K. Boriboonsomsin, and M. J. Barth, "Prediction-based Eco-approach and departure strategy in real traffic environment," in *Proc. Transp. Res. Board 96th Annu. Mtg.*, Washington, DC., 2017.
  8. **F. Ye**, G. Wu, K. Boriboonsomsin, Matthew J. Barth, "A hybrid approach to estimating electric vehicle energy consumption for Eco-driving applications," in *Proc. 19th Int. IEEE Conf. Intell. Transp. Syst. (ITSC)*, Rio de Janeiro, Brazil, 2016, pp. 719–724.

The commercialization office of UC Riverside and Honda R&D America Inc. have jointly filed a patent application for the proposed Lane Hazard Prediction (LHP) application described

in Chapter 5. In addition, Mitsubishi Electric Research Laboratories (MERL) has filed a patent application for the work in Chapter 6.

### **7.3 Future Work**

While this dissertation has presented contributions to various aspects of integrating predictive models with energy-efficient driving algorithms, and it has also addressed concrete challenges in the mixed traffic and anomaly traffic in connected vehicle environments, there are still several directions in which further research could be conducted that built upon the results presented in this work.

- Predictive Powertrain Optimization

The several different predictive models proposed in this dissertation are all developed and integrated for improving the performance of vehicle dynamics. The future work will be focused on integrating the prediction on preceding traffic with the powertrain-level optimization. The energy efficiency is expected to be further improved with the help of this predictive powertrain optimization.

- Vehicle Future Trajectory Prediction Considering Social Interactions

The several predictive models of vehicles' future motion presented in this dissertation are all developed based on a sequence-to-sequence modeling approach, in which the future trajectory prediction of a vehicle is based on its historical trajectory and some scene context. This can be further improved by considering the traffic context and interactions between vehicles that also affect the motion of vehicles in traffic.

# Bibliography

- [1] Californian Air Resource Board, *California greenhouse gas emission inventory*, [Online]. Available: <https://www.arb.ca.gov/cc/inventory/inventory.htm>,
- [2] U.S. Energy Information Administration, *Monthly energy review*, [Online]. Available: <https://www.eia.gov/totalenergy/data/monthly>,
- [3] J. B. Kenney, "Dedicated short-range communications standards in the United States," *Proc. IEEE*, vol. 99, no. 7, pp. 1162–1182, Jul. 2011.
- [4] U.S. Department of Transportation, *Applications for the environment: Real-time information synthesis (aeris)*, [Online]. Available: <http://www.its.dot.gov/aeris/>, Accessed: Aug. 2015.
- [5] European Commission (EC), *Ecomove – cooperative mobility systems and services for energy efficiency*, [Online]. Available: [https://www.its.dot.gov/research\\_archives/aeris/index.htm](https://www.its.dot.gov/research_archives/aeris/index.htm),
- [6] Iteris, *Connected vehicle reference implementation architecture*. [Online]. Available: <http://local.iteris.com/cvria/html/applications/applications.html..>
- [7] Waymo), *Safety report and first responders*, [Online]. Available: <https://storage.googleapis.com/sdc-prod/v1/safety-report>,
- [8] European Commission, *The compass4d project*, [Online]. Available: <https://trimis.ec.europa.eu/project/compass4d>,
- [9] P. Hao, G. Wu, K. Boriboonsomsin, and M. J. Barth, "Preliminary evaluation of field testing on eco-approach and departure (ead) application for actuated signals," in *Proc. Int. Conf. Connected Veh. Expo (ICCVE)*, 2015, pp. 279–284.
- [10] B. Asadi and A. Vahidi, "Predictive cruise control: Utilizing upcoming traffic signal information for improving fuel economy and reducing trip time," *IEEE Trans. Control Syst. Technol.*, vol. 19, no. 3, pp. 707–714, May 2011.

- [11] H. Yang, H. Rakha, and M. V. Ala, “Eco-cooperative adaptive cruise control at signalized intersections considering queue effects,” *IEEE Trans. Intell. Transp. Syst.*, vol. 18, no. 6, pp. 1575–1585, Jun. 2017.
- [12] A. Stevanovic, N. Mitrovic, N. Dobrota, D. Mitrovic, and S.-E.-S. Chowdhury, “Glosa (green light optimal speed advisory)-concept for future connected and automated vehicles,” in *Miami Book Fair*, Nov. 2017.
- [13] Z. Chen, Y. Zhang, J. Lv, and Y. Zou, “Model for optimization of ecodriving at signalized intersections,” *Transportation Research Record*, vol. 2427, no. 1, pp. 54–62, 2014. DOI: 10.3141/2427-06. eprint: <https://doi.org/10.3141/2427-06>. [Online]. Available: <https://doi.org/10.3141/2427-06>.
- [14] Q. Jin, G. Wu, K. Boriboonsomsin, and M. J. Barth, “Power-based optimal longitudinal control for a connected eco-driving system,” *IEEE Trans. Intell. Transp. Syst.*, vol. 17, no. 10, pp. 2900–2910, Oct. 2016.
- [15] X. Huang and H. Peng, “Speed trajectory planning at signalized intersections using sequential convex optimization,” in *Proc. Amer. Control Conf. (ACC)*, 2017, pp. 2992–2997.
- [16] M. Barth, S. Mandava, K. Boriboonsomsin, and H. Xia, “Dynamic eco-driving for arterial corridors,” in *Proc. IEEE Forum Integr. Sustain. Transp. Syst.*, Jun. 2011, pp. 182–188.
- [17] H. Jiang, J. Hu, S. An, M. Wang, and B. B. Park, “Eco approaching at an isolated signalized intersection under partially connected and automated vehicles environment,” *Transp. Res. C, Emerging Technol.*, vol. 79, pp. 290–307, 2017.
- [18] X. He, H. X. Liu, and X. Liu, “Optimal vehicle speed trajectory on a signalized arterial with consideration of queue,” *Transp. Res. Part C: Emerg. Technol.*, vol. 61, pp. 106–120, 2015.
- [19] G. Mahler and A. Vahidi, “An optimal velocity-planning scheme for vehicle energy efficiency through probabilistic prediction of traffic-signal timing,” *IEEE Transactions on Intelligent Transportation Systems*, vol. 15, no. 6, pp. 2516–2523, 2014, ISSN: 1524-9050. DOI: 10.1109/TITS.2014.2319306.
- [20] P. Hao, G. Wu, K. Boriboonsomsin, and M. J. Barth, “Eco-approach and departure (EAD) application for actuated signals in real-world traffic,” *IEEE Trans. Intell. Transp. Syst.*, vol. 20, no. 1, pp. 30–40, 2019.
- [21] M. Brackstone and M. McDonald, “Car-following: A historical review,” *Transportation Research Part F: Traffic Psychology and Behaviour*, vol. 2, no. 4, pp. 181–196, 1999, ISSN: 1369-8478.

- [22] M. Saifuzzaman and Z. Zheng, "Incorporating human-factors in car-following models: A review of recent developments and research needs," *Transportation Research Part C: Emerging Technologies*, vol. 48, pp. 379–403, 2014, ISSN: 0968-090X.
- [23] P. Gipps, "A behavioural car-following model for computer simulation," *Transp. Research Part B: Methodological*, vol. 15, no. 2, pp. 105–111, 1981.
- [24] S. Krauss, "Microscopic modeling of traffic flow: Investigation of collision free vehicle dynamics," PhD thesis, 1998.
- [25] M. Treiber, A. Hennecke, and D. Helbing, "Derivation, properties, and simulation of a gas-kinetic-based, non-local traffic model," 1999. DOI: 10.1103/PhysRevE.59.239. eprint: arXiv:cond-mat/9901240.
- [26] S. Panwai and H. Dia, "Comparative evaluation of microscopic car-following behavior," *IEEE Transactions on Intelligent Transportation Systems*, vol. 6, no. 3, pp. 314–325, 2005, ISSN: 1524-9050.
- [27] G. han Peng and R. jun Cheng, "A new car-following model with the consideration of anticipation optimal velocity," *Physica A: Statistical Mechanics and its Applications*, vol. 392, no. 17, pp. 3563–3569, 2013, ISSN: 0378-4371.
- [28] A. Khodayari, A. Ghaffari, R. Kazemi, and R. Braunstingl, "A modified car-following model based on a neural network model of the human driver effects," *IEEE Transactions on Systems, Man, and Cybernetics - Part A: Systems and Humans*, vol. 42, no. 6, pp. 1440–1449, 2012, ISSN: 1083-4427. DOI: 10.1109/TSMCA.2012.2192262.
- [29] F. Wu and D. B. Work, "Connections between classical car following models and artificial neural networks," in *2018 21st International Conference on Intelligent Transportation Systems (ITSC)*, 2018, pp. 3191–3198. DOI: 10.1109/ITSC.2018.8569333.
- [30] V. Kanagaraj, G. Asaithambi, C. N. Kumar, K. K. Srinivasan, and R. Sivanandan, "Evaluation of different vehicle following models under mixed traffic conditions," *Procedia - Social and Behavioral Sciences*, vol. 104, pp. 390–401, 2013, 2nd Conference of Transportation Research Group of India (2nd CTRG), ISSN: 1877-0428.
- [31] G. Agamennoni, J. I. Nieto, and E. M. Nebot, "A bayesian approach for driving behavior inference," in *2011 IEEE Intelligent Vehicles Symposium (IV)*, 2011, pp. 595–600. DOI: 10.1109/IVS.2011.5940407.
- [32] J. Morton, T. A. Wheeler, and M. J. Kochenderfer, "Analysis of recurrent neural networks for probabilistic modeling of driver behavior," *IEEE Transactions on Intelligent Transportation Systems*, vol. 18, no. 5, pp. 1289–1298, 2017, ISSN: 1524-9050. DOI: 10.1109/TITS.2016.2603007.

- [33] M. T. Arne Kesting and D. Helbing, “Enhanced intelligent driver model to access the impact of driving strategies on traffic capacity,” *Philosophical Transactions of the Royal Society A: Mathematical, Physical and Engineering Sciences*, vol. 368(1928), 4585–4605, 2010.
- [34] S. Cui, B. Seibold, R. Stern, and D. B. Work, “Stabilizing traffic flow via a single autonomous vehicle: Possibilities and limitations,” in *2017 IEEE Intelligent Vehicles Symposium (IV)*, 2017, pp. 1336–1341. DOI: 10.1109/IVS.2017.7995897.
- [35] S. Yang, M. Li, Y. Lin, and T. Tang, “Electric vehicle’s electricity consumption on a road with different slope,” *Physica A: Statistical Mechanics and its Applications*, vol. 402, pp. 41–48, 2014.
- [36] R. Zhang and E. Yao, “Eco-driving at signalised intersections for electric vehicles,” *IET Int. Transp. Syst.*, vol. 9, no. 5, pp. 488–497, 2015.
- [37] F. Caouche, R. Trigui, N. E. El Faouzi, and R. Billot, “Energy Consumption Assessment For Electric Vehicles,” in *Proc. Int. symp. Recent Adv. Transp. Modeling*, Apr. 2013, 5 p.
- [38] A. Diaz Alvarez, F. Serradilla Garcia, J. E. Naranjo, J. J. Anaya, and F. Jimenez, “Modeling the driving behavior of electric vehicles using smartphones and neural networks,” *IEEE Int. Transp. Syst. Mag.*, vol. 6, no. 3, pp. 44–53, Jul. 2014.
- [39] N. Chang, D. Baek, and J. Hong, “Power consumption characterization, modeling and estimation of electric vehicles,” in *Proc. IEEE/ACM Int. Conf. CAD (ICCAD)*, Nov. 2014, pp. 175–182.
- [40] E. Yao, M. Wang, Y. Song, and Y. Zhang, “Estimating energy consumption on the basis of microscopic driving parameters for electric vehicles,” *Transp. Res. Record*, vol. 2454, no. 1, pp. 84–91, 2014.
- [41] X. Wu, D. Freese, A. Cabrera, and W. A. Kitch, “Electric vehicles’ energy consumption measurement and estimation,” *Transp. Res. Part D: Transp. Environment*, vol. 34, pp. 52–67, 2015.
- [42] M. Ehsani, Y. Gao, S. Longo, and K. Ebrahimi, *Modern electric, hybrid electric, and fuel cell vehicles*. CRC press, 2018.
- [43] J. Felipe, J. C. Amarillo, J. E. Naranjo, F. Serradilla, and A. Díaz, “Energy consumption estimation in electric vehicles considering driving style,” in *Proc. IEEE Intell. Transp. Syst. Conf. (ITSC)*, Sep. 2015, pp. 101–106.
- [44] G. Turin, “An introduction to matched filters,” *IRE Trans. Inf. Theory*, vol. 6, no. 3, pp. 311–329, Jun. 1960.

- [45] R. Maia, M. Silva, R. AraŹžjo, and U. Nunes, “Electrical vehicle modeling: A fuzzy logic model for regenerative braking,” *Expert Systems with Applications*, vol. 42, no. 22, pp. 8504–8519, 2015.
- [46] R. J. Hyndman and A. B. Koehler, “Another look at measures of forecast accuracy,” *Int. J. Forecasting*, vol. 22, no. 4, pp. 679–688, 2006.
- [47] R. C. Team *et al.*, “R: A language and environment for statistical computing,” 2013.
- [48] D. Anderson and K Burnham, “Model selection and multi-model inference,” *Second. NY: Springer-Verlag*, p. 63, 2004.
- [49] G. Schwarz *et al.*, “Estimating the dimension of a model,” *The Annals Statistics*, vol. 6, no. 2, pp. 461–464, 1978.
- [50] *Next Generation SIMulation: Improved Simulation of Stop Bar Driver Behavior at Signalized Intersections – Los Angeles, CA and Atlanta, GA Data sets*, [Online]. Available: <http://www.webpages.uidaho.edu/ngsim/ATL/ATL.htm>, Accessed: Nov. 2014.
- [51] H. Xia, K. Boriboonsomsin, and M. Barth, “Dynamic eco-driving for signalized arterial corridors and its indirect network-wide energy/emissions benefits,” *J. Intell. Transp. Syst.*, vol. 17, no. 1, pp. 31–41, 2013.
- [52] R. K. Kamalanathsharma and H. Rakha, “Agent-based modeling of eco-cooperative adaptive cruise control systems in the vicinity of intersections,” in *Proc. IEEE Intell. Transp. Syst. Conf. (ITSC)*, Sep. 2012, pp. 840–845.
- [53] V. A. Butakov and P. Ioannou, “Personalized driver/vehicle lane change models for adas,” *IEEE Trans. Veh. Technol.*, vol. 64, no. 10, pp. 4422–4431, Oct. 2015.
- [54] H. Xia, K. Boriboonsomsin, F. Schweizer, A. Winckler, K. Zhou, W. Zhang, and M. Barth, “Field operational testing of eco-approach technology at a fixed-time signalized intersection,” in *Proc. IEEE Intell. Transp. Syst. Conf. (ITSC)*, Sep. 2012, pp. 188–193.
- [55] H. Xia, G. Wu, K. Boriboonsomsin, and M. J. Barth, “Development and evaluation of an enhanced eco-approach traffic signal application for connected vehicles,” in *Proc. IEEE Intell. Transp. Syst. Conf. (ITSC)*, Oct. 2013, pp. 296–301.
- [56] P. Hao, G. Wu, K. Boriboonsomsin, and M. J. Barth, “Developing a framework of eco-approach and departure application for actuated signal control,” in *Proc. IEEE Intell. Veh. Symp. (IV)*, Jun. 2015, pp. 796–801.

- [57] C. Sun, X. Hu, S. J. Moura, and F. Sun, "Velocity predictors for predictive energy management in hybrid electric vehicles," *IEEE Trans. Control Syst. Technol.*, vol. 23, no. 3, pp. 1197–1204, May 2015.
- [58] C. Sun, F. Sun, and H. He, "Investigating adaptive-ecms with velocity forecast ability for hybrid electric vehicles," *Appl. Energy*, vol. 185, pp. 1644–1653, 2017.
- [59] D. Zhou, F. Gao, A. Ravey, A. Al-Durra, and M. G. Simões, "Online energy management strategy of fuel cell hybrid electric vehicles based on time series prediction," in *Proc. IEEE Transp. Electrific. Conf. & Expo (ITEC)*, Jun. 2017, pp. 113–118.
- [60] R. Schubert, E. Richter, and G. Wanielik, "Comparison and evaluation of advanced motion models for vehicle tracking," in *Proc. Int. Conf. Inf. Fusion*, Jun. 2008, pp. 1–6.
- [61] S. Lefevre, C. Sun, R. Bajcsy, and C. Laugier, "Comparison of parametric and non-parametric approaches for vehicle speed prediction," in *Proc. Amer. Control Conf. (ACC)*, Jun. 2014, pp. 3494–3499.
- [62] M. Elhenawy and H. A. Rakha, "Traffic stream speed short-term prediction using machine learning techniques: I-66 case study," Tech. Rep., 2016.
- [63] A. Houenou, P. Bonnifait, V. Cherfaoui, and W. Yao, "Vehicle trajectory prediction based on motion model and maneuver recognition," in *Proc. IEEE/RSJ Int. Conf. Intell. Robot. Syst.*, Nov. 2013, pp. 4363–4369.
- [64] J. Wiest, M. Häuffken, U. Kreßel, and K. Dietmayer, "Probabilistic trajectory prediction with gaussian mixture models," in *Proc. IEEE Intell. Veh. Symp. (IV)*, Jun. 2012, pp. 141–146.
- [65] J. Park, D. Li, Y. L. Murphey, J. Kristinsson, R. McGee, M. Kuang, and T. Phillips, "Real time vehicle speed prediction using a neural network traffic model," in *Proc. Int. Joint Conf. Neural Netw.*, Jul. 2011, pp. 2991–2996.
- [66] B. Jiang and Y. Fei, "Traffic and vehicle speed prediction with neural network and hidden markov model in vehicular networks," in *Proc. IEEE Intell. Veh. Symp. (IV)*, Jun. 2015, pp. 1082–1087.
- [67] —, "Vehicle speed prediction by two-level data driven models in vehicular networks," *IEEE Trans. Intell. Transp. Syst.*, vol. 18, no. 7, pp. 1793–1801, Jul. 2017.
- [68] S. Elanayar V.T. and Y. C. Shin, "Radial basis function neural network for approximation and estimation of nonlinear stochastic dynamic systems," *IEEE Trans. Neural Netw.*, vol. 5, no. 4, pp. 594–603, Jul. 1994.

- [69] U.S. Environmental Protection Agency (USEPA), *Moves (motor vehicle emission simulator)*, Final Report, EPA 430-R-16-002, Apr. 2016.
- [70] B. Chen and H. H. Cheng, “A review of the applications of agent technology in traffic and transportation systems,” *IEEE Trans. Intell. Transp. Syst.*, vol. 11, no. 2, pp. 485–497, Jun. 2010.
- [71] H. Rakha and R. K. Kamalanathsharma, “Eco-driving at signalized intersections using V2I communication,” in *Proc. IEEE Intell. Transp. Syst. Conf. (ITSC)*, 2011, pp. 341–346.
- [72] C. Winter, P. Ritzer, and J. Brembeck, “Experimental investigation of online path planning for electric vehicles,” in *Proc. IEEE Intell. Transp. Syst. Conf. (ITSC)*, 2016, pp. 1403–1409.
- [73] P. Hao, K. Boriboonsomsin, G. Wu, Z. Gao, T. J. LaClair, and M. J. Barth, “Deeply integrated vehicle dynamic and powertrain operation for efficient plug-in hybrid electric bus,” in *Proc. Transp. Res. Board Annu. Mtg.*, Jan. 2019.
- [74] A. Vahidi and A. Sciarretta, “Energy saving potentials of connected and automated vehicles,” *Transp. Res. Part C: Emerg. Technol.*, vol. 95, pp. 822–843, 2018.
- [75] P. Vissim, *PTV Vissim Group*. [Online]. Available: <http://vision-traffic.ptvgroup.com/en-us/products/ptv-vissim/>.
- [76] R. Arora, A. Basu, P. Mianjy, and A. Mukherjee, “Understanding deep neural networks with rectified linear units,” *arXiv preprint arXiv:1611.01491*, 2016.
- [77] Transportation Research Board, *Highway capacity manual, sixth edition: A guide for multimodal mobility analysis*. [Online]. Available: <https://trrjournalonline.trb.org/doi/book/10.5555/9780309441483>.
- [78] Riverside Transit Agency, *14 – GALLERIA AT TYLER – DOWNTOWN 14 RIVERSIDE – LOMA LINDA VA HOSPITAL*. [Online]. Available: <https://www.riversidetransit.com/images/stories/DOWNLOADS/ROUTES/014.pdf>.
- [79] The U.S. Department of Transportation’s National Highway Traffic Safety Administration, [Online]. Available: <https://www.nhtsa.gov/press-releases/usdot-releases-2016-fatal-traffic-crash-data>, Accessed: Oct. 2017.
- [80] *Vehicle-to-vehicle communications: Readiness of V2V technology for application*, Accessed: Oct. 2017.
- [81] US Department of Transportation (USDOT), *Connected vehicle safety pilot*, [Online]. Available: [http://www.its.dot.gov/safety\\_pilot/index.htm](http://www.its.dot.gov/safety_pilot/index.htm), Accessed: Oct. 2015.

- [82] ———, *Dynamic Mobility Applications (DMA)*, [Online]. Available: <http://www.its.dot.gov/dma/index.htm>, Accessed: Oct. 2015.
- [83] D. Krajzewicz, M. Heinrich, M. Milano, P. Bellavista, T. Stützle, J. Härrä, T. Spyropoulos, R. Blokpoel, S. Hausberger, and M. Fellendorf, “Colombo: Investigating the potential of v2x for traffic management purposes assuming low penetration rates,” *ITS Europe*, 2013.
- [84] C. Zinoviou, K. Katsaros, R. Kernchen, and M. Dianati, “Performance evaluation of an adaptive route change application using an integrated cooperative its simulation platform,” in *Proc. Int. Wireless Commun. Mobile Comput. Conf. (IWCMC)*, Aug. 2012, pp. 377–382.
- [85] European Commission, *PRE-DRIVE C2X: PREparation for DRIVING implementation and Evaluation of C2X communication technology*, Technical Report, 2010.
- [86] G. S. Nair, M. E. Eltayeb, R. W. Heath Jr, C. R. Bhat, and N. R. Juri, “A microsimulation approach to quantify the safety benefits of connected vehicles: A road hazard warnings application,” in *Proc. Transp. Res. Board Annu. Mtg.*, 2017.
- [87] H. Yeo, S. E. Shladover, H. Krishnan, and A. Skabardonis, “Microscopic traffic simulation of vehicle-to-vehicle hazard alerts on freeway,” *Transp. Res. Record*, vol. 2189, no. 1, pp. 68–77, 2010.
- [88] J. Liu and A. J. Khattak, “Delivering improved alerts, warnings, and control assistance using basic safety messages transmitted between connected vehicles,” *Transp. Res. Part C: Emerg. Technol.*, vol. 68, pp. 83–100, 2016.
- [89] J. A. Hanley and B. J. McNeil, “The meaning and use of the area under a receiver operating characteristic (roc) curve.,” *Radiology*, vol. 143, no. 1, pp. 29–36, 1982.
- [90] Federal Highway Administration, *Surrogate safety assessment model and validation*, Final Report, FHWA-HRT-08-051, 2008.
- [91] Traffic Count Database System, [Online]. Available: <http://www.ms2soft.com/products/traffic-counts>,
- [92] D. Schrank, B. Eisele, T. Lomax, and J. Bak, “2015 urban mobility scorecard,” 2015.
- [93] R. Ramakrishnan, V. Arvinth, *et al.*, “A look at motion planning for autonomous vehicles at an intersection,” *arXiv preprint arXiv:1806.07834*, 2018.
- [94] K. Dresner and P. Stone, “Multiagent traffic management: A reservation-based intersection control mechanism,” in *Proc. Int. Joint Conf. Auton. Agents Multiagents Syst.*, Jul. 2004, pp. 530–537.

- [95] F. Zhu and S. V. Ukkusuri, “A linear programming formulation for autonomous intersection control within a dynamic traffic assignment and connected vehicle environment,” *Transp. Res. C, Emerging Technol.*, vol. 55, pp. 363–378, 2015.
- [96] H. Ahn and D. Del Vecchio, “Safety verification and control for collision avoidance at road intersections,” *IEEE Trans. Autom. Control*, vol. 63, no. 3, pp. 630–642, Mar. 2018.
- [97] R. Scarinci, B. Heydecker, and A. Hegyi, “Analysis of traffic performance of a ramp metering strategy using cooperative vehicles,” in *Proc. IEEE Intell. Transp. Syst. Conf.(ITSC)*, Oct. 2013, pp. 324–329.
- [98] H. Yang and H. Rakha, “Reinforcement learning ramp metering control for weaving sections in a connected vehicle environment,” Tech. Rep., Jan. 2017.
- [99] J. Rios-Torres, A. Malikopoulos, and P. Pisu, “Online optimal control of connected vehicles for efficient traffic flow at merging roads,” in *Proc. IEEE Intell. Transp. Syst. Conf. (ITSC)*, Sep. 2015, pp. 2432–2437.
- [100] D. Miculescu and S. Karaman, “Polling-systems-based control of high-performance provably-safe autonomous intersections,” in *Proc. IEEE Annu. Conf. Decision Control*, Dec. 2014, pp. 1417–1423.
- [101] J. R. Scariza, “Evaluation of coordinated and local ramp metering algorithm using microscopic traffic simulation,” PhD thesis, Massachusetts Institute of Technology, 2003.
- [102] P. Jaworski, “Cloud computing based adaptive traffic control and management,” PhD thesis, Coventry University in collaboration with MIRA Limited, 2013.
- [103] B. Varghese, N. Wang, S. Barbhuiya, P. Kilpatrick, and D. S. Nikolopoulos, “Challenges and opportunities in edge computing,” in *Proc. IEEE Int. Conf. Smart Cloud (SmartCloud)*, Nov. 2016, pp. 20–26.
- [104] S. A. Fayazi, A. Vahidi, and A. Luckow, “Optimal scheduling of autonomous vehicle arrivals at intelligent intersections via milp,” in *Proc. IEEE Amer. Control Conf. (ACC)*, May 2017, pp. 4920–4925.
- [105] *IBM ILOG CPLEX optimization studio*, [Online]. Available: <https://www.ibm.com/products/ilog-cplex-optimization-studio>, Accessed: Dec. 2018.
- [106] W. L. Winston, M. Venkataramanan, and J. B. Goldberg, *Introduction to mathematical programming*. Thomson/Brooks/Cole Duxbury; Pacific Grove, CA, 2003, vol. 1.
- [107] F. Ye, P. Hao, X. Qi, G. Wu, K. Boriboonsomsin, and M. J. Barth, “Prediction-based eco-approach and departure at signalized intersections with speed forecasting on preceding vehicles,” *IEEE Trans. Intell. Transp. Syst.*, vol. 20, no. 4, pp. 1378–1389, Apr. 2019.

- [108] M. Behrisch, L. Bieker, J. Erdmann, and D. Krajzewicz, “Sumo–simulation of urban mobility: An overview,” in *Proc. Int. Conf. Adv. Syst. SIMUL*, ThinkMind, 2011, pp. 63–68.